



Establishing Three-Dimensional *Ex-Vivo* Culture Platforms of Human Pancreatic Ductal Adenocarcinoma as Pre-clinical Models for the Development of Oncolytic Virotherapy

Reem Mahmoud Elghazawy

Submitted in accordance with the requirements of MD,
Doctor of Medicine

The University of Leeds

Leeds School of Medicine

June 2023

Supervisors: Prof GE Blair, Prof JP Lodge and Prof CS Verbeke

Intellectual Property and Publication Statement

I confirm that the work submitted is my own, except where work which has formed part of jointly authored publications has been included. My contribution and the other authors to this work has been explicitly indicated below. I confirm that appropriate credit has been given within the thesis where reference has been made to the work of others.

- No chapter is based on work from jointly authored publications. The work has been referenced in the Introduction, page 13. A copy of the publication is provided in the appendices (see section 7.4).
- Publication details:

Elghazawy RM, Verbeke CS. Pathology of Pancreatic Tumours. *Surgery*. 2010;28(5): 189-197. (Review).

- The above is a literature review that was a collaboration between myself and Professor CS Verbeke (consultant histopathologist, Oslo University Hospital), on which I was first named author and Prof. Verbeke second.

This copy has been supplied on the understanding that it is copyright material and that no quotation from the thesis maybe published without proper acknowledgement.

“The right of Reem Mahmoud Elghazawy to be identified as Author of this work has been asserted by Reem Mahmoud Elghazawy in accordance with the Copyright, Designs and Patents Act 1988”

Acknowledgements

I am forever indebted to Professor GE Blair for his years of unrelenting support, understanding and for always believing in me. Without him as a positive constant throughout the trials and tribulations of this endeavour I could never have reached the end goal. Thank you.

To my husband, who has made many sacrifices over the years, been the best father to our beautiful children Lianne and Omar, the most wonderful husband who has seen me through the most troubling of times and always picked me up so I can carry on, thank you.

I am so sorry that you are now battling this dismal disease with your nearest and dearest but I promise you we will get through this together and I will never leave your side.

To the woman who made me, my mother, whose years of infinite love, kindness, support, tolerance and understanding has gotten me to where I am today; Mummy you are my back bone, you are life. Thank you.

Finally, and most importantly to my Pappy, whom I lost to this ugly, ugly disease two years ago. My father, my soulmate, my confidante and best friend. I am so lucky and so proud to be able to call myself your daughter. Writing this after losing you has been nothing short of torment but I know how much you wanted me to do this, and were it not for you, I never would have put myself through it. I just wish you were here so I could tell you. Pappy, this is for you.

Abstract

Pancreatic ductal adenocarcinoma (PDAC) is one of the deadliest human neoplasms which remains poorly understood. There is a pressing need to develop a research platform that better recapitulates the in-vivo tumour microenvironment in order to develop better therapeutics and understand the biologics of PDAC. In this study we evaluate two such models; i) organotypic tissue slices and ii) multicellular tumour spheroids (MCTS). Our aims were to i) optimize the culture conditions for the tissue explants and devise a comprehensive method for their analysis and ii) generate MCTS using three PDAC cell lines, Panc-1, Capan-1 and MiaPaCa-2, both as homotypic MCTS or heterotypic MCTS, the latter upon co-culture of the PDAC cell lines with either fibroblasts (MRC5) or epithelial cells (DEChTERT). We also aim to infect both the tissue slices and spheroids with Ad5-based oncolytic viruses and evaluate their response.

Ultra-thin tissue slices were cut from freshly retrieved Whipple's resections. Several variables were modified to establish their ideal culture conditions. We assessed tissue i) integrity using immunohistochemical analysis ii) viability using a TUNEL assay and iii) functionality using an amylase assay. We found that tissue explants can be maintained in culture for ≥ 3 days, longer for tumour tissue, whilst retaining excellent morphology and viability.

We co-cultured PDAC cell lines with fibroblasts or epithelial cells, to form heterotypic MCTS and observed them over a 7-days using immunofluorescence microscopy. These were infected with a wild type and recombinant Adenovirus 5 (Ad5)-based viruses in order to evaluate the i) oncolytic efficacy of Ad5, ii) selectivity for cancer cells, and iii) effect of fibroblasts and epithelial cells on the response of the heterotypic MCTS to viral oncolysis. Homotypic MCTS were blown apart by both viruses with minimal-to-no residual spheroid, with the exception of MiPaCa-2. Heterotypic MCTS showed a subverted response to viral oncolysis highlighting the importance of the tumour microenvironment.

Contents

Intellectual Property and Publication Statement	1
Acknowledgements	2
Abstract	3
Contents	4
Tables and Illustrative Material	8
List of Tables	8
List of Illustrative Material	8
Glossary of Abbreviations	10
1. Introduction & Literature Review	12
1.1. Introduction	12
1.2. Literature Review	14
1.2.1. Pancreatic Adenocarcinoma	14
1.2.2. Tumour Models in Preclinical Research	15
1.2.3. Two-Dimensional Cellular Monolayers versus Three-Dimensional Tumour Models	15
1.2.4. The ex-vivo Tissue Slice Model	19
1.2.5. Oncolytic Viruses	20
1.3. Aims and Plan of Work	22
1.3.1. Ex-Vivo Tissue Slice Model	22
1.3.2. Three-dimensional Multicellular Tumour Spheroids (MCTS)	22
2. Materials and Methods	23
2.1. The ex-vivo Tissue Slice Model	23
2.1.1. Tissue Procurement and Culture	23
2.1.1.1. Tissue Slicing	24
2.1.1.2. Tissue Culture	25
2.1.2. Assessment of Tissue Integrity	27

2.1.2.1.	Tissue Morphology	27
2.1.2.2.	Tissue Functionality.....	29
2.1.2.3.	Tissue Viability –TUNEL Assay.....	34
2.2.	Three-dimensional Multicellular Tumour Spheroids (MCTS)	37
2.2.1.	Cell & Spheroid Culture	38
2.2.1.1.	Cell culture	38
2.2.1.2.	Three-dimensional (3D) spheroid culture.....	40
2.2.1.3.	Pilot Study:.....	40
2.2.1.4.	Preparation of DMEM/Methylcellulose Stock Solution	42
2.2.2.	Generation of 3D Spheroids	43
2.2.2.1.	Homotypic MCTS:	43
2.2.2.2.	Heterotypic MCTS	45
2.3.	Adenoviral Infection	49
2.3.1.	Ascertaining Viral Titres in 2D Monolayers	49
2.3.2.	Flow Cytometry Assessment of Viral Uptake in 2D Monolayers	51
2.3.3.	Homotypic MCTS Transduction & Infection	52
2.3.4.	Heterotypic MCTS Transduction & Infection	54
2.3.5.	Flow Cytometry Assessment of Viral Uptake	56
2.3.5.1.	Hexon Staining.....	56
2.3.5.2.	Flow Cytometry	57
2.3.6.	Spheroid Harvest & Fixation for IHC.....	59
3.	Results.....	60
3.1.	The ex-vivo Tissue Slice Model.....	60
3.1.1.	Tissue Morphology	60
3.1.2.	Tissue Functionality	64
3.1.2.1.	Tissue Irradiation.....	64
3.1.2.2.	Amylase Standard Curve.....	66
3.1.2.3.	Amylase Assay	69
3.1.3.	Tissue Viability.....	72

3.2.	Multicellular Tumour Spheroids.....	74
3.2.1.	Optimisation of spheroid generation	74
3.2.2.	Homotypic MCTS	78
3.2.3.	Heterotypic Multicellular Tumour Spheroids.....	82
3.2.3.1.	Optimizing cell tracker dye labelling in monolayers.....	82
3.2.3.2.	Heterotypic Multicellular Spheroids	86
3.2.4.	Adenoviral Transduction and Infection.....	91
3.2.4.1.	Ascertaining Viral Titres in 2D Monolayers	91
3.2.4.2.	Flow Cytometry	93
3.2.4.3.	Homotypic MCTS Infection.....	95
3.2.4.4.	Heterotypic MCTS Infection.....	103
3.2.4.5.	Flowcytometric Analysis of Viral Selectivity.....	107
4.	Discussion	108
4.1.	The ex-vivo Tissue Slice Model.....	108
4.1.1.	Tissue Morphology	108
4.1.2.	Tissue functionality	110
4.1.3.	Tissue viability	112
4.2.	Multicellular Tumour Spheroids.....	113
4.2.1.	Homotypic Multicellular Spheroids.....	114
4.2.2.	Heterotypic Multicellular Tumour Spheroids.....	118
4.2.3.	Adenoviral Transduction, Infection and Oncolysis.....	122
4.2.3.1.	Homotypic MCTS Infection.....	122
4.2.3.2.	Heterotypic MCTS Infection.....	126
5.	Future Work	132
5.1.	The ex-vivo Tissue Slice Model.....	132
5.2.	Multicellular Tumour Spheroids.....	133
6.	References	135
7.	Appendices.....	146
7.1.	Appendix 2 Manufacturer’s Amylase standard curve.....	147

7.2.	Appendix 3 Ethical approval letter.....	149
7.3.	Appendix 1 Consent form.....	152
7.4.	Publications	153

Tables and Illustrative Material

List of Tables

Table 1 - Cell Lines and their Characteristics	37
--	----

List of Illustrative Material

Figure 1 – Histological viability grading of pancreatic tissue slices	28
Figure 2 – Dilutions of α -amylase from a stock solution to produce a standard curve for amylase activity.....	32
Figure 3 – Ultra-low adherence 96-well plate setup of homotypic MCTS.....	44
Figure 4 – Viability grading of tissue explants from normal pancreas	61
Figure 5 – Viability grading of tissue explants from pancreatic adenocarcinoma	62
Figure 6 – Example of a Day 1 pancreatic cancer section.....	63
Figure 7 – Amylase activity in the medium of normal pancreatic explants after x-irradiation	65
Figure 8 – Standard curves of purified α -amylase activity on storage at 4°C over four consecutive days	66
Figure 9 – Standard curve of purified α -amylase activity on storage at -80°C.....	67
Figure 10 - Pattern of amylase activity of normal pancreas explants over 3 days in culture	70
Figure 11 – Pattern of amylase activity of pancreatic adenocarcinoma tissue explants over two days in culture	71
Figure 12 – Apoptotic body staining of normal and pancreatic cancer after 24hrs in culture using TUNEL.....	72
Figure 13 – Apoptotic body staining in pancreatic adenocarcinoma after 1, 2 and 3 days in culture	73
Figure 14 – Sample images from the Panc-1 trial plate to optimize spheroid culture conditions.....	76
Figure 15 – 911 Homotypic MCTS	79
Figure 16 – Homotypic MCTS	81
Figure 17 – Capan-1 Test sections for autofluorescence.....	83
Figure 18 – MiaPaCa-2 Test sections for autofluorescence.....	84
Figure 19 - Examples of fluorescence in cancer and normal cell lines labelled with cell tracker dyes	85
Figure 20 – 3 examples of the heterotypic MCTS formed of Panc-1 and MRC5.....	87

Figure 21 – Uninfected Panc-1/DEChTERT Heterotypic MCTS	89
Figure 22 – Uninfected Capan-1/DEChTERT Heterotypic MCTS	90
Figure 23 – Cell tracker dye labelling of 911 and Capan-1 monolayers	92
Figure 24 – Cell tracker dye labelling of MiaPaCa-2 and Panc-1 monolayers	92
Figure 25 – Flowcytometric analysis of fluorescent tracker dye uptake	94
Figure 26 – 911 Homotypic MCTS; Uninfected and infected with Ad5F35-EGFP as positive control.....	96
Figure 27 – Panc-1 Homotypic MCTS Infection.....	98
Figure 28 – Capan-1 Homotypic MCTS Infection	99
Figure 29 – MiaPaca-2 Homotypic MCTS Infection	100
Figure 30 – “Infected Halos”	101
Figure 31 – Example Z-Stack images of MCT at preset sequential depths.....	102
Figure 32 - Panc-1/DEChTERT Heterotypic MCTS infection	104
Figure 33 - Capan-1/DEChTERT Heterotypic MCTS infection.....	105
Figure 34 – Infected 911 Homotypic MCTS	106

Glossary of Abbreviations

Adenoviruses	Ads
Adenovirus species-5	Ad5
Coxsackie Adenovirus Receptor	CAR
Hours	hrs
Minutes	mins
National Health Service	NHS
Dulbecco's Modified Eagle's Medium	DMEM
Phosphate-Buffered Saline	PBS
DPX-Mounting Medium	DPX
Haematoxylin and Eosin	H&E
Hertz	Hz
Millimetres per Second	mm/s
Microliters	µl
Microns	µm
Micrograms	µg
Degrees Celsius	°C
Deoxynucleotidyl Transferase	TdT
Borminated Nucleotide	BrdU
Adenoviruses	Ads
Adenovirus Species-5	Ad5
Coxsackie Adenovirus Receptor	CAR
Hours	hrs
Minutes	mins
National Health Service	NHS
Dulbecco's Modified Eagle's Medium	DMEM
Phosphate-Buffered Saline	PBS
DPX-Mounting Medium	DPX
Haematoxylin and Eosin	H&E
Hertz	Hz
Millimetres per Second	mm/s
Microliters	µl
Microns	µm

Micrograms	µg
Degrees Celsius	°C
Deoxynucleotidyl Transferase	TdT
Brominated Nucleotide	BrdU
Multicellular tumour spheroids	MCTS
MOI	Multiplicities of Infection
Viral particles per microlitre	Vp/µl
Nanometres (absorbance unit)	Nm
Pancreatic ductal adenocarcinoma	PDAC
Adenovirus	Ad
Normal goat serum	NGS
Paraformaldehyde	PFA
Immunohistochemistry	IHC
Carbon dioxide	CO₂
Extracellular matrix	ECM
Epithelial mesenchymal transition	EMT
Average	\bar{X}

1. Introduction & Literature Review

1.1. Introduction

Pancreatic cancer is a major leading cause of cancer death in the Western world, with approximately 40,000 deaths per year occurring in Europe and around 26,000 in the USA¹. The incidence of pancreatic adenocarcinoma has been steadily increasing over the past 20 years and it is now the fourth most common cause of cancer deaths and the epidemiologic projections indicate that it will be second only to lung cancer in its lethality by 2025². Fatality is due to a lack of effective screening strategies, inconspicuous early symptoms and poor response to existing therapies leading to a median survival of around one year^{3,4}. New forms of treatment for this disease are therefore urgently needed and this has led to research on the use of human viruses as therapeutic gene delivery systems for the treatment of pancreatic tumours.

A critical requirement for pre-clinical studies is a suitable model system in which to analyse targeting of viral vectors and their penetration/expression in tumour cells as well as virus vs host interactions. Most in-vitro models fail to reflect the complex tissue architecture of an individual tumour. In this study human pancreatic tissue samples, both malignant and normal, were obtained from surgical specimen and processed to produce precision-cut uniform 250µm x 0.5cm slices. Various elements to the modelling system were introduced in order to maximise the yield from minimal amounts of tissue and to optimise their culture conditions. Maximal viability and yield were obtained by minimising the time from surgical resection to culture, using 3% low melting point agarose in coated 6-well plate without the need for agitation. This work has been directed towards devising a comprehensive system to analyse tissue morphology, function and viability and has established that histopathological examination together with a morphological grading was the best method of analysis. It was found that cellular death in such slices in the modelling system appears to occur by necrosis rather than apoptosis. With increased tissue availability, this organotypic culture model presents a representative and reproducible system of the in-vivo situation that will allow the prediction of the clinical efficacy of novel therapies.

Given the limited number of surgical resections and hence availability of human tissue, both of which underpin the inadequate knowledge of this disease and consequently advances in improved therapies, we moved to the development of an alternative culture platform.

It is recognised that three-dimensional cultures are a relevant pre-clinical model as they more accurately reflect the architecture and biomechanical properties of the in-vivo solid tumour.

Three-dimensional (3D) multicellular tumour spheroids (MCTS) are becoming an essential tool in cancer research as it provides a model intermediate in complexity between 2D monolayers and in vivo solid tumours. Spheroids are cell aggregates, self-assembling in an environment that prevents attachment to a flat surface^{5,6}. MCTS closely resemble solid tumours in many aspects such as i) their heterogeneous architecture and ii) internal gradients of signalling factors, nutrients, and oxygenation⁷. MCTS also have growth kinetics similar to those of in vivo tumours and cells within the spheroids mimic the physical interaction of the tumours such as cell-to-cell and cell-to-extracellular matrix interactions. These similarities provide great potential for studying the biological properties of tumours and a promising platform for pre-clinical drug screening and therapeutic efficacy evaluation.

It is well documented that PDAC solid tumours contain a dense fibrous stroma that gives PDAC its chemoresistant phenotype. Furthermore, like many solid tumours, PDAC undergo epithelial-mesenchymal-transition (EMT), a process whereby tumour cells undergo a transition from tightly bound epithelial cells to a more mobile mesenchymal phenotype resulting in local invasiveness and the formation of distant metastasis.

Oncolytic viruses have long been viewed as tools for directly killing cancer cells. Oncolytic viruses can specifically target tumour cells and replicate indefinitely until they kill tumour cells⁸. Adenovirus 5, a species C adenovirus, is one of the most studied.

In this study, and for the first time, we individually co-culture pancreatic ductal adenocarcinoma (PDAC) cell lines with two different normal cell lines that exist in the normal microenvironment of the in vivo solid tumours, fibroblasts and epithelial cells to form heterotypic MCTS. Their characteristics are observed for a 7-day growth period using immunofluorescence microscopy. We also infected these heterotypic MCTS with both a wild type and in-house generated recombinant Adenovirus 5 (Ad5) in order to evaluate the i) efficacy of Ad5 as an oncolytic virus ii) selectivity for cancer cells and iii) the effect of the presence of either fibroblasts or epithelial cells on the response of the heterotypic MCTS to viral oncolysis compared to their absence in their homotypic counterparts.

1.2. Literature Review

1.2.1. Pancreatic Adenocarcinoma

Pancreatic Adenocarcinoma is the fourth leading cause of cancer death in the Western world and remains one of the deadliest human neoplasms⁸. Survival rates have remained relatively unchanged for the last 40 years, with the incidence rate approximating the mortality rate⁹. The poor outcome is largely due to the late detection of the cancer, as most patients remain asymptomatic until the disease is at an advanced stage. Extensive local tumour progression and distant dissemination are frequently found at the time of diagnosis, resulting in a 5-year survival of less than 5%³.

In addition to ductal adenocarcinoma, which is by far the most frequent tumour, an array of different neoplasms can develop in the pancreas. This is in part explained by the normal cellular composition of the pancreas. There are three main cell populations that exist in the gland – acinar cells, duct epithelial cells and islet cells – whereby each of these can undergo neoplastic transformation into one or more tumour entities. Ductal adenocarcinomas are by far the most frequent malignant pancreatic tumours and represent 85-90% of all pancreatic neoplasms⁹. It is a disease of the elderly with a slight male preponderance (male:female ratio = 1.6:1)^{10,11}. Sixty to seventy percent of ductal adenocarcinomas occur in the pancreatic head, and obstructive jaundice, with or without weight loss, is the characteristic presentation in these patients¹². Cancers arising in the body or tail of the pancreas (15 - 20%) lead to mass-related symptoms. Approximately 85% of patients present with an unresectable tumour due to advanced loco-regional and/or metastatic disease¹³. Their median survival is 4 - 8 months³. Surgical resection is currently the only curative treatment option but approximately only 20% of patients are eligible¹⁴. However, the rate of disease recurrence – local, distant or both – is high, amounting to approximately 80%, and results in a postoperative 5-year survival of, at most, 20 - 25% and a median survival of only 20 months¹⁵. The high recurrence rate probably reflects microscopically incomplete resection in the majority of patients¹⁶.

Although the exact pathogenesis of PDAC remains poorly understood, it is thought to be linked to i) smoking, family history of chronic pancreatitis, advancing age, male sex, diabetes mellitus, obesity, occupational exposures, African-American ethnic origin, a high-fat diet, diets high in meat and low in vegetables and folate and possibly *Helicobacter pylori* infection⁸. Although pancreatic cancers overall have a low tumour mutation burden, there are some genes that show recurrent mutations. The most frequent of these include mutations in

the KRAS oncogene observed in 65% to 90% of cases and the TP53 gene encoding for p53 protein, a major tumour suppressor⁹.

Genetic alterations in pancreatic cancer result in an aggressive cancer that is resistant to medical intervention and despite the introduction of new chemotherapeutic agents and combination regimens, it remains a chemo and radioresistant tumour¹⁷. This is mainly due to the influence of the tumour stroma, which promotes tumours growth, early invasion and resistance to chemoradiation^{18,19}. Therefore, the need for new experimental models to better recapitulate this unique tumour environment and the role it plays on the biologics of PDAC is imperative. Furthermore, novel therapies, such as viral-vector-mediated gene therapy, are required to improve the survival of patients with this dismal disease.

1.2.2. Tumour Models in Preclinical Research

Cancer models are either naturally existing or artificially prepared experimental systems that show similar features with human tumours²⁰. However, given the heterogeneity of most solid tumours, the choice of the most fitting model to best reflect the given tumour system is one of the real difficulties for cancer research.

Vast studies have been conducted on cancer models to develop a better understanding of cancer invasion, progression, and early detection. These models give an insight into cancer aetiology, their molecular basis, host tumour interactions, the role of the microenvironment, tumour heterogeneity and tumour metastasis.

Some of these models are briefly explored as well as the role they play in cancer and therapeutic research.

1.2.3. Two-Dimensional Cellular Monolayers versus Three-Dimensional Tumour Models

The inability of in-vitro cancer models to mimic the heterogeneity of human cancer, its microenvironment, and the stromal compartment has hindered the thorough understanding of tumour pathogenesis, therapeutic responses, and adverse reactions²¹.

Two-dimensional (2D) cell culture monolayers are commonly used for toxicological assessments of nanomaterials. The convenience and reproducibility of cancer cells derived from human tumours makes them very attractive to work with as they, in particular, provide important insights into cancer cell phenotypes²². Cancer cell lines can be easily maintained

and can be stored and shared between different laboratories. Of particular significance, the NCI 60 platform, a collection of 60 cell representatives of 9 prevalent cancer types, has led to many important discoveries including P-glycoprotein expression in cancer, a major mechanism of drug resistance²³.

Unfortunately, the efficacy of anticancer drugs on tumour cell lines in-vitro shows little correlation with its success on patients²⁴. Moreover, cancer is as not a single characterized tumour but a heterogeneous system with vast inter cancer variability. This, therefore, means that despite their easy handling, simple cell lines exhibit several significant limitations in reproducing the complexity and pathophysiology of in-vivo tumours in comparison with three-dimensional (3D) in-vitro cell models, such as spheroids²⁵. They omit the complex multicellular effect that influences tumours and their treatment, making them poor predictors of clinical outcomes²⁴.

The limitations of simple cell line research are many and include:

- i) tumour cells grown in vitro undergo phenotypic drifts secondary to extensive passaging and are grown in a fundamentally different microenvironment to solid tumours^{26,27},
- ii) the number of cells grown in vitro are always significantly greater than those in solid tumours, they therefore display greater susceptibility to antitumour drugs that cannot be replicated in vivo^{28,29},
- iii) cell cycle discrepancies, important for cancer gene therapy, differ between cell lines and clinical disease³⁰,
- iv) oncolytic vaccines rely on microenvironmental components that are simply not represented in monolayer cultures³¹,
- v) non-transformed cells within solid tumours, such as fibroblasts and immune cells, provide a complex microenvironment, such as a thick extracellular matrix that supports tumour growth and is radioprotective^{32,33},
- vi) hypoxic cores render tumours chemoresistant³³, and
- vii) localised tumour immunosuppressive networks subvert effective antitumour immune response^{32,34}.

It is clear therefore that despite their availability and reproducibility, simple in-vitro 2D cancer cell models are simply not representative of the complex tumour milieu nor of the interplay within this that gives cancer its growth characteristics and responsiveness to therapy. It is therefore imperative that we continue to develop three-dimensional models that more closely recapitulate the unique tumour microenvironment.

Amongst the most common genetic mutations in cancer are missense mutations in the K-RAS oncogene and p53 tumour suppressor gene. The role of the K-RAS oncogene is the regulation of cell division as a result of its ability to relay external signals to the cell nucleus³⁵. The tumour suppressor gene p53 is a nuclear transcription factor with a pro-apoptotic function³⁶.

K-RAS appears in greater than a quarter of all human neoplasms³⁷; with >90% of PDAC exhibiting the missense mutation. It is also seen in colorectal carcinoma (45%), lung adenocarcinoma (25%) and endometrial carcinoma (20%)^{15,38}.

P53 mutation occurs in 50–75% of human PDAC following activation of mutation in the KRAS gene. Furthermore, p53 and K-RAS co-occur in approximately 70% of patients³⁹.

Since the turn of the century, scientists have focused on the generation of genetically engineered mutant mouse (GEM) models, K-RAS and KPC (The KPC mouse contains a conditional point mutation in the transformation related p53 gene plus K-RAS), that reproduce the natural history of the human disease and closely recapitulate the biology of human PDAC in terms of histopathological and clinical features⁸. Mice have many comparable human anatomical, cellular, and molecular properties known to be critical and functional in cancer⁴⁰. These models have been instrumental in identifying targets with therapeutic properties in PDAC tumours.

However, the genetic profile of PDAC induced by carcinogens in mice is not yet defined and thus limits their applications in studies involving molecular genetics and signalling pathway analyses⁴¹. Moreover, the carcinogens often produce adverse effects on tissues other than the pancreas, thus reducing the value of carcinogen-induced mouse models in preclinical trials⁴²⁻⁴⁴.

Although genetically engineered mouse models have an array of advantages, despite their value as a pre-clinical tool predominantly for the study of cellular phenotypes in PDAC, their value remains limited in the clinical setting particularly in assessment of drug responsiveness. There remains a need therefore to develop other ex-vivo tumour models that better represent in-vivo PDAC solid tumours.

One such model is the 3D multicellular tumour spheroid (MCTS). Spheroids are three-dimensional (3D) cell aggregates that can mimic tissues and microtumours. Spheroids are believed to mimic tumour behaviour more effectively than regular 2D cell cultures.

Much like tumours, spheroids contain both surface-exposed and deeply buried cells, proliferating and non-proliferating zones, hypoxic and nutrient gradient and a rich extracellular matrix. These unique features of the spheroid structure permit cell-cell and cell-

extracellular matrix interactions that is present in in-vivo solid tumours. As a result, spheroids are thought to represent a model that is intermediary in complexity between 2D-monolayers and in-vivo solid tumours. Furthermore, more than one cell population can be co-cultured, such as cancer cell with fibroblasts and/or endothelial cells, both of which are present in the normal milieu of solid tumours. In doing so, the heterotypic MCTS further recapitulates the normal tumour microenvironment.

Moreover, considerable differences have been observed in migration potential and receptor and gene expression of tumour cells grown in 2D monolayers and 3D spheroids, which is thought to be as high as 30%⁴⁵. Therefore, the 3D microenvironment of tumours deserves careful consideration.

Much like solid tumours spheroids display differential oxygen gradients, which is important in the assessment of therapies that can be influenced by tissue hypoxia, such as radiotherapy⁴⁶. Furthermore, the different proliferative regions seen in spheroids, outer proliferative zone and inner quiescent core, can be used to assess responsiveness to therapies that solely target highly proliferative cells^{47,48}.

The fibrous stroma has become increasingly recognised for the role that it plays in cancers, especially PDAC²². It has been reported that there is an interpatient variability in stromal density in PDAC solid tumours, in the range of 40-70%, and it is this high stromal density that gives PDAC its aggressive phenotype, propensity for invasion, migration and radiation resistance^{22,49}. These stromal cells, as well as other stromal components, can be readily co-cultured with primary PDAC cell lines to form heterotypic MCTS which more closely represent the in-vivo solid tumour. This allows for more accurate evaluation of tumour behavioural characteristics and response to therapy, a model that is explored further in this study.

The spheroid model therefore represents an important platform to study the three-dimensional nature of in vivo tumours as well as being an attractive model for the screening of drugs and other therapeutics such as gene and immune therapies^{50,51}.

However, the most major drawback of MCTS is that, although cells are retrieved from human neoplasms, they are cultured in the laboratory and undergo multiple passages in vitro. This results in phenotypic drifts and unwanted clonal dominance⁵².

One way to overcome this phenotypic variation is the use of more “organotypic” spheroids – organoids^{53,54}. Organoids are tiny, self-organized, mini organ-like three-dimensional tissue cultures that are derived from patient derived stem cells that are left to differentiate and

ultimately accurately represent the diverse genetic, cellular and pathophysiological hallmarks of cancer⁵⁵.

1.2.4. The ex-vivo Tissue Slice Model

The limited intervention options for advanced and metastasised pancreatic cancer require new treatment modalities, such as gene therapy. The majority of preclinical studies of viral vectors have relied on the use of human pancreatic cancer cell lines growing subcutaneously in a nude mouse model. However, these are inadequate models for several reasons. Firstly, pancreatic cancer cell lines acquire new genetic alterations upon multiple passages in-vitro and after subcutaneous injection in-vivo¹⁰. As these cell lines undergo multiple changes, it influences their biological behaviour and hence they no longer reflect the primary tumour of origin. In addition, it is difficult to adapt the cells of many tumour cells to in-vitro conditions when establishing a primary culture¹³. Furthermore, xenograft tumours lack the physiological interaction between tumour cells, stromal cells, normal cells and extracellular matrix. This is a very important drawback, given that anatomical barriers, such as fibrosis, act as a major hurdle for adenoviruses to spread through the tumour^{4,12}. The discrepancies in efficacy of novel treatments seen in these preclinical trials and subsequent clinical trials demonstrate that these models are not ideal for a number of reasons:

- i) mouse models do not assess the cellular heterogeneity of solid tumours,
- ii) mouse models do not accumulate an extracellular matrix, which occurs in human tumours, and
- iii) the lack of normal human pancreas cells makes the mouse models unsuitable for demonstrating the increased specificity of the retargeted viral vectors- sensitivity of anticancer drugs depend upon dynamic interactions between tumour cells and their microenvironment¹⁷.

Therefore, to investigate tumour cell behaviour ex-vivo it is necessary to maintain or reconstitute an environment closely resembling the tumour tissue, and hence the in-vivo situation. Tissue explants are a good alternative to mice and cell line models, as they retain the interaction between heterogeneous cell types, comprising both normal and cancer tissue. In addition, these ultra-thin slices also contain an extracellular matrix. As these tissue explants more closely represent the architecture of the original organ, it makes this technique a powerful instrument to perform toxicity and drug-metabolizing studies, as well as the evaluation of the transduction efficiency of viral vectors, such as adenoviruses^{57,58}.

A recent global genomic analysis has identified at least 12 signal transduction pathways in which components were altered in most pancreatic cancers, implying that complex drug combinations may be necessary⁵⁹. An alternative approach to pancreatic cancer therapy is the use of viruses to exploit specific features of cancer cells that make them particularly susceptible to killing by the virus⁶⁰.

1.2.5. Oncolytic Viruses

Most studies that use GEM models, have used strategies in which the target gene was ablated or inactivated before or at the time of tumour initiation, hence limiting the translational value of the results to a clinical scenario⁴². This is exemplified by the fact that as of today, not a single targeted drug has been approved to treat K-RAS mutant cancers^{42,43}. Given the technical difficulties that arise from developing drugs that selectively target gene mutations in cancers, the development of alternative therapeutics, is imperative.

Oncolytic virotherapy constitutes an upcoming alternative treatment option for a broad spectrum of cancer entities, including PDAC. However, to date, despite great research efforts, only four oncolytic viruses been approved by the FDA for treatment of cancer globally, although only one is widely approved, T-VEC⁶². T-VEC is indicated for the treatment of patients with recurrent melanoma after initial surgery and was initially approved in 2015⁶².

One approach to pancreatic cancer therapy is the use of recombinant or oncolytic human adenoviruses (Ads). The Ads appear to be able to infect a wide variety of human cell types, can be grown and purified to high titres using simple cell culture systems and can be genetically modified with relative ease⁶². As well as delivering toxic gene products to tumour cells, the Ads can also target tumour cells for selective replication, the so-called oncolytic virus. Here, mutants of Ad5 target tumour cells that are deficient in expression of the tumour suppressor gene p53⁹.

Precise targeting of the recombinant Ad to the tumour is crucial, since inappropriate uptake into surrounding tissues can result in inflammation and undesired toxicity⁶⁴. The receptor for most human Adenoviruses has been identified as a 46 kD protein which is also utilised by Coxsackie B viruses and has been termed the Coxsackie B and adenovirus receptor, CAR⁶⁵. CAR is an adhesion molecule, and in the preliminary work to this project, our group has shown that loss of CAR expression has been noted in a number of tumour cell types, including pancreatic cancer.

This has given an impetus to research directed towards re-targeting of the Ad5 fibre by genetic modification, ablating CAR interaction and engineering new receptor specificities into

the fibre^{64,66,67}. Re-targeted Ads, however, require specialised cell lines to support their replication and high-titre viral stocks which are difficult to achieve⁶⁸. Most studies using Ads as oncolytic viruses have been based on the species C virus Ad5 and have not attained their expected clinical potential⁶⁵. This may be due to the limited efficiency of Ad infection, due to loss of CAR and poor spread throughout tumours.

There is a clear need to develop new Ads that have broad cell tropism and efficient replication in cancer but not normal cells^{66,67}. However, thus far, the tissue slice method has not been applied to human pancreatic tumour tissue and the selectivity of Ad targeting to cell types within tumours has not been determined. Consequently, one of the long-term aims of this research is to use the tissue slice model for pancreatic cancer and attempt to transduce the tissue slices with Ad and further investigate its potential use, specificity and sensitivity as a novel therapy for pancreatic cancer.

1.3. Aims and Plan of Work

1.3.1. Ex-Vivo Tissue Slice Model

The aim of the first part of the project is to collect resected pancreatic normal tissue and adenocarcinoma from freshly resected surgical specimens. The tissue will be used to produce and maximise the yield of uniform tissue slices using an electronic slicer. The next phase of the research will be to optimise the culture conditions for these explants using various methods in order to prolong survival whilst retaining the best morphology, ultrastructure and function of the tissue. Finally, a comprehensive method of analysis for both normal and cancerous tissue explants will be created looking at tissue viability, function and death.

1.3.2. Three-dimensional Multicellular Tumour Spheroids (MCTS)

Generate MCTS using three PDAC cell lines, Panc-1, Capan-1 and MiaPaCa-2, both as homotypic MCTS or heterotypic MCTS, the latter upon co-culture of the PDAC cell lines with cells which are naturally occurring in the microenvironment of *in-vivo* solid tumours, fibroblasts (MRC5) or epithelial cells (DEChTERT). We aim to infect the spheroids with two Ad5-based oncolytic viruses, Ad5F35-Wild Type (WT) and the in-house generated recombinant Ad5F35-CDC20, to evaluate their oncolytic response, cancer cell selectivity and whether the presence of the fibroblasts and epithelial cells has an effect on this response.

2. Materials and Methods

2.1. The ex-vivo Tissue Slice Model

2.1.1. Tissue Procurement and Culture

To date, a total of eight fresh human pancreatic tissue samples (malignant and normal) have been retrieved from patients undergoing a Whipple's resection (pancreaticoduodenectomy or a pylorus-preserving pancreaticoduodenectomy depending on the extent of the disease; c/o Mr Andrew Smith, Consultant HPB Surgeon, St James' University Hospital). Two of these were not useable. In one specimen the incubator used for culture overheated during the night to 39.5°C. The second specimen was heavily microbially contaminated after 24hrs in culture. Bacterial or fungal contamination has otherwise not at all been observed because of the broad-spectrum antibiotics used and the strict sterile conditions under which the culturing process is performed. In the latter case, contamination was presumed to be due to non-sterile material being present in the incubator, which was in use by others and all material was contaminated on that day. Therefore, data for only five specimens are included in this report.

Investigation was approved by the local ethics committee (see Appendices for ethical approval letter), and informed consent was obtained from all patients (see Appendices for consent form).

The numbers for this type of model and tumour entity are low for several different reasons. These include:

- i) Unresectable tumours at time of presentation – 85% of patients present with unresectable disease,
- ii) patient co-morbidities – although some patients have surgically operable disease, some are deemed unfit for surgery secondary to medical co-morbidities,
- iii) tumour entities other than ductal adenocarcinoma,
- iv) unresectable tumours at the time of surgery (intra-operatively),
- v) waiting lists; unfortunately, patients with resectable tumours ultimately end up having inoperable disease because of waiting time and funding issues,
- vi) late procedure cancellations due to:
 - patient factors: i.e., patients unfit for surgery,
 - NHS management factors: lack of high dependency or intensive care beds

- vii) leave of surgeon and/or pathologist, and
- viii) tissue sharing – half the specimens were used for adenoviral transduction/infection by a colleague.

The specimens are collected immediately after surgical resection and taken to the pancreatic pathologist for cut-up. The amount of tissue given for experimentation is limited and dependent upon:

- i) tumour size,
- ii) ease of macroscopically identifying tumour from surrounding reactive inflammation and normal pancreatic tissue,
- iii) no sampling from areas that are decisive for tumour staging i.e., invasion of bile duct, duodenum, peripancreatic soft issue etc., and
- iv) not compromising the resection margin – this is imperative as the specimens are primarily used for clinical diagnosis and grading,

Both cancerous and normal tissue were used, whenever possible, the latter as a control.

Upon retrieval from the pathologist, the tissue was handled, slice and cultured as follows:

2.1.1.1. Tissue Slicing

Materials

- 2% Virkon
- 70% Ethanol
- DMEM (Sigma D6429)
- Tissue coring tool (5mm in diameter - TSE systems MP0143)
- Agar (Sigma A7002)
- Leica VT1000s vibrating blade microtome
- DMEM + antibiotics:
 - 10ml Pen/Strep (Sigma P4458)
 - 500µl Gentamicin solution (Sigma G1397)
 - 25µl Amphotericin B at 5mg/ml (Sigma A2411)
 - Top up to 500ml with sterile DMEM
- 10% Trigene (Medichem International TR093)

Method

The tissue was stored in DMEM + antibiotics, in order to avoid contamination, (see materials) on ice until use. Tissue cores were obtained using a handheld tissue coring tool and the cylinders of tissue embedded in 3% Agar in PBS and left to set at 4°C. From the cylinders, precision-cut 250µm x 5mm sections were produced (speed setting = 2.5 mm/s frequency setting = 10 Hz) using the Leica vibrating blade microtome. In order to avoid contamination all parts of the slicer in contact with the tissue were cleaned with 2% Virkon, followed by 70% ethanol. Cut sections were transferred into a 6-well plate containing ~ 3ml of warmed DMEM + antibiotics per well and stored in a 37°C incubator to maintain tissue in optimal conditions until cutting is complete. Waste tissue was discarded initially in Trigene and then incinerated.

2.1.1.2. Tissue Culture

Materials

- Shaking platform (Heidolph, Titramax 1000)
- CO₂ incubator at 37°C (Sanyo, MCO-20A1C)
- Treated 6-well plate (Costar 3516)
- Untreated 6-well plate (Sarstedt 83.1839.500)
- PET membrane transwells (Thincert) with either 0.4 µm or 3.0µm pores (greiner bio-one)
- Ex-vivo tissue culture media:
 - 10% Heat inactivated FCS (50ml)
 - 5ml Glutamine (Sigma G7513)
 - 10ml Pen/strep (Sigma P4458)
 - 5ml 100x vitamins (Invitrogen 11120)
 - 10ml 50x amino acids (Invitrogen 11130)
 - 500µl Gentamicin (Sigma G1397)
 - 5ml 100x insulin/transferrin/selenium solution (Invitrogen)
 - 25µl Amphotericin B at 5mg/ml (Sigma A2411)
 - The above components were made up with 500ml with DMEM (Sigma D6546)

Method

Under sterile conditions (using a sterile tissue hood), sections were transferred into a 6-well plate, 1 section per well, containing 3ml of ex-vivo tissue culture media (see below). If a transwell was used, a further 2mls of culture medium was added to the transwell, with a total of 5mls in all wells. The tissue was incubated at 37°C in a 5% CO₂ incubator containing, in certain cases, a shaking platform at 150rpm. After 24 hours in culture and ensuring there was no contamination, the culture was aspirated and replaced with fresh medium. This was then repeated every 48 hours.

In order to optimise the culture conditions for the tissue slices, several variables were introduced to their environment to observe if any of these helped maintain and prolong the tissue morphology, ultrastructure, functionality and viability. These variables included:

6-well culture plates: normal culture plates are treated and hence bear a positive-charge. This could draw the cut slices (given their relatively large dimensions) to the bottom of the culture well, therefore preventing adequate exposure of their undersurface to the culture medium. In order to overcome this, a comparison was made between treated and untreated 6-well plates.

Transwells: to further combat the 'sinking' effect of the slices, transwells with a PET membrane were used to suspend the slices in the wells so that equal amounts of medium, and hence nutrients, covered both upper and undersurfaces of the slices. Transwells with either a 0.4µm or a 3.0µm pore size were used for comparison. These were also used as an air-medium interface to allow adequate oxygenation of the slices.

Shaking platform: to keep the slices constantly moving, hence preventing further sinking and allowing uniform exposure to the culture medium at all times, a shaking platform was used at 150rpm. For each specimen, a direct comparison was made between those slices cultured whilst on the shaking platform and those that were not.

2.1.2. Assessment of Tissue Integrity

The aim of the first part of the study was to optimise the culture conditions for the pancreatic tissue slices. The effectiveness of these was assessed using three approaches in order to examine morphology, viability and functionality over time of normal and malignant pancreatic explants. Furthermore, we examined these three different components with the aim of compiling a comprehensive analysis system for pancreatic explants using this culture model.

2.1.2.1. Tissue Morphology

a. Haematoxylin & Eosin Staining

Materials

- 10% phosphate-buffered formalin (Sigma HT501182)
- 1% PBS
- 70% Ethanol
- tissue cassettes
- paraffin for embedding
- graded xylene and alcohol for dewaxing
- Mayer's haematoxylin
- Scott's tap water
- Eosin
- Alcohol and xylene for dehydrating
- Glass cover slips
- DPX mounting medium
-

Method

Under sterile conditions, individual tissue slices were removed from culture at 24hour time points and washed in 1% PBS for 5 minutes. The slices were then fixed in 10% phosphate-buffered formalin for 10 minutes at room temperature and then washed again in 1% PBS. Individual tissue slices were then transferred into cassettes and left in 70% ethanol for processing. After processing sections were embedded in paraffin and then cut into 3µm sections using a standard microtome. Paraffin sections were then stained with haematoxylin and eosin for histopathological examination using standard laboratory protocol.

b. Histopathological Examination & Viability Grading

Materials

- Leica DMR light microscope, magnification 100x
- SPOT camera, Diagnostic Instruments Inc., Sterling Heights, Michigan, USA
- SPOT Advanced software

Method

The H&E - stained sections examined were examined using a standard light microscope and pictures were taken at a magnification of 100x. Using the Spot Advanced software, individual areas within each tissue section were demarcated according to their viability and assigned a viability grade 0, 1 or 2 as detailed below:

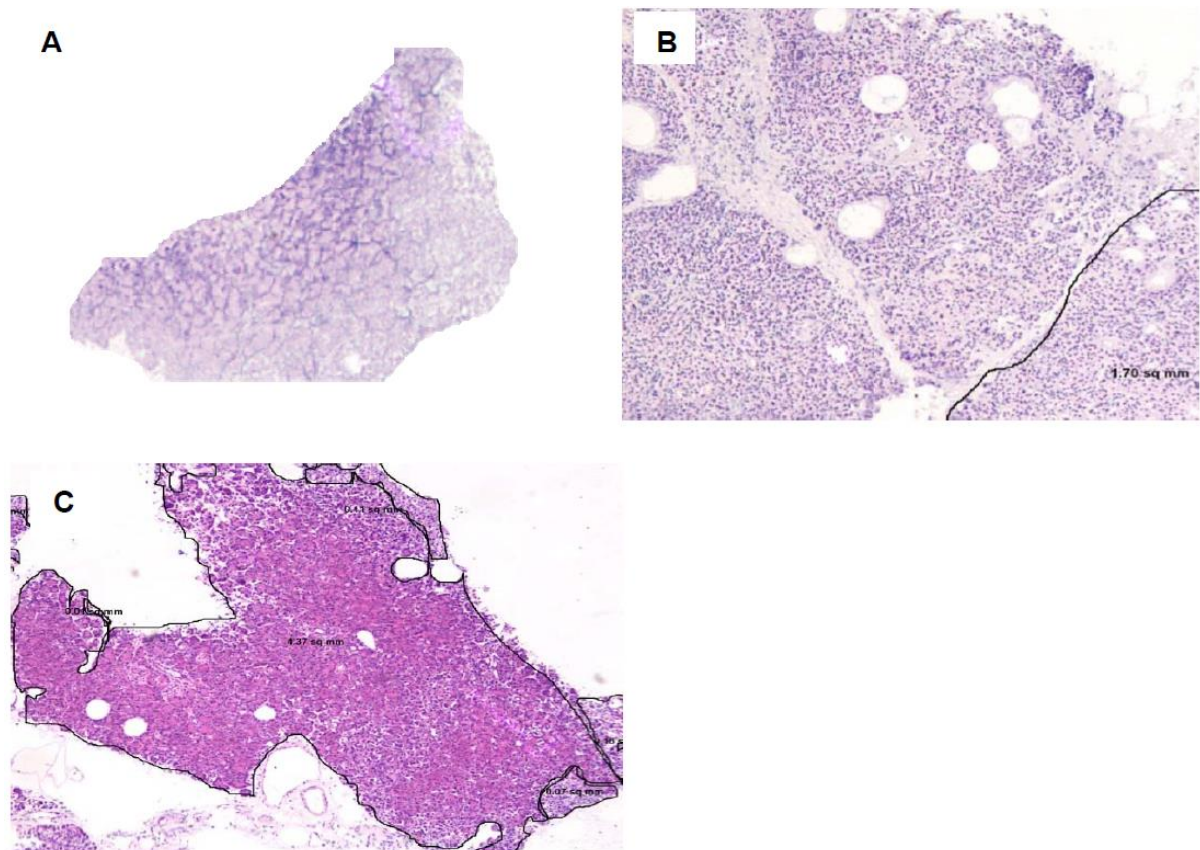


Figure 1 – Histological viability grading of pancreatic tissue slices

Slices of normal and cancerous pancreatic tissue were assessed according to the same scheme, magnification 100x. A: Grade 0: non-viable cells, absence of nuclear staining, loss of cytoplasmic staining; B: Grade 1: withered cells, preserved nuclear staining, shrunken cytoplasm; C: Grade 2: fully viable cells of normal size, with preserved nuclear and cytoplasmic staining.

2.1.2.2. Tissue Functionality

In addition to viability and morphology, the functionality of pancreatic slices was tested by determining amylase activity in the medium.

A major function of the exocrine pancreas is to secrete pancreatic enzymes, one of which is amylase, released by the pancreatic acinar cells for the digestion of carbohydrates. In the clinical setting, a hyperamylasaemia is associated with pancreatic cell damage or trauma, such as pancreatitis. To this end, there is a laboratory reference range for normal amounts of serum amylase, and a 3-4-fold increase in serum amylase is evidence of pancreatic trauma, injury or disease. However less is known about the significance of amylase levels at the lower end of the normal range.

In the context of pancreatic explants secreting amylase into culture medium, the same "normal" reference range cannot be applied given the differences in the environment, method of secretion and the significance of a high or low level.

In vivo, amylase is secreted from the acinar cells in a very controlled manner, however, in the case of tissue slices, the enzyme will be released in an uncontrolled manner, as it is not under the influence of any feedback mechanisms. There are currently no reports in the literature regarding levels of amylase released from pancreatic tissue explants in the surrounding medium and what this may represent. For example, do high levels represent diseased/damaged cells (as is the case with hyperamylasemia in acute pancreatitis), "leaky" ducts as a result of the slicing process or might this be an optimal function?

To address these questions, slices from normal pancreatic tissue were irradiated in their media and analysed as outlined below:

a. Tissue Irradiation

Explants from normal pancreatic tissue were irradiated in their culture medium and the amylase content before and after irradiation was measured in order to answer the question:

“Does a high amylase level in the ex-vivo culture medium of pancreatic explants represent optimally functioning pancreatic tissue or functionally failing acini?”

The intention of irradiation was to kill the cells so that they would no longer be functional and to determine the effect of this treatment on amylase concentration. As the literature did not provide any guidance regarding either the dose or the length of time required to kill the cells, a range of durations, at the maximal output of the irradiator, were tested.

Materials

- Irradiator 320 (NDT equipment services Ltd)
- 6-well plate
- DMEM with additives
- PBS
- 10% formalin
- Bijou tubes (Sterlin)
- Phadebas amylase tablets

Method

Six slices from normal pancreatic tissue were produced and established in culture for 24 hours, as above (section 2.1). After 24 hours, each individual slice was then transferred to a bijou, within its culture medium. The slices were then irradiated in turn at the maximal output of the irradiator, 1.84Gy/minute, for 10, 20, 30, 40, 50 and 60mins respectively. Once irradiated, the slices were washed in PBS and then immediately fixed in formalin. Fixed slices were then paraffin blocked, cut and H&E stained for analysis.

The medium from each slice was then assayed for its amylase content, as described below.

b. Amylase Standard Curve

Although the Phadebas α -amylase reagent used came with its own standard curve to read the amylase activity, in order to assess the reliability of this, an independent standard curve was performed using a lyophilised powder of α -amylase from human pancreas. This was done in order to:

- optimise the assay
- assess the reliability of the manufacturer's standard curve
- assess the stability of amylase enzyme and hence establish optimal conditions for its assay

Materials

- 100 µg of α-amylase from human pancreas at 100units/mg (Sigma A9972)
- 200µl 25mM Tris-HCl solution, pH 7.5
- 100mM KCl solution
- Distilled water
- Eppendorf tubes (Sarstedt)
- Jenway 6303 spectrophotometer

Method

The α-amylase was reconstituted in 200µl (the minimum volume required for the Phadebas assay) of 25mM Tris-HCl pH 7.5, 100mM KCl according to the manufacturer's instructions. This therefore produced a final concentration of 10 units of α-amylase in the 200µl or 50,000units/litre. As spectrophotometer readings >1.5nm are considered unreliable, the highest standard for the curve used was at 1000 units/l of α-amylase. For this, the standard curve provided by Phadebas was used as a guide, and at this concentration the spectrophotometer reading anticipated was ~1.7nm.

The 200µl stock solution was divided into 20x10µl aliquots (at 50,000units/L). The 10µl solutions were then diluted in 490µl of distilled water to produce the 1000unit/L top standard in a total volume of 500µl. Five of these were stored at 4°C and the rest at -80°C. This was done in order to evaluate whether the purified amylase (and hence eventually the supernatants from the tissue explants):

- is best preserved at 4°C or at -80°C
- undergoes significant loss of activity overtime and hence determine if best assayed on the day of collection
- is subject to loss of activity by freeze-thawing

The amylase content of the five samples stored at 4°C was assayed (see below for procedure) at 24-hour time points, between days 0 – day 5, in order to evaluate amylase activity over time at 4°C. From each of these stock solutions (at 1000units/L) a range of serial two-fold dilutions were then produced in order to produce a standard curve. These dilutions were produced as follows:

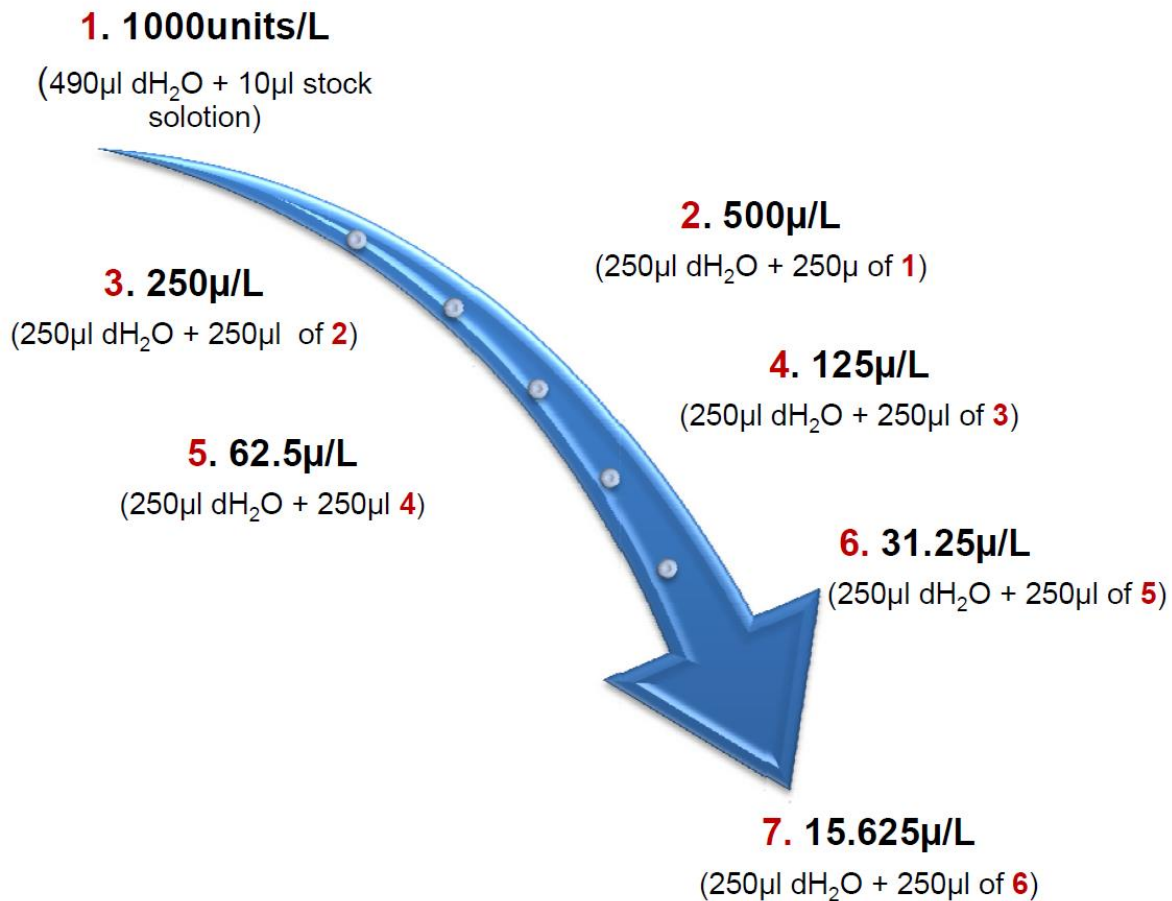


Figure 2 – Dilutions of α -amylase from a stock solution to produce a standard curve for amylase activity
Diagrammatic representation of α -amylase from stock solution to produce an inhouse standard curve to test versus the manufacturer's

Once the dilutions were produced, they were kept on ice until use. At both 1000 units/l and 500units/l of amylase, the spectrophotometer was unable to read the amylase content as the concentration was too high (i.e., readings >1.5nm). These were therefore diluted further, and only 50ul of the reconstituted amylase was added to 250ul of distilled water. The absorbance reading of these was as a result multiplied by a factor of four.

A single stock solution was removed from the -80°C freezer and thawed at room temperature. A series of dilutions were made in the same way (as above) to produce a standard curve of amylase activity.

c. Amylase Assay

This was performed using an enzyme-based colorimetric assay on a Jenway 6303 spectrophotometer.

Materials

- Phadebas reagent - Amylase tablets (Pharmacia Diagnostics, Sweden)
- Phadebas standard curve (provided)
- Water bath at 37°C, Tempette TE-8A (Techne,)
- Centrifuge capable of producing 1500g, Eppendorf 5810-R
- Plastic centrifuge tubes (Costar Corning, UK)
- Jenway Spectrophotometer 6303
- Vortex mixer, Rotamixer (Hook & Tucker instruments)
- Distilled water
- 0.5 M, Sodium Hydroxide solution (VWR, UN1823)

Method

Medium from the tissue slices was analysed for as many consecutive days as the pancreatic explants were kept in culture. The supernatants from each well were collected at 24-hour time points. Frozen samples were thawed in a waterbath at 37°C. Aliquots of 200mls of the sample was mixed with 4 ml distilled water in a 10 ml tube and returned to the water bath. To each tube a tablet of Phadebas reagent was added and vortexed for 10secs. This contained a water-soluble, cross-linked starch polymer which was hydrolysed by α - amylase to generate a water-soluble blue dye. Tubes were left for 15 minutes, after which the reaction was terminated by the addition of 1ml 0.5M sodium hydroxide. After centrifugation at 1500g for 5 minutes, the clear supernatant was aspirated into spectrophotometer cuvettes and the absorbance measured at 620nm wavelength against a blank cuvette containing the supernatant of the reaction with the reagent only and distilled water. The absorbance of the blue solution was proportional to the α -amylase in the sample. Absorbance readings above 1.5 were considered inaccurate. Samples with high amylase content were diluted by either 5 or 10-fold using distilled water and the amylase activity in units/l (read from the standard curve) was in turn multiplied by the same factor as that of the dilution.

2.1.2.3. *Tissue Viability –TUNEL Assay*

In order to assess tissue viability quantitatively, apoptotic bodies were detected by immunohistochemical staining. Apoptosis is characterised by a number of intracellular phenomena such as membrane blebbing, chromatin condensation and nuclear DNA fragmentation. Detection of nuclear DNA fragmentation is a widely accepted method to assay for apoptosis and can be performed in situ by incorporating labelled nucleoside triphosphate at the free 3-OH ends of DNA fragments using the terminal deoxynucleotidyl transferase (TdT) enzyme. This assay, often referred to as the TUNEL assay, allows monitoring of apoptosis in cell samples or tissue sections, providing a histological localisation of apoptotic events. A brominated nucleotide (BrdU) is more efficiently incorporated by TdT than biotinylated nucleotides at the sites of DNA fragmentation. The TACS-blue label provides an intense blue staining in cells in which DNA is fragmented.

Materials

- TACS.XL – Blue Label in Situ Apoptosis Detection Kit (4828-30-BK, Trevigen), contents:
 - Proteinase K
 - Cytonin
 - 10x TdT Labelling buffer
 - 10x TdT Stop Buffer
 - B-dNTP Mix
 - TdT Enzyme
 - Strep-HRP
 - TACS Blue Label Solution
 - Anti-BrdU Antibody
 - Strep-Diluent
 - TACS-Nuclease
 - TACS-Nuclease Buffer
 - Nuclear Fast Red Counterstain
- Proteinase K Solution = (n x 1µl Proteinase K) + (n x 50µl dH₂O)
- Quenching Solution = 45mls methanol + 5mls 30% hydrogen peroxide
- 1x TdT Labelling Buffer = 10x TdT Labelling Buffer diluted using dH₂O
- Labelling Reaction Mix = (n x 1µl B-dNTP Mix) + (n x 1 µl TdT Enzyme) +(n x 50µl 1x TdT Labelling Buffer)
- 1x TdT Stop Buffer = 10x TdT Stop Buffer diluted using dH₂O

- Antibody Solution = (n x 1µl Anti-BrdU) + (n x 50 µl Strep-Diluent)
- PBST = 200ml 1x PBS + 100µl Tween20
- Strep-HRP Solution = (n x 50µl 1x PBS) + (n x 1µl Strep-HRP); where n = number of assays
- 37°C incubator
- Microcentrifuge (Eppendorf, Centrifuge 5415D)
- Coplin jar
- Humidity chamber
- Distilled water
- 1x PBS
- Tween 20
- Xylene
- 30% Hydrogen peroxide (Sigma H1009)
- Methanol
- Hydrophobic coverslips (Deckglaser)
- Millipore S7101 apoptosis detection kit

Method

Tissue slices were removed from culture at 24-hr time points, formalin-fixed and then paraffin- embedded (see 2.2.1a). Paraffin sections were de-waxed in graded xylene and alcohol. The samples were then immersed in PBS for 10 minutes. Sections were then covered with 50µl of 2% Proteinase K Solution in a humid chamber for 30 minutes at room temperature. Hydrophobic cover slips were applied to ensure the sections were uniformly covered with the solution and to prevent dehydration. Samples were then washed twice in deionised water for 2mins each. The slides were immersed in 50ml Quenching solution for 5mins, washed in 1x PBS for 1 min and then immersed in 50ml of 10% TdT labelling buffer for 5mins. Each section was then covered with 50 µl of Labelling Reaction Mix and incubated overnight at 37°C in a humid chamber. The samples were then immersed in 50ml of 10% TdT Stop Buffer, followed by two washes in PBS for 2mins each. The sections were replaced in the humid chamber and covered with 50µl of Antibody Solution for 60mins at 37°C. Given the high frequency of cell death by apoptosis in salivary gland tissue, this was used as a positive control (obtained from surplus archived material). Addition of the Antibody Solution was omitted on one of the salivary gland sections as a negative control. The slides were washed twice in PBST for 2mins each, before covering with 50µl of Strep-HRP solution and incubated for 10mins at room temperature in a humid chamber. This was followed by 2

washes in PBS for 2mins each, then 2mins in deionised water. TACS Blue Label (50µl) was added to cover each sample for 5mins, and after washing in deionised water, slides were immersed for 5mins in 50ml of nuclear fast red to counterstain. After washing in deionised water, the slides were then dehydrated in 100% ethanol followed by xylene, before mounting glass coverslips using DPX.

Slides were examined using a standard light microscope.

To establish whether apoptosis in the tissue explants was indeed due to the culture conditions or present, in the first instance, in the pancreatic specimens (and hence independent of the culturing procedure), tissue sections from each sample were retrieved from surplus archived material from the Pathology Department and TUNEL stained using the same procedure above.

a. Optimisation

To ensure maximal sensitivity and specificity in apoptotic body detection, several components of the assay were first optimised using control tissue:

- Trevigen vs. Millipore (S7101) apoptosis detection (TUNEL) kits: much greater sensitivity was obtained with the Trevigen kit and higher specificity (significantly less background staining)
- Use of DAB vs. TACS-Blue Label: greater sensitivity and a stronger signal were seen with the TACS-Blue label
- Incubation time of primary antibody: maximal labelling was obtained after 60mins of incubation as opposed to 30mins (the manufacturer's instructions)
- Incubation time of nucleotide mix: incorporation was maximal after an overnight incubation as opposed to 60mins (the manufacturer's instructions)
- Prostate vs. Salivary gland tissue as positive control: many more apoptotic bodies were noted in salivary gland tissue.

2.2. *Three-dimensional Multicellular Tumour Spheroids (MCTS)*

Three pancreatic cancer cell lines were investigated in this study; Panc-1, MiaPaCa-2 and Capan-1 for their ability to form spheroids in culture. The origin of each cell line was tracked back to the respective sources to ensure that they were truly generated from pancreatic ductal adenocarcinoma and ascertain if they originated from a primary tumour or a metastasis. 911 cells, an Ad5 immortalised human, retinoblast cell line, were used as a positive control. DEChTERT, a ductal pancreatic epithelial cell line immortalised by hTERT, was used to represent normal epithelial cells present in PDAC in vivo solid tumours and used to form heterotypic MCTS with each of the PDAC cell lines. MRC5, is a diploid cell line composed of human foetal fibroblasts, was used to represent stromal fibroblasts in PDAC solid tumours and again were co-cultured with each of the PDAC to form mixed spheroids. Both the epithelial and fibroblast cell lines were used to emulate the normal cancer milieu of PDAC solid tumours and ultimately determine whether Ad5 selectively infects cancerous over normal cells.

Cell Lines used

Cell Line	Source of cells	Normal or Malignant	Differentiation	Histology	Supplier
911	Ad immortalised human retinoblasts	Normal	N/A	Human retinoblasts	Laboratory Stock
MRC5	Human foetal fibroblasts	Normal	N/A	Diploid human fibroblasts	Laboratory Stock
DEChTERT	hTERT immortalised ductal pancreatic epithelial cells	Normal	N/A	Ductal pancreatic epithelium	Laboratory Stock
TC32	Primary Tumour	Malignant	Poor	Human Ewing's sarcoma	c/o Prof GP. Cook, LIMR
Capan-1	Liver Metastasis	Malignant	High	PDAC	Laboratory Stock
Panc-1	Primary Tumour	Malignant	Moderate	PDAC	Laboratory Stock
MiaPaCa-2	Primary Tumour	Malignant	Poor	PDAC	Laboratory Stock

Table 1 - Cell Lines and their Characteristics

2.2.1. Cell & Spheroid Culture

2.2.1.1. Cell culture

Materials

- DMEM (Sigma D6429)
- 10ml Pen/Strep (Sigma P4458)
- 50ml FBS (Hyclone)
- TC grade culture T25 culture flasks, (Corning)
- TC grade T75 culture flasks, (Corning)
- 37°C Water bath
- Centrifuge
- Trypsin (Sigma)
- CO₂ incubator [(5% CO₂, 95% air in humidified chamber at 37°C) (Sanyo, MCO-20A1C)]
- Gilson micropipettes
- 50ml universal tubes (Corning)
- Sterile (autoclaved) PBS (Oxoid; one tablet/100ml)

Method

Cells were grown in complete DMEM with 10% foetal bovine serum and 1% Penicillin/Streptomycin under standard culture conditions (5% CO₂, 95% air in humidified chamber at 37°C) using the following method:

Cells were thawed from -80°C/liquid Nitrogen in a water bath at 37°C. Once thawed, the cells were removed from original Eppendorf and transferred to a clear universal tube containing 50ml of DMEM under sterile culture conditions. The tube was centrifuged at 1500g for 5 minutes to pellet the cells. The resultant supernatant was removed and discarded and the pellet was resuspended in 5ml of warmed complete DMEM. This cell solution was transferred to a T25 culture flask with sterile filter cap. The flask was transferred to an incubator under standard culture conditions (5% CO₂, 95% air in humidified chamber at 37°C) until the cells reached confluence.

Once confluent, the cells were trypsinised and transferred to a T75 flask. Firstly, the medium was removed from the flask and the cells were washed with 1ml of PBS. The PBS was then

removed and 1ml of thawed, warmed Trypsin was added to the flask, ensuring the base was covered. The Trypsin containing flask was transferred to an incubator and left for 5-10 min until the adherent cells were floating. In the culture hood, 5ml of complete DMEM was added to the flask and cells were thoroughly resuspended, transferred to a T75 flask and supplemented with complete medium to a total volume of 12ml. The cells were incubated under standard culture conditions and the medium was changed every 2-3 days, as necessary.

Cells cultures were sub-cultured every 3 days (when they had reached at least 80% confluence) into a T75 flasks using the above method by transferring half of the trypsinised cell suspension from the original T75 flask into a second, and adding Complete DMEM medium. Cell expansion was continued until a sufficient cell population was established for the formation of spheroids at the required seeding density (see section 2.2.2.1; 43).

2.2.1.2. Three-dimensional (3D) spheroid culture

For the generation of spheroids, cells were trypsin-treated (see section 2.2.2.1; 43) and counted using the Neubauer chamber (haemocytometer) according to the manufacturer's instructions. Subsequently the cells were seeded onto round bottomed ultra-low adherence 96 well plates at the required seeding densities in 200µl of DMEM containing 10% FBS and supplemented with 20% methylcellulose stock solution, a crowding agent that facilitates spheroid formation. Each well was subsequently topped up with medium to a total volume of 200µl.

2.2.1.3. Pilot Study:

TC32, a Ewing sarcoma cell line, was used by a sister laboratory to form spheroids with a well-established methodology. A pilot study was performed using this cell line in order to establish the techniques required for spheroid formation prior to experimenting with the pancreatic cancer cell lines.

Materials:

- TC32 – from sister laboratory (Professor GP Cook, LIMR, St James' University Hospital, Leeds).
- RPMI R98758, (SIGMA)
- Trypsin (laboratory stock)
- Haemocytometer
- Light microscope
- Corning Costar ultra-low adherence 96 well plates (#7007)
- Gilson pipettes and tips
- Sterile hood
- 37°C Water bath
- Humidified incubator

Methods:

TC32 was grown in RPMI under standard culture conditions (see section 2.2.1.1; 38). Cells were treated with 2ml of trypsin at 37°C in a CO₂ incubator for approximately 15 min. The cells were then resuspended in 3ml of medium and counted using a haemocytometer (see

section 2.2.2.1; 43) to get 605 cells/ μ l. A ten-fold dilution was made from this (1 μ l aliquot added to 9 μ l of medium) and this was used to seed cells at different concentrations in a 96 well ultra-low adherence plate.

Ten wells were seeded with the TC32 starting with 1000 cells/well, going up in increments of 1000 up to 10,000 cells/well using the x10 diluted solution. Each aliquot of cells was pipetted into a single well and supplemented with 200 μ l of RPMI

This was done in order to establish the ideal number of cells required for spheroid generation. The culture plate was microscopically assessed every 24 hrs for effective spheroid formation, spheroid size, size of hypoxic core and evidence of disaggregation.

2.2.1.4. Preparation of DMEM/Methylcellulose Stock Solution

Much of the literature reported the difficulty in spheroid generation using some pancreatic cancer cell lines, particularly Panc-1 and Mia-PaCa-2 and these formed spheroids much more readily with the use of a crowding agent. The one most frequently and successfully used was DMEM/Methylcellulose.

Materials:

- Methylcellulose (Sigma, M0262)
- Flask with magnetic stirrer
- Autoclave
- DMEM
- DMEM with 20% FBS
- Cold room at 4°C

Method:

6g of methylcellulose powder was autoclaved in a 500ml flask with a magnetic stirrer. The autoclaved powder was dissolved in 250ml preheated (to 30°C) basal (without FBS or antibiotics) DMEM at 60°C for 20 min using the magnetic stirrer. Thereafter, 250ml of medium at room temperature containing double the amount of FBS (20%) which was added to a final volume of 500ml DMEM and the whole solution mixed overnight at 4°C. The final stock solution was aliquoted and cleared by centrifugation (5000g, 2hrs, room temperature). Only the clear highly viscous supernatant was used for the spheroid assay. For spheroid generation, 20% of the stock solution and 80% culture medium corresponding to a final 0.24% methylcellulose, was used. Lastly, 5ml of this solution was removed and replaced by 5ml (1%) of Penicillin/Streptomycin.

2.2.2. Generation of 3D Spheroids

All three PDAC lines, 911 and DEChTERT were used to form both homotypic and heterotypic MCTS. The homotypic MCTS were formed from each of the cell lines individually and the heterotypic were formed by combining each of the PDAC with DEChTERT to emulate the milieu of in-vivo cancers. Optimisation of the culture conditions was performed in order to define the ideal conditions for the formation of the homotypic and heterotypic 3D MCTS.

2.2.2.1. Homotypic MCTS:

Materials:

- Trypsin (laboratory stock)
- Haemocytometer
- Corning Costar ultra-low adherence (#7007)
- DMEM/Pen/Strep
- DMEM/Methylcellulose/Pen/Strep stock solution
- Gilson pipettes and tips
- Sterile hood
- 37°C Water bath
- Humidified incubator
- Light microscope

Methods:

The required cell line was grown under standard culture conditions (see section 2.2.1.1; 38). Cells were trypsin treated (2ml) and counted using a haemocytometer (see section 2.2.1.1; 38) and the number of cells/ μ l deduced.

Using the Corning Costar ultra-low adherence (to prevent cells adhering to wells and encourage clustering and formation of spheroids), the outer two rows and two columns of wells were filled with 200 μ l of medium to prevent uneven evaporation of medium from the inner wells. In the rest of the plate, cells were seeded (at the required density) on a bed of DMEM/methylcellulose and supplemented with warmed complete DMEM at a ratio of 20%:80% DMEM/Methylcellulose:complete DMEM.

The plates and were set up as follows:

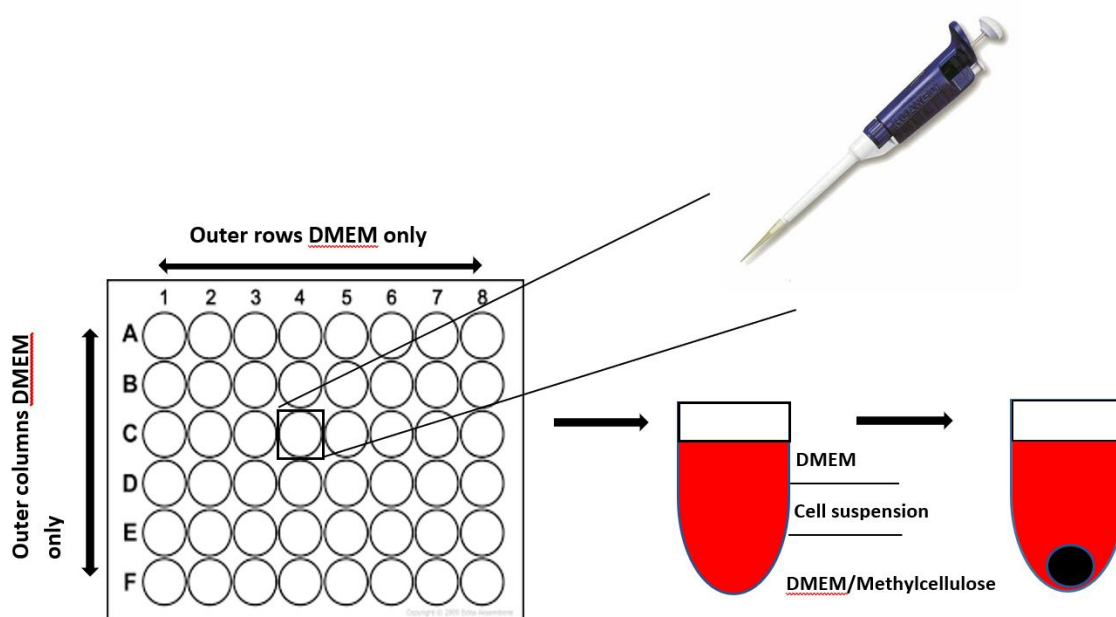


Figure 3 – Ultra-low adherence 96-well plate setup of homotypic MCTS

Diagrammatic representation of 96 well plate lay out for spheroid generation. Outer wells contained medium only to prevent dehydration of cell containing wells. Call containing wells were plated in the order as shown; DMEM/methylcellulose solution first, followed by cell suspension and topped up with complete DMEM to a total volume of 200µl.

Each seeding density/variable was set up in duplicate or triplicate and plates were incubated at standard culture conditions for the required number of days until required size/state of hypoxia achieved. Plates were inspected daily under light microscopy and depending on the cell line, spheroid formation occurred at 24-72hrs.

The spheroid culture medium was changed every 72 hrs by removing 100µl of medium and replacing it with 100µl of fresh warmed medium. This was carefully done by inserting a pipette tip down one wall of the well and keeping it near the surface, being careful not to aspirate the spheroid.

To ascertain the optimal seeding density for each cell line for spheroid formation, each cell line was experimentally seeded at 2500, 4000, 5500, 7000, 8000 and 10000 cells per well in a 96 well plate. Each cell line was microscopically assessed every 24 hrs for effective spheroid formation, spheroid size, size of hypoxic core and disaggregation if any. The optimal seeding density for all cell lines was observed to be 2500 cells/well and this density was used for all spheroid generation from this point onwards.

2.2.2.2. Heterotypic MCTS

Tumours are not unicellular entities. They are formed of both malignant and normal cells and so in order to more closely emulate the tumour structure, heterotypic MCTS were formed. Each of these contained two cellular populations – one of the pancreatic cancer cell lines and DEChTERT, a primary immortalised epithelial cell line as a normal control. Furthermore, if adenoviruses are to be used as vectors for chemotherapeutics, a prerequisite will be that they exclusively target and transduce malignant cells. Therefore, the heterotypic MCTS can be used to assess this.

In order to identify the cell type within the heterotypic MCTS, fluorescent cell tracker dyes in DMSO were used to track each of the cell types. This would also illustrate which of the cell types the adenovirus had entered, cancerous or normal.

a. Optimising Cell Tracker Dye Labelling in Monolayers

Materials:

- Cell tracker green (Molecular Probes, ThermoFisher)
- Cell tracker orange (Molecular Probes, ThermoFisher)
- Cell tracker violet (Molecular Probes, ThermoFisher)
- 6-well culture plates
- T75 cell culture flasks
- DMEM
- Trypsin, laboratory stock
- Humidified CO₂ incubator, 37°C
- Gilson pipettes
- Cell culture hood
- EVOS microscope

Methods:

To evaluate which of the cell tracker dyes resulted in the best cellular uptake and therefore signal, monolayers of each of the pancreatic cancer cell lines and MRC5 were set up and incubated with the dyes.

A confluent T75 flask of each of the pancreatic cancer cell lines was trypsinised and resuspended in 6ml of medium to a total volume of 8ml.

One 6 well plate was set up per cell line. One millilitre of the resuspended cells was aliquoted into each of the wells and topped up with 4ml of complete DMEM. The plates were incubated in normal conditions overnight until 60-70% confluent.

The green, orange and violet fluorescent cell tracker dyes were warmed to room temperature and dilutions of 1:1000 and 1:2000 of these were made up using serum free medium. The medium was removed from the 6-well plates for all cell lines and 1 ml of each dilution from all 3 cell tracker dyes was added one per well for all cell lines. The cell plates were incubated for one hr and then the medium removed and complete medium was added for imaging in the EVOS microscope. The strongest signal for each of the dyes was resolved for all cell lines and this was used for making the heterotypic MCTS. Cell tracker violet imaged poorly with too much background noise and therefore was not taken any further.

Heterotypic MCTS were made using one of the three pancreatic cancer lines and MRC5, a human foetal lung fibroblast, which grow adherently in culture and exhibited fibroblast morphology.

b. Heterotypic MCTS generation:**Materials:**

- Panc-1 cell line
- Capan-1 cell line
- DEChTERT cell line
- MRC5 cell line
- Cell tracker green
- Cell tracker orange
- Serum free DMEM
- DMEM (Sigma) with foetal bovine serum (laboratory stock)
- Trypsin, laboratory stock

- T75 culture flasks
- Sterile culture hood
- Humidified incubator
- 6-well culture plates
- Sterile falcons
- DMEM/methylcellulose solution
- 96-well ultra-low adherence plate
- Haemocytometer
- Light microscope
- Zeiss inverted (fluorescent) microscope
- EVOS microscope

Methods:

A preliminary experiment was performed using MRC-5 cell line in order to determine the ideal number of cells for spheroid formation and this was found to be 750 and therefore it was decided to form the heterotypic MCTS at a ratio of 750:750 of Pancreatic Cancer Cell Line:MRC-5.

To make the heterotypic MCTS, pancreatic cancer cells were always labelled green and MRC-5 always orange.

The ideal concentration that returns the best signal of cell tracker green (see section 2.2.2.2) for each of the pancreatic cancer cell lines was made up using serum free medium, this was 1:1000 for Panc-1 and 1:2000 for both Capan-1 and MiaPaCa-2. Cell tracker orange was used at 1:1000 for MRC-5.

After confluent T75 flasks of each of the cell lines was cultured and became 60-70% confluent, these were trypsinised (as above) and resuspended in 6 ml of medium to make a total volume of 8ml.

A 6-well plate was set up per cell line using the resuspended cells, aliquoting 1ml in each well and topped up with 4ml of complete DMEM. The plates were incubated in normal conditions overnight until 60 -70% confluent. The medium was removed from the 6-well plates for all cell lines and 1 ml of the ideal dilution of cell tracker green was added per well for the three pancreatic cancer cell lines and 1ml in each well of 1:1000 of cell tracker orange to the MRC-5 plate. The cell plates were incubated for one hr and then each well of green labelled cells of the pancreatic cancer cell lines was trypsinised with 0.5ml of trypsin,

reconstituted in 0.5ml of complete medium and 20µl of this was used for cell counting using the neubar chamber as per the manufacturer's instructions.

The cell counts deduced 152 cells/µl of Panc-1, 510cells/µl of Capan-1, 510 cells/µl, 557c/µl of MipaCa-2 and 57.5cells/µl for MRC-5. Therefore, to get a total of 750 cells per cell line $750/152 = 4.9$ µl of the reconstituted labelled Panc-1 cells was used, $750/510 = 1.47$ µl of Capan-1, $750/557 = 1.3$ µl of MiaPaCa-2 and $750/57.5 = 13$ µl of MRC-5.

Each of the pancreatic cancer cell line volumes was aliquoted with a volume of MRC-5 at the base of each well of 96-well ultra-low adherence plate, 40 µl of DMEM/methylcellulose solution was added to this and each well topped up with 160 µl of complete medium. Again, the outer two rows and columns were filled with medium only to ensure that there is not uneven evaporation of liquid from the peripheral rows and columns of cell filled wells.

In order to assess the development and formation of the heterotypic MCTS compared to their homotypic counterparts, a plate of homotypic MCTS was set up from each of the unlabelled pancreatic ductal adenocarcinoma (PDAC) and MRC5 cell lines at a seeding density of 1500 cells per well to mirror the heterotypic MCTS cell number.

This was done as above from confluent T75 flasks of each of the cell lines that were trypsinised, reconstituted with 3ml of medium to a total volume of 5ml, 20µl of which was used for cell counting and the rest of the reconstituted cells were made up to 13ml total volume and re incubated. After the cells were counted, the correct volume of each of the unlabelled cell lines was deduced that gave a total of 1500 cells/cell line. Each of the cell volumes was aliquoted into a well of a 96 well plate to which 40 µl of DMEM/methylcellulose solution was added and topped up with 200 µl of complete DMEM.

The spheroid plates were reviewed every 24 hrs using:

- Light microscopy for presence/absence of spheroid formation and their progression
- Fluorescence (Zeiss inverted) microscopy for assessment of presence or absence of fluorescence and whether there is a mixed cell progeny of both cell populations, the PDAC and MRC-5, present in the heterotypic MCTS; and
- EVOS microscope to image, measure and produce overlaid images of each spheroid for as long as they were viable.

MiaPaCa-2 multiplied very rapidly as a cell line but formed only loose aggregates and failed to form spheroids and therefore its use was discontinued beyond this point.

2.3. Adenoviral Infection

2.3.1. Ascertaining Viral Titres in 2D Monolayers

Ad5F35-EGFP was used to infect 911 cells with Ad5F35-CDC20 and Ad5F35-WT used to infect the PDAC cell lines.

Materials:

- 6-well culture plates (Thermoscientific #130184, LOT 12EA75G107)
- Ad5F35-EGFP
- Ad5F35-CDC20
- Ad5F35-WT
- DMEM
- Bovine foetal serum
- Sterile culture hood
- Gilson pipetes
- Trypsin
- PBS
- EVOS microscope
- Panc-1 cell line
- Capan-1 cell line
- DEChTERT cell line
- 911 cell line
- MRC-5 cell line

Methods:

Each of the cell lines; Panc-1, MiaPaCa-2, 911, Capan-1 and DEChTERT; was cultured as a monolayer in 6 well plates.

Confluent and established culture flasks of each of cell line was trypsinised with 2ml (see section) and then resuspended in 9ml of DMEM. Four x1ml of the cell suspension were aliquoted in 4 wells of a 6 well plate and topped up with 1 ml of DMEM then left to grow under standard culture conditions. 1 well was used as a negative control, i.e., no viral titre added, 1 well to trypsinised and perform a cell count and the remaining two were used to infect with two different Multiples of infection (MOI) of the chosen virus.

Once the Monolayers became confluent, one well from each cell line was trypsinised by removing the medium, washing with 1ml PBS and then adding 0.5ml trypsin. This was incubated for 10min. The trypsinised solution was resuspended in 1ml PBS and 20µl of this was used to do a cell count in order to calculate the viral concentration required for infection.

The neat concentration of the two viruses used were AD5F35-CDC20 5.5×10^8 viral particles (vp)/µl and Ad5F35-EGFP 4.4×10^9 vp/µl. Two multiplicities of infection (MOI), 100 vp/µl and 1000 vp/µl, of each virus were tested to ascertain the optimal MOI required for each of the cell lines.

To work out the volume of the neat virus required for each of the MOIs (x100) a cell count was done and viral volume calculated using the following formula:

$$MOI = \frac{\text{Plaque forming units (pfu) of virus used for infection}}{\text{Number cells}}$$

For the 100 vp/µl, 1µl of the neat virus was added to 9µl of serum free medium. One microlitre of this resultant solution was again added to 9µl of serum free medium to make for the 1000 vp/µl.

The medium was removed from all three remaining wells of each cell line and each monolayer was washed with 1ml PBS. One millilitre of serum free medium was added to each well and the pre-prepared viral titres was added to two of the wells. The remaining well had no virus added and was used as a negative control. Once the virus was added the plates were agitated slightly and then incubated for 30 min. They were then topped up with a further 2ml of serum free medium and incubated overnight.

In order to conclude which viral MOI was most effective for each of the cell lines, The cell lines transduced with Ad5F35-EFGP were initially imaged using the EVOS microscope and then fixed for flow cytometry in order to show which MOI gave better viral uptake and therefore signal.

2.3.2. *Flow Cytometry Assessment of Viral Uptake in 2D Monolayers*

Materials:

- Sterile culture hood
- Gilson pipetes
- PBS
- CO₂ humidified incubator
- Trypsin
- 15 ml sterile Falcon tubes
- Centrifuge
- 4% PFA
- Flowcytometer

Methods:

The medium was removed from each well and cells washed with 0.5ml of PBS. The PBS was then removed and 0.5ml of trypsin was added and plates incubated under standard conditions for 5 – 10min. Once detached, the cells were resuspended in 2ml of complete medium (DMEM) and transferred to 15 ml falcons, one per well. The falcons were then centrifuged at 1400rpm for 5min at 4°C. The supernatant was then discarded and pellet resuspended in 200µl of PBS and then recentrifuged under the same conditions. The supernatant was again discarded and pellet resuspended in 4% PFA in PBS and incubated for 10min at room temperature. The suspensions were recentrifuged under the same conditions, supernatant discarded and the pellet resuspended in 200µl of PBS. Each falcon was wrapped in foil and stored at 4°C until flowcytometry was performed.

Both EVOS images and flowcytometry data showed that 1000vp/µl of Ad5F35-EGFP gave better cellular uptake of the virus and therefore signal in all cell lines. This was therefore used for both viruses and all spheroids for infection.

2.3.3. Homotypic MCTS Transduction & Infection

Materials:

- Costar 96-well ultra-low adherence plates
- Panc-1 cell line
- Capan-1 cell line
- 911 cell line
- DEChTERT cell line
- Sterile culture hood
- CO₂ humidified incubator
- Trypsin
- Haemocytometer
- Light microscope
- PBS
- Ad5F35-CDC20
- Ad5F35EGFP
- Ad5F35-WT
- DMEM
- Foetal bovine serum
- EVOS microscope

Methods:

All four cell lines were set up in a 96-well ultra-low adherence plates at 1 row and 8 spheroids per cell line. The plates were set up as above (see section 2.2.2.1; 43) using sterile techniques and incubated in standard culture conditions.

Forty-eight hours after seeding, a representative spheroid from each cell line was trypsinised for cell counting. The medium from each of these was removed and spheroids were washed in 100µl of PBS. The PBS was removed and 100µl of Trypsin added and plates subsequently incubated for 35 min. Tightly bound spheroids did not disaggregate and for these the cell count was guesstimated using the 24 hrs monolayer cell count as a guide and doubled as the spheroid cell count was performed at 48 hrs.

Two spheroids per cell line were infected with Ad5F35-CDC20 and Ad5F35-WT except the 911 spheroids, which were infected with Ad5F35EGFP as a positive control. To run in parallel

as negative controls, two spheroids per cell line were left uninfected. For this, the medium from the representative spheroids was removed, spheroids washed with 100µl of PBS and 100µl of serum free medium added. After calculation, the viral aliquots were added to the wells, plate shaken a little and then incubated in standard conditions for 30min. The infected spheroid wells were then topped up with 100µl of serum free medium.

All spheroids were measured and imaged every 48 hrs using EVOS microscope and Z-stacks performed on all infected spheroids. Furthermore, one infected and one uninfected spheroid from each cell line was fixed and paraffin embedded every 48 hrs for immunohistochemical analysis.

2.3.4. Heterotypic MCTS Transduction & Infection

Materials:

- 96 ultra-low adherence plates
- PBS
- Gilson pipetes
- Sterile culture hood
- Trypsin
- Ad5F35-CDC20
- Ad5F35EGFP
- Ad5F35-WT
- DMEM
- Humidified CO2 incubator
- EVOS microscope

Methods:

Labelled heterotypic MCTS were generated using the green and orange cell tracker dyes (see section 3.2.3.1; 81). Each of the PDAC cell lines was labelled green and combined with DEChTERT labelled orange. 911 were set up as homotypic MCTS and left unlabelled to be used as a positive control. These were set up in 96 well ultra-low adherence plates at 1 row and 8 spheroids per cell line. The plates were set up under sterile techniques and incubated in standard culture conditions.

Forty-eight hours after seeding, a representative spheroid from each cell line was trypsinised for cell counting. The media from each of these was removed and spheroids were washed in 100µl of PBS. The PBS was removed and 100µl of Trypsin added and plates subsequently incubated for 35min. Tightly bound spheroids did not disaggregate and for these the cell count was guesstimated using the 24 hrs monolayer cell count as a guide and doubled as the spheroid cell count was performed at 48 hrs.

Two spheroids per PDAC/DEChTERT were infected with Ad5F35-CDC20 and two infected with Ad5F35-WT, with the exception of the 911 spheroids, which were infected with Ad5F35EGFP as a positive control. To run in parallel as negative controls, two spheroids of each heterotypic entity were left uninfected. For this, the medium from the representative spheroids was removed, spheroids washed with 100µl of PBS and 100µl of serum free

medium added. After calculation, the viral aliquots were added to the wells, plate shaken a little and then incubated in standard conditions for 30min. The infected spheroid wells were then topped up with 200µl of serum free medium and incubated in standard conditions.

All spheroids were measured and imaged every 48 hrs using EVOS microscope and Z-stacks performed on all infected spheroids. Furthermore, one infected and one uninfected spheroid from each cell line was fixed and paraffin embedded every 48 hrs for immunohistochemical analysis.

2.3.5. Flow Cytometry Assessment of Viral Uptake

Some of the spheroids infected were completely disaggregated by the virus and therefore could not be harvested for paraffin fixation and immunohistochemical staining. The residual cells were suspended in their medium, hexon stained and used for flow cytometry assessment of viral uptake as an alternative. For heterotypic MCTS, cancer cells were labelled green and normal cells left unlabelled. We performed hexon staining to look for viral uptake and used flowcytometry to evaluate whether there was increased hexon content in the green coloured (cancer) cells and hence proving Ad cancer cell specificity.

2.3.5.1. Hexon Staining

Materials:

- 2Hx2 Anti-Ad5 hexon mouse antibody, produced in house, 1:1000
- Alexa Fluor 488-goat anti-mouse IgG; Invitrogen; A11029; 1:500
- Serum-free DMEM
- 6-well plates
- Trypsin, Sigma
- Serum
- Centrifuge
- PBS
- Microcentrifuge tubes
- 15ml centrifuge tubes
- PFA
- Triton X-100 (Sigma)
- 10% Normal Goat Serum
- Isotype-matched control (Sigma M5409)

Methods:

Serum-free DMEM medium was removed from transduced or infected cells in a 6-well plate, the cells were washed with 1ml of PBS, 0.5ml of 1xTrypsin (Sigma,UK) was added and the cells were incubated at 37°C until the cells were round and detached. Two ml of DMEM medium containing serum was added to neutralise the trypsin. Cells were transferred to 15 ml centrifuge tubes and centrifuged for 5 minutes at 350xg at 4°C. The supernatant was removed and cells were resuspended in 200 µl of PBS and transferred to 1.5ml

microcentrifuge tubes. Cells were centrifuged at 350xg at 4°C for 5 mins. The supernatant was removed, cell pellets were resuspended in 200µl of 4% paraformaldehyde (PFA) and incubated for 10 mins at room temperature. Cells were centrifuged in the same conditions; supernatants were removed and cell pellets were resuspended in 200µl of 1% Triton X-100 in PBS and incubated for 5 mins. The cells were centrifuged, cell pellets were resuspended in 200µl of 10% Normal Goat Serum (NGS) in PBS and 100µl of resuspended cells was transferred to a new 1.5ml microcentrifuge tube. After 10 mins of incubation, cells were centrifuged and the pellets were resuspended in 50µl of 2Hx2 antibody (diluted 1:1000 in 1% NGS and 0.1% Triton X-100 in PBS); the second tube was resuspended in isotype-matched control (Sigma M5409 diluted 1:150 in 1%NGS and 0.1% Triton X-100 in PBS), and incubated for 1 hour. Cells were centrifuged and the pellets were resuspended in 50µl Alexa 488-labelled goat anti-mouse antibody (diluted 1:500 in 1%NGS and 0.1% Triton X-100 in PBS) and incubated for 30 mins at room temperature in the dark. After the incubation, cells were centrifuged and the pellets were resuspended in 500µl of PBS and stored at 4°C in the dark until analysis by flow cytometry.

2.3.5.2. Flow Cytometry

Materials:

- 15ml Falcon tubes
- Centrifuge
- Refrigerator
- Gilson pipetes
- PBS
- 4% PFA
- Flowcytometer

Methods:

Cells suspensions were transferred to 15 ml falcons, one per well. The falcons were then centrifuged at 1400rpm for 5min at 4°C. However, no pellet was formed and therefore the RPM was gradually increased until 10,000 and at this speed a small pellet was formed. The supernatant was then discarded and pellet resuspended in 200µl of PBS and then recentrifuged under the same conditions. The supernatant was again discarded and pellet resuspended in 4% PFA in PBS and incubated for 10min at room temperature. The suspensions were recentrifuged under the same conditions, supernatant discarded and

resuspended in 200µl of PBS. Each falcon was wrapped in foil and stored at 4°C until flowcytometry performed.

2.3.6. Spheroid Harvest & Fixation for IHC

Materials:

- 1% PBS
- tissue cassettes
- paraffin for embedding
- 4% PFA
- Pipette tips
- Eppendorfs
- Molten 1% agar
- Water bath at 55°C

Methods:

Representative infected spheroids were fixed and paraffin embedded for immunohistochemical analysis every 48 hrs to run in parallel with the EVOS imaging in order to provide 3D spatial distribution of viral uptake.

From these spheroids, the medium was removed and spheroids washed in 100µl PBS. With a cut pipette tip, each spheroid was carefully aspirated out of the wells and transferred into an Eppendorf containing 300µl 4% PFA and incubated at room temperature for 2hrs. The spheroids were then transferred to another Eppendorf containing 1ml of PBS and washed and then into another containing 300µl of molten 1% Agar and then transferred to a 55°C water bath for 30min to allow full impregnation. After cooling, the agar embedded spheroids were transferred to histopathology cassettes and sent to the processing laboratory for dehydration and alcohol processing. These were then blocked out in liquid paraffin set on cold block ready for microtome cutting.

3. Results

3.1. *The ex-vivo Tissue Slice Model*

3.1.1. *Tissue Morphology*

Unlike solid organs, such as the liver, which slice readily, it was not previously possible to use tissue slice technology for organotypic culture models of the human pancreas mainly because the tissue is too soft.

This problem was overcome in this study by embedding the pancreatic tissue in 3% low melting point agarose for support, hence allowing it to be processed using a slicer. With the aid of a tissue corer to make cylinders of pancreatic tissue, the Leica VT1000s vibrating microtome was used to produce uniform 250µm x 5mm circular sections. Initially the tissue corer was not available and instead the tissue was cut by hand into approximately equal cubes. This produced highly variable pancreatic slices in terms of size and integrity, as well as producing tissue fragments that were often not suitable for further experimentation. Before the use of the low melting point agar, normal agar was used but this was not found to support the tissue firmly. Other materials such as cork and felt were used but these also failed. Even with the use of low melting point agar, the fibrous nature of the pancreatic tissue often meant that as the blade cut into the cylinders and once it hit a fibrous strand it dragged the entire cylinder out of the agar block, and hence no more slices could be produced. This was overcome by experimenting with both the speed and frequency of the blade vibrations. It was found best to use the blade at maximum frequency of 10 Hz and a relatively low speed, 3.5 mm/s. As cancer tissue is often much firmer due to calcification, this was cut with much more ease.

The study of Wang *et. al*⁶⁹ suggested that supplementing the culture medium with amino acids and vitamins extended tissue survival and therefore this was included in the medium of the slices, which were then cultured in a sterile CO₂ incubator at 37°C.

To assess the quality, viability and preservation of ultrastructure over time of the cultured pancreatic slices, this was first done by histology. Slices from three normal pancreas specimens and two pancreatic adenocarcinomas were included. Tissue slices were removed after culturing for 24hrs, formalin-fixed and paraffin-embedded for H&E staining. All slices were scored for viability. Each slice was examined at a magnification of 100x with a normal light microscope. Areas of tissue were demarcated and assigned a viability grade of 0 to II

(see Materials & Methods, section 2.1.2.1; pg 27) and an overall percentage calculated for each grade. This was done in order to determine whether any of the variables added to the culturing system improved the viability of the pancreatic tissue. Normal pancreatic slices were cultured for 3 days with very good/excellent morphology (sections mostly scored a viability grade II) and with moderate morphology for 4 days (sections around 50% grade II) see figure 4. Slides were reviewed by an experienced pancreatic pathologist. (Dr CS Verbeke, Consultant Hisopathologist)

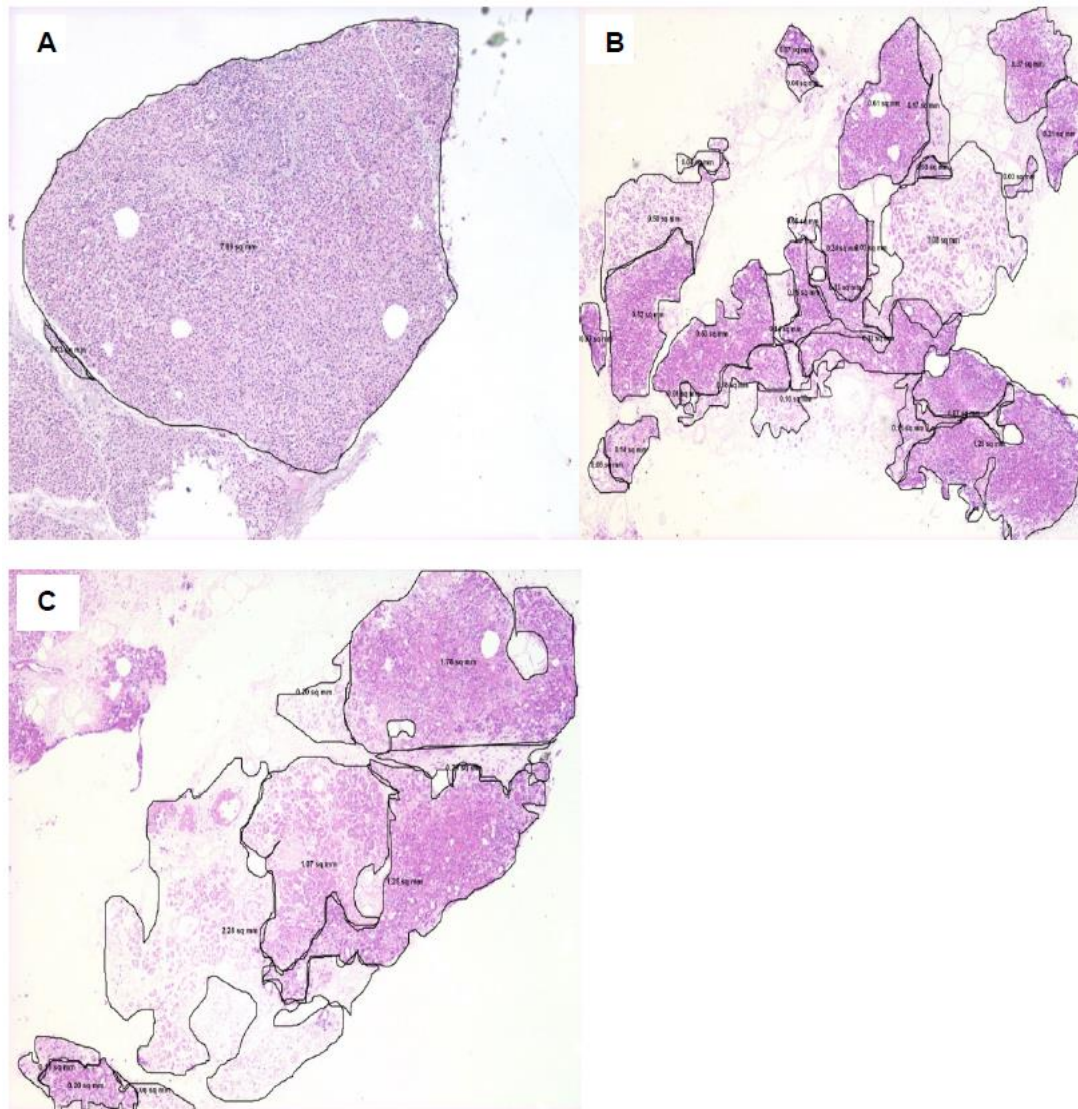


Figure 4 – Viability grading of tissue explants from normal pancreas

A: Day 0 from a normal pancreatic section, demonstrating 100% of the section at Grade II; B: Day 3 from a normal pancreatic section (with a coated 6-well plate without the shaking platform and 0.4µm transwell) demonstrating very good morphology with 86.8% at Grade II, 32.1% at Grade I and 3.1% Grade 0; C: Day 4 from a normal pancreatic section (with a uncoated 6-well plate with the shaking platform and 3.0µm transwell) demonstrating average morphology with 46% at Grade II, 18.1% at Grade I and 35.9% Grade 0.

In the case of pancreatic cancer however, the slices were preserved with excellent morphology throughout, i.e., 100% at grade II (see figure 5), after 48 hours in culture.

Unfortunately, due to tissue limitation, there was insufficient surplus tumour tissue from the Whipple's resections to allow the observation of the viability of these pancreatic adenocarcinoma slices for longer periods in culture.

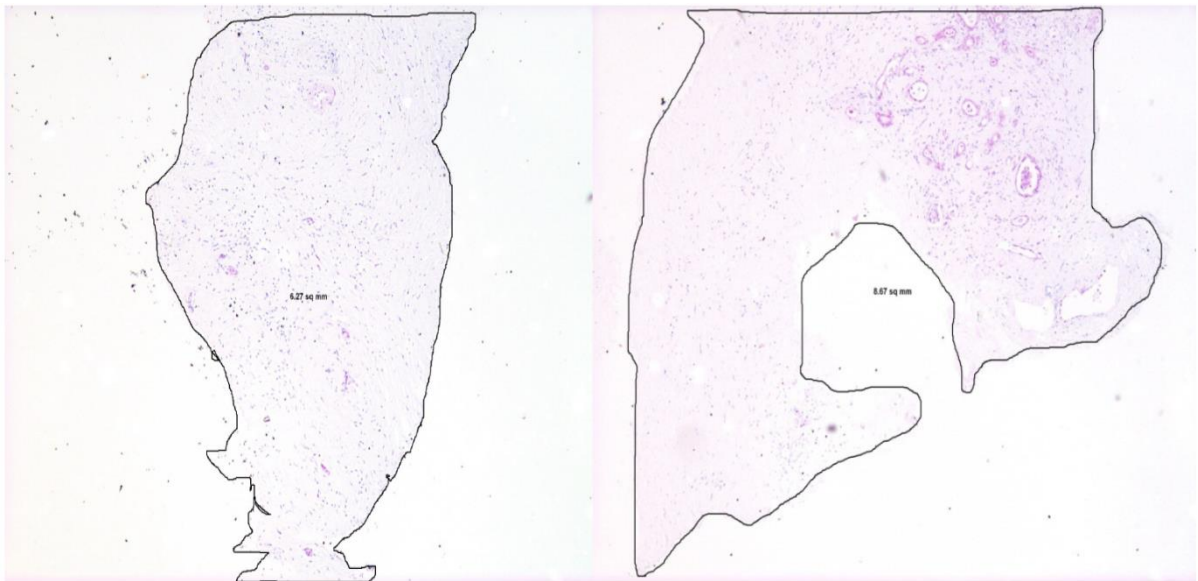


Figure 5 – Viability grading of tissue explants from pancreatic adenocarcinoma

A: Day 0 from a pancreatic cancer section, demonstrating 100% of the section at Grade II; B: Day 0 from a pancreatic cancer section, demonstrating 100% of the section at Grade II

One very interesting observation noted in all pancreatic cancer sections, is that very quickly after they were set up in culture, new tumour cells begin to grow and at quite a marked rate. This new growth occurred only at the very peripheries of the tissue slices (see figure 6).

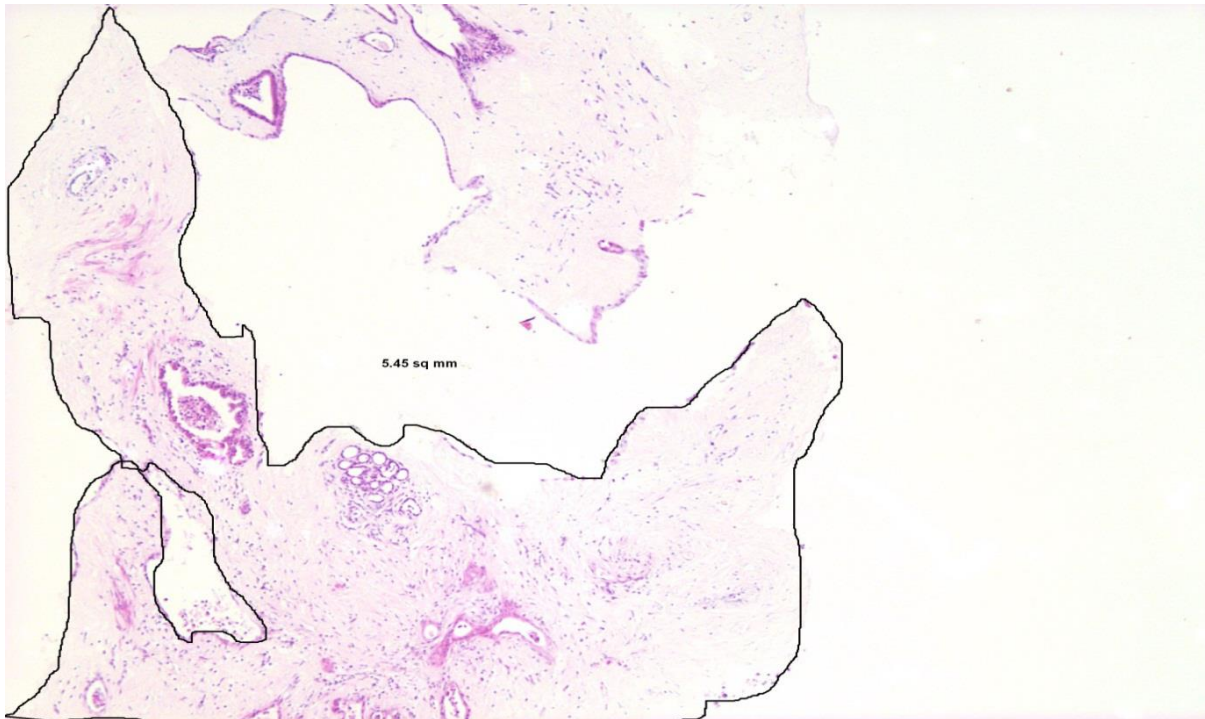


Figure 6 – Example of a Day 1 pancreatic cancer section

Day 1 of a pancreatic cancer section cultured in a 6-well plate, without a shaking platform and 0.4µm transwell. Note the “edge” effect.

This new growth of tumour cells was noted within 24 hours of culturing and was a consistent finding in all pancreatic cancer slices regardless of any variable added to the conditions (i.e., the shaker, transwells etc.).

Although the numbers are too low for statistical analysis, qualitative assessment of the H&E - stained sections showed that none of the variables added to the culture conditions, (i.e., the transwells, the shaking platform and the uncoated 6-well plates) made much difference to the viability of either normal or cancerous pancreatic tissue. This is consistent when looking at the amylase activity in the supernatants of the slices, in that there was no difference in activity between the various culturing conditions.

Unsurprisingly, keeping the time between resection and tissue culture as short as possible improved the viability of the slices. This was aided by keeping the freshly cut slices in a 37°C incubator until slicing was completed, rather than at room temperature until all tissue was sliced.

3.1.2. Tissue Functionality

3.1.2.1. Tissue Irradiation

This experiment was done with the aim of defining the effects of amylase activity in the supernatants of the pancreatic explants over time.

There was no data available in the literature to indicate the dose or length of irradiation required to kill the tissue slices. Using the maximal output of the irradiator (1.84Gy/min), six individual tissue slices in their culture media were irradiated in increments of 10 minutes. The slices were then immediately fixed and paraffin-embedded for H&E staining. The supernatant from each slice was collected and its amylase activity measured, as shown in figure 7 below.

Superficially, this did not reveal a clear pattern of amylase activity in relation to increased cell death. There seemed to be dramatic peaks and troughs of amylase activity, hence not answering the question of whether the amylase activity increases or decreases as more pancreatic cells die.

However, on assessing the H&E sections of the slices, it was clear that the tissue was completely devitalised and hence cells were 100% necrotic after the first 10 minutes of irradiation. However, there was minimal tissue, and hence few acini on the H&E section of the concurrent slice. This seemed to correspond to the first trough in the amylase activity graph.

After 20mns of irradiation, the H&E stain revealed that all cells are dead but remain intact. The amylase activity in the supernatant peaks at this point despite maintenance of structural integrity of the cells. Morphologically however it is not possible to ascertain how truly intact the cells are and whether they may indeed have leaky membranes, hence explaining the peak in amylase activity.

Morphological examination of the tissue section exposed to 40mns of irradiation shows loss of structural integrity and this may account for a burst in amylase release into the surrounding supernatant as cells lyse, and hence accounting for the peak in the amylase activity shown in figure 7. There is a further increase in amylase activity after 50mns of irradiation. The H&E section of this tissue slice, although does not show any further cellular lysis, does reveal more tissue surface area and hence more amylase secreting acini.

After 60mns of irradiation there is another dip in amylase activity in the supernatant of the slice, and morphologically there was a mixture of both dead intact and dead lysed cells.

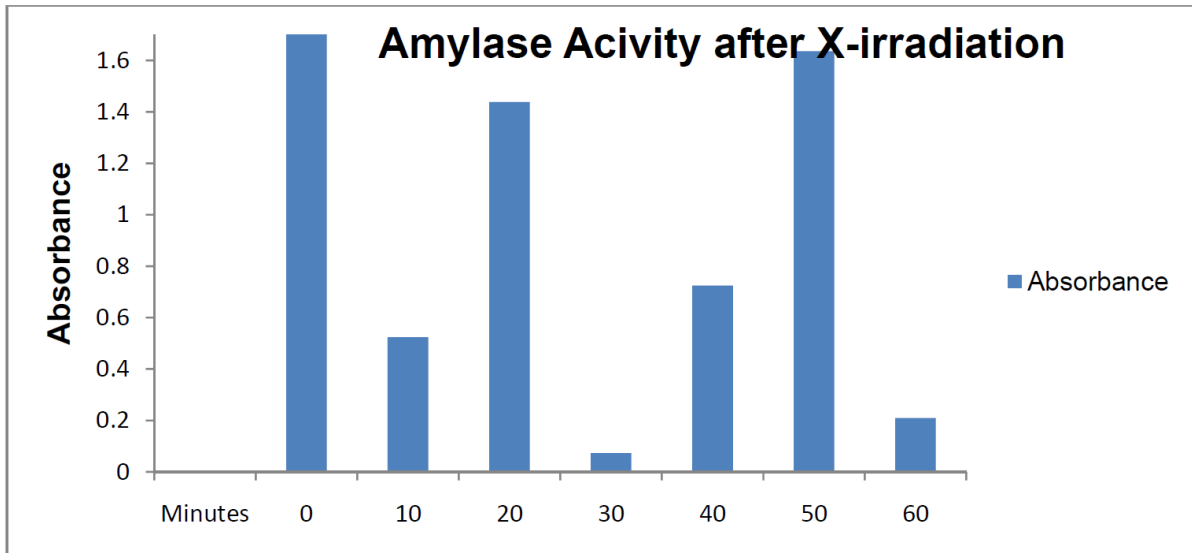


Figure 7 – Amylase activity in the medium of normal pancreatic explants after x-irradiation

Bar graph displaying light absorbance in nm, proportional to amylase concentration in the medium (y-axis), vs number of minutes of irradiation of normal pancreatic explants (x-axis). This displays peaks and troughs that don't demonstrate a direct relationship except to the amount of tissue on the corresponding H&E-stained sections; fewer acini, less amylase in the medium.

Looking at the amylase activity in the supernatants of the irradiated slices alongside their corresponding H&E stain, there is no direct explanation for the peaks and troughs in amylase activity based on cellular morphology. All slides showed dead tissue, which were largely structurally intact. This therefore does not allow a conclusion to be drawn on the cell membrane as a barrier; i.e., despite the presence of intact necrotic cells, the cellular membranes may become leaky and hence release amylase into the surrounding culture medium.

3.1.2.2. Amylase Standard Curve

Using purified α -amylase as a standard, amylase enzyme activity was assayed in order to assess the stability of the enzyme when stored at 4°C over four consecutive days and to observe whether there was a freeze-thaw effect on enzyme activity. The results show that there was significantly reduced enzyme activity at 4°C with every consecutive 24 hours of storage, with the greatest loss occurring in the first 24 hours (figure 8).

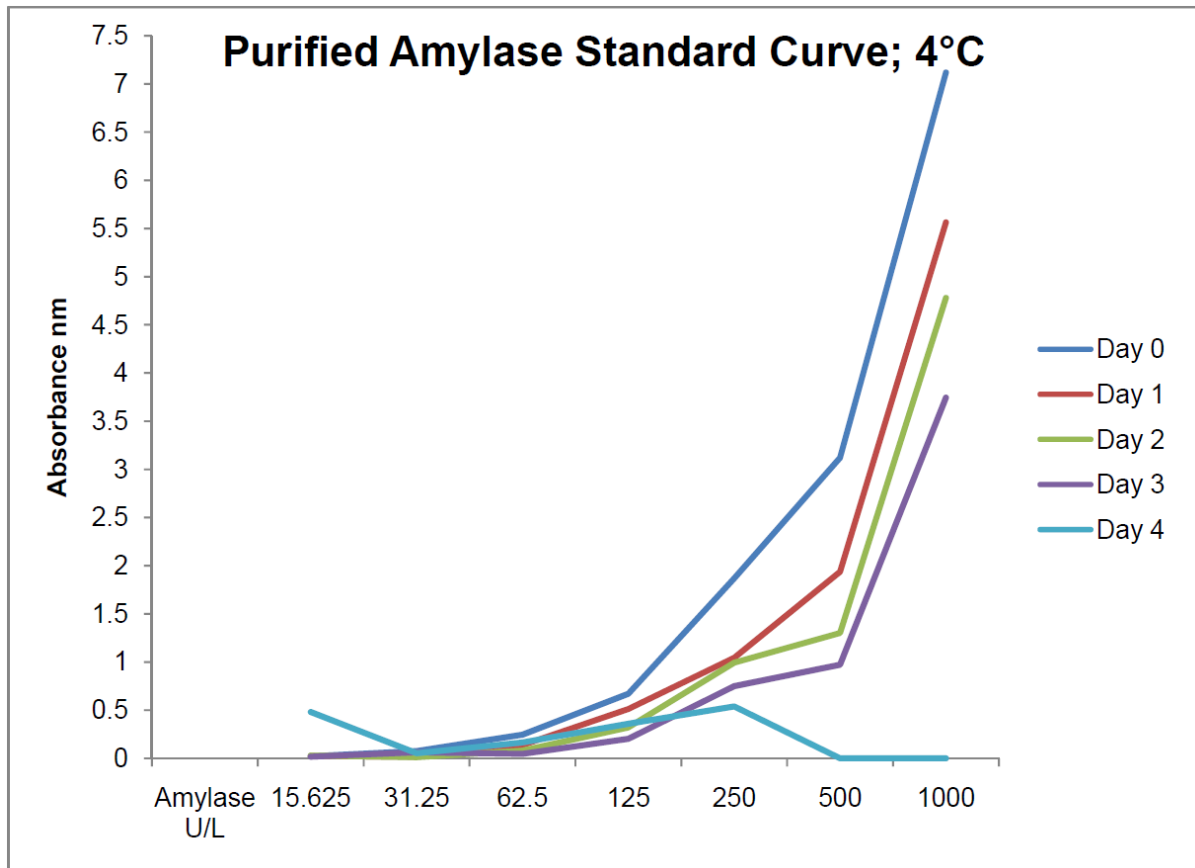


Figure 8 – Standard curves of purified α -amylase activity on storage at 4°C over four consecutive days

Graphical representation of α -amylase concentration in U/L (x-axis log₁₀ scale) upon storage at 4°C vs absorbance in nm (y-axis) (read at 620nm) from the medium of pancreatic explants over a 4-day period. This was performed to deduce i) the ideal storage conditions for α -amylase, ii) assess if there was enzyme degradation and hence loss of activity over time and iii) deduce whether there was freeze-thaw affect when they were comparatively stored at -80°C (figure 9 below). This demonstrates a loss of enzyme concentration over the 4-day period.

On storage at -80°C there was a minimal freeze-thaw effect on enzyme activity, with the absorbance curve being very similar to that after 24 hours at 4°C (see figure 8). However, although there was some loss of enzyme activity after freezing and thawing, because the standard curve follows a very similar pattern to that on day zero of testing, this method of

storage was considered to be adequate as absolute amylase activities are not necessarily relevant, but the pattern of loss is.

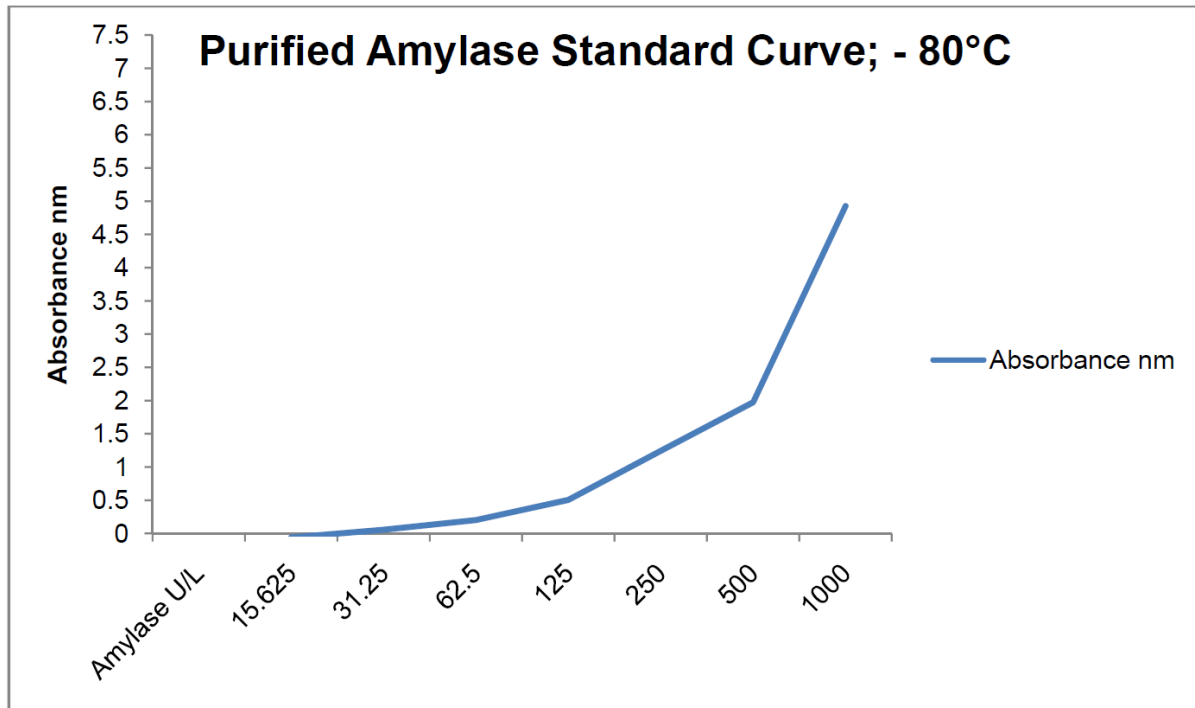


Figure 9 – Standard curve of purified α -amylase activity on storage at -80°C

Comparative assessment to ascertain whether there was a freeze-thaw effect after supernatant storage at -80°C showing minimum loss at -80°C compared to 4°C (see figure 8 above). Again, α -amylase concentration in U/L (x-axis log₁₀ scale) vs absorbance in nm (y-axis) (read at 620nm).

The standard curves produced following both storage conditions, i.e., 4°C and -80°C followed a very similar line and hence a similar pattern of enzyme loss. However, both of these were very different from the manufacturer's own. The manufacturer's standard curve (also produced using human α -amylase) demonstrated a perfectly linear relationship between amylase activity and absorbance (see Appendices for an example of manufacturer's standard curve). This was vastly different from all the standard curves produced in this study; across a range of amylase concentrations, with or without storage and using different storage conditions.

These results therefore indicate that: i) at 4°C there is gradual loss of amylase activity with every 24 hours of storage, ii) storage at -80°C causes minimal enzyme loss and hence a safe way of storing the amylase-containing supernatants from pancreatic explants (figure 8) and iii) unlike the manufacturer's standard curve, the relationship between enzyme activity and absorbance is not a linear relationship and hence the manufacturer's data is not reliable for the purposes of this study.

3.1.2.3. Amylase Assay

In normal pancreas, the amylase activity seemed to decline with every 24 hours of culture. The amylase activity was very high after the first 24 hours of culture and very low after 72 hours. This was true regardless of the differing culture conditions to which pancreatic explants from the same specimen were exposed to (see figure 10 below). Although the numbers are too low for statistical analysis, the figures below indicate that for normal pancreatic tissue, none of the variables added to the culture conditions made a significant difference to the amylase activity in the supernatants. This was also true when looking at the concurrent H&E stains for each specimen (figure 1).

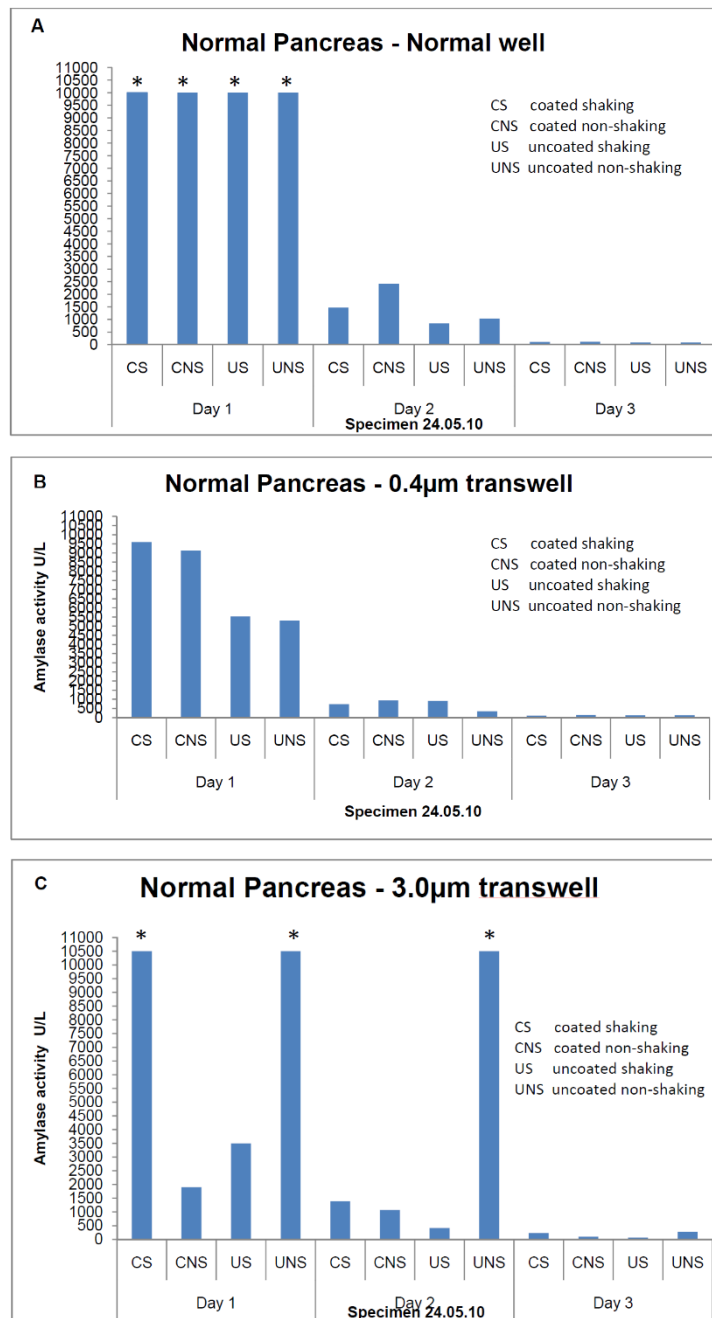


Figure 10 - Pattern of amylase activity of normal pancreas explants over 3 days in culture

These figures demonstrate that for normal pancreas, there is a general decline in amylase activity with increased time in culture. This is true regardless of variables added to the culturing system including uncoated well plates and the use of 0.4µm (B) and 3.0µm (C) transwells. Note after the first 24hrs in culture in A, the amylase activity was very high, higher than the recommended reliable cut-off for the spectrophotometer (readings >1.5) despite attempts at x5 and x10 dilutions. This is true for all bars with "*" above them. Further dilutions were advised against by the manufacturer.

In contrast to normal pancreatic tissue, the amylase activity in the supernatants of the pancreatic cancer slices was minimal, and barely above zero. This did not decrease with increasing time in culture. This was true of all cancer specimens analysed. An example of this is demonstrated in the graphs below (figure 11). When the H&E - stained sections

relating to these supernatants were examined, the tissue slices were entirely composed of tumour cells, with a total absence of normal pancreatic cells.

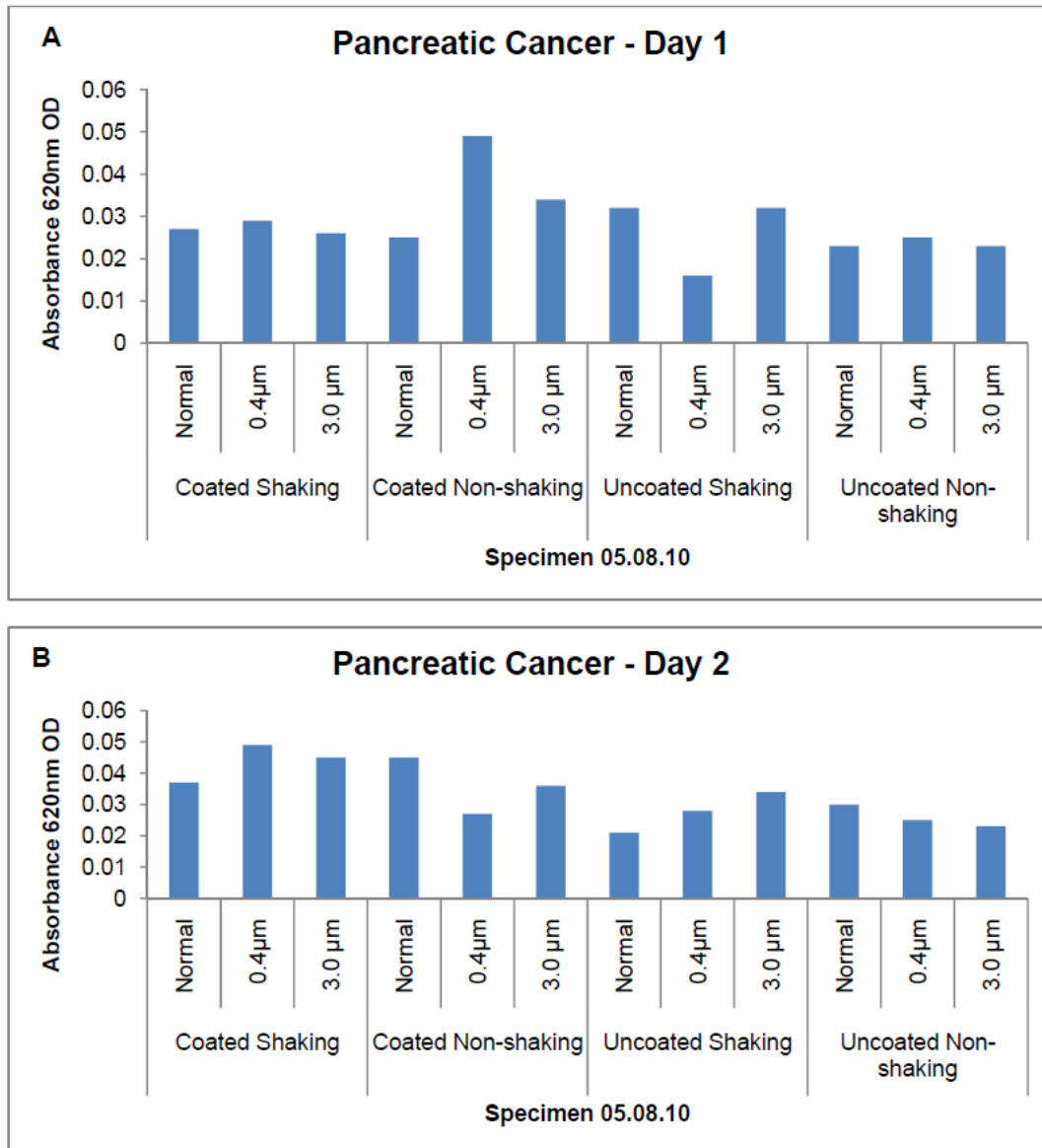


Figure 11 – Pattern of amylase activity of pancreatic adenocarcinoma tissue explants over two days in culture

As the tissue slices represented in this figure were 100% tumour tissue, there was an absence of normal acini and hence amylase secretion. The y-axis in these graphs is the spectrophotometer absorbance reading as oppose to amylase activity as represented in those for normal tissue. This is because the absorbance readings were so low that the values were lower than the minimum equivalent value for amylase activity in the conversion table provided by the manufacturer.

3.1.3. **Tissue Viability**

After optimising the assay, a series of both normal and cancerous slides were TUNEL stained for apoptotic bodies, using salivary gland sections as a positive control. The TACS-XL blue label generates an intense blue staining in cells with DNA fragmentation, easily visualised against a pale red counterstain. Apoptotic bodies were recognised from positively stained extracellular debris by being:

- small
- greeny/blue
- extracellular, and
- well-defined

A high level of specificity for the staining of apoptotic bodies in both normal and cancerous pancreatic tissue was achieved. The salivary gland controls were highly positive for apoptosis, without false negatives.

The level of staining, i.e., number of apoptotic bodies, did not differ between normal and cancerous tissue (figure 12), nor was there increased apoptosis with every successive 24-hour time point (figure 13).

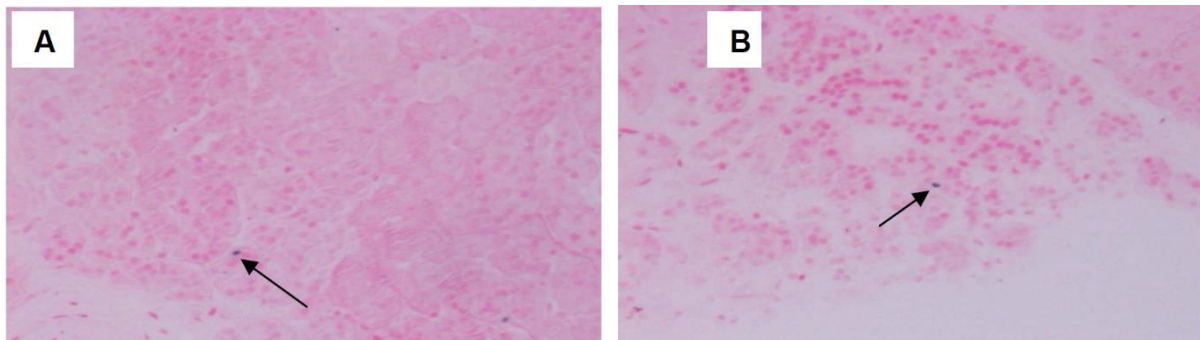


Figure 12 – Apoptotic body staining of normal and pancreatic cancer after 24hrs in culture using TUNEL

A: Normal pancreas; B: Pancreatic adenocarcinoma. TUNEL staining showed little death by apoptosis in both normal and cancerous tissue.

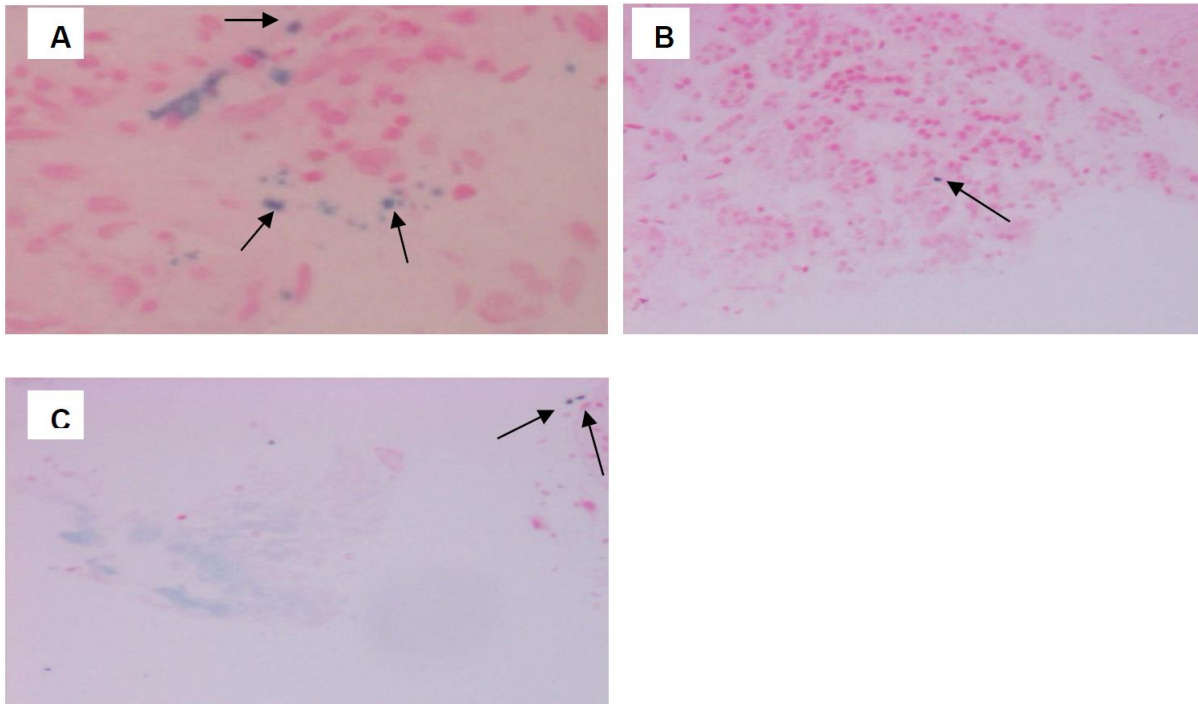


Figure 13 – Apoptotic body staining in pancreatic adenocarcinoma after 1, 2 and 3 days in culture

A: apoptosis, day 1; B: apoptosis, day 2; C: apoptosis day 3. These stains show that in pancreatic adenocarcinoma there was little death by apoptosis with increasing time in culture.

On comparing each TUNEL-stained slide with its corresponding H&E stain, it was apparent that the overall level of apoptosis in the pancreatic tissue was low. This did not correlate with the degree of tissue viability. The pattern of cell death in the pancreatic tissue was more consistent with necrosis than apoptosis.

Because of this, and in order to minimise wasting time on a lengthy procedure and the use of costly materials, all H&E slides from all cases were studied for number of apoptotic bodies and those with a high level of apoptosis would then be TUNEL stained.

However, the finding that cell death in pancreatic tissue was predominantly by necrosis and minimally by apoptosis was consistent throughout. This was true for all of the following:

- both cancerous and normal pancreatic tissue
- regardless of culture conditions
- not related to number of days in culture, i.e., apoptosis did not increase as time progresses but necrosis does

3.2. Multicellular Tumour Spheroids

3.2.1. Optimisation of spheroid generation

Multiple pilot studies were performed in order to optimise the culture conditions for MCTS formation.

Initially TC32, a Ewing's sarcoma cell line, was cultured and used with an established protocol for their spheroid formation from a partner laboratory. This was because it was known that TC32 cells readily formed spheroids (doi:10.4049). TC32 cells were seeded in increments of 1000 cells/well up to 10,000/well in order to establish the optimal number of cells for spheroid formation and to observe the behaviour of spheroids over time at different seeding densities. Each seeding density was repeated in triplicate.

The TC32 plate was reviewed every 24 hrs using light microscopy. TC32 is a rapidly growing cell line which readily formed compact, regular and spheroidal-shaped spheroids within 24 hrs even at the lowest seeding density without the need for DMEM/methylcellulose solution (a crowding agent that aids cell clustering). The size of the spheroids increased as the seeding density increased. At greater than 1000 cells/well, the spheroids had a diameter > 500µm after 24 hrs and given there is substantial evidence to show that a hypoxic core begins to develop at a diameter of 200-300µm and necrosis at 500 µm^{22,70,71}, seeding densities above 1000 cells/well would not allow for many days of experimentation. One of the ultimate goals of this study is to grow viable spheroids imitating the cancer milieu and assess the oncolytic efficacy of adenovirus 5-based viruses. Furthermore, at a seeding density of ≥5000 cells/well, the spheroids were so large after 24 hrs that a large necrotic centre had already developed and cells had begun to slough off and outgrow the size of the well.

A similar process was performed to ascertain the ideal seeding density for each of the other cell lines used; namely Panc-1, Capan-1, MiaPaCa2, DEChTERT, MRC5 and 911. In the TC32 pilot study, it was found that a seeding density of 1000 cells/well was enough to form spheroids within 24 hrs and this was the initial established seeding density for all cell lines. However, keeping all other variables constant, PDAC (pancreatic ductal adenocarcinoma) cell lines, DEChTERT and MRC5 cells did not form spheroids. Therefore, a trial was done for each of these cell lines to establish their individual optimal seeding density, starting at 1000cells/well and going up in increments of 500 to a maximum of 10,000 cells/well. The ideal seeding density was found to be 1500cells/well for all cell lines. Fewer cells took too long to form sizeable spheroids and more than 1500cells/well-formed large spheroids(>500µm)/loose aggregates quickly. Furthermore, the size of the spheroids and

their hypoxic cores remained small at 1500 cells for all cell lines after 24 hrs allowing a seven-day period of experimentation.

Homotypic (containing one cell type) and heterotypic (containing more than one cell type) MCTS plates were set up with the experimentally deduced optimal seeding density for each of the cell lines; 1500 per cell line for the homotypic MCTS and 1500 of each cell line at a 50:50 ratio of PDAC:Normal cells for the heterotypic MCTS. Each well included DMEM/methylcellulose in the base, followed by the cell aliquots and topped up with 200µl of supplemented DMEM. After 72 hrs, neither plate showed formation of spheroids, at best some had formed loose aggregates despite previous successful formation of spheroids with all cell lines. In order to ascertain the ideal conditions for spheroid formation, Panc-1 and 911 cell lines were used to further optimize the culture conditions of spheroids. Several factors were tested that were thought could contribute to successful spheroid formation.

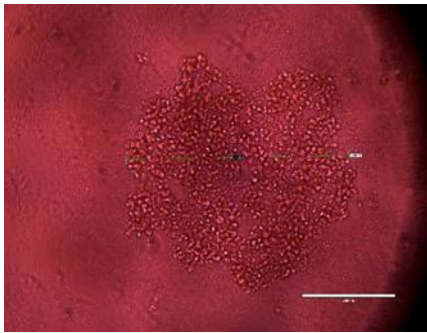
These factors included:

1. Presence or absence of DMEM/Methylcellulose solution
2. DMEM/Methylcellulose solution was prepared as a large volume stock solution, frozen in aliquots and thawed for every use. The thawing process may have affected the structural integrity of the solution and therefore a fresh solution of DMEM/Methylcellulose was prepared and tested vs the thawed solution.
3. The addition of cell aliquots first in the wells followed by the DMEM/Methylcellulose solution or vice versa.
4. Once cells were trypsinised, it was ensured that the cells were adequately resuspended in medium and therefore there was an accurate full cell count before dispensing into culture plates.
5. The optimal cell number per homotypic MCTS for each cell line, although previously experimentally deduced to be 1500, was increased to 2500 and tested vs 1500 cells/well.
6. To ascertain the ideal seeding density for each of the PDAC, 911, DEChTERT and MRC5 cell lines.

Using light microscopy, it was found that the addition of DMEM/methylcellulose solution and its addition prior to the aliquot of cells resulted in better cell aggregation and the formation of tighter spheroids in a shorter time period. This was in comparison to its absence or its addition after the aliquot of cells. This was particularly true for the PDAC cell lines which did not form spheroids as readily as the normal cells. The absence of DMEM/Methylcellulose yielded looser aggregates as opposed to compactly formed spheroids that also took longer to form.

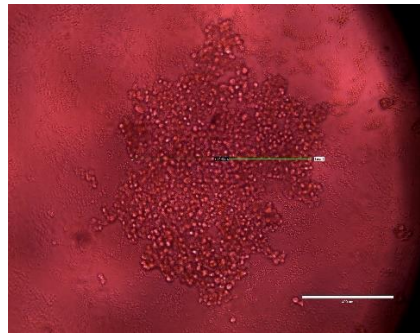
The Panc-1 spheroid trial plate was imaged 48 hrs after set up and two sample images were taken of each variable:

A1



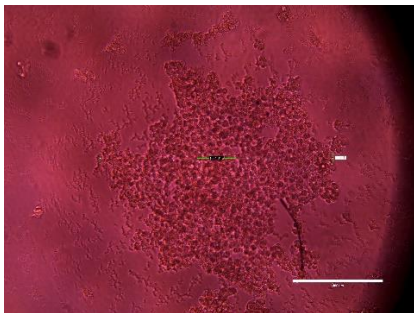
954 μm

A2



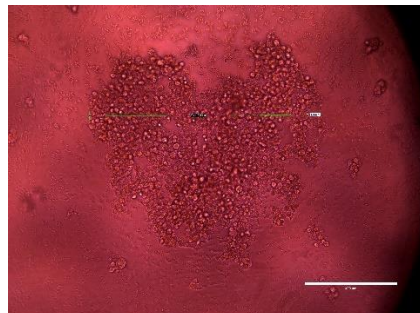
782 μm

B1



1032 μm

B2



941 μm

Figure 14 – Sample images from the Panc-1 trial plate to optimize spheroid culture conditions. Bar represents 1000 μm

Sixteen wells of Panc-1 cells were seeded at 2500 cells/well; 8 with DMEM/Methylcellulose prior to the cells and in the other 8 wells, the cells were aliquoted first. Set A are imaged spheroids with DMEM/Methylcellulose solution added first followed by the Panc-1 cells. Set B are images of spheroids with the cells aliquoted prior to DMEM/Methylcellulose. Set A show tighter spheroids with fewer sloughed cells from the periphery.

Once cells were confluent in the culture flasks and ready to be used for spheroid formation, they were trypsinised, counted and cell aliquots were made in Eppendorfs ready for dispensing into each well. This was performed as the first step each time a spheroid plate was set up. When spheroids failed to form, it was hypothesised that the cells in the suspensions settled to the base of the Eppendorfs and the supernatant was mainly medium that contained much fewer cells than those counted resulting in very low cell counts per well. The low cell count may have resulted in minimal cell-cell contact, lack of crowding and therefore aggregation for adequate spheroid formation. By resuspending the cells adequately in their medium using a Gilson pipette immediately before plating out, it was ensured that the full cell count was added to each well.

Initially after deducing the ideal cell density for each cell line and using the freshly made DMEM/Methylcellulose solution at the base of each well, tightly formed spheroids were

formed for each of the cell lines however this could not be duplicated despite trying to adjust other experimental factors. DMEM/Methylcellulose was made as a large batch stock solution, frozen and thawed every time a plate of spheroids was set up. Given that all other factors were kept constant, it was hypothesised that the repeated thawing process of the DMEM/Methylcellulose solution may have affected its structural integrity and therefore its crowding function/ability. A fresh batch was therefore made and spheroid plates of each cell line in duplicates was set up in order to compare thawed DMEM/Methylcellulose to that freshly made. Indeed after 24 hrs spheroids were beginning to form from all cell lines in the plate with freshly made DMEM/Methylcellulose and only loose aggregates in the plate with the frozen then thawed DMEM/Methylcellulose. From 48 hours onwards no spheroids were formed in the thawed DMEM/Methylcellulose plate but those with the freshly made DMEM/Methylcellulose continued to get more compact and larger for at least the first 72hrs. Therefore, fresh DMEM/Methylcellulose was made, filter sterilised and divided into 20ml aliquots in sterile Falcon tubes, each aliquot only being used for a day's experimentation and any remaining discarded. The rest was frozen and each Falcon only thawed and used once. This seemed to yield better spheroids every time.

After all of the aforementioned factors were optimised, the ideal seeding density for each cell line was again reassessed with increments of 500 cells/well starting at 500 cells/well. Although 911, DEChTERT and MRC5 formed compact spheroids of approximately 300µm in diameter within 24 hrs at 1000 cells/well, this was not the case for the PDAC. After the process was repeated and all other factors optimised, 1500 cells/well was again found to be the optimal density for the PDAC. For the sake of consistency and comparability, 1500 cells/well was therefore used for all homotypic and heterotypic MCTS; the latter being made of 750 of each cell line to a total of 1500 cells/well. Although 911 and the fibroblast cell lines formed good spheroids at 1000 cells/well, using 1500 cells/well, the formed spheroids were not too large after 24 hrs for 911, MRC5 or DEChTERT.

3.2.2. Homotypic MCTS

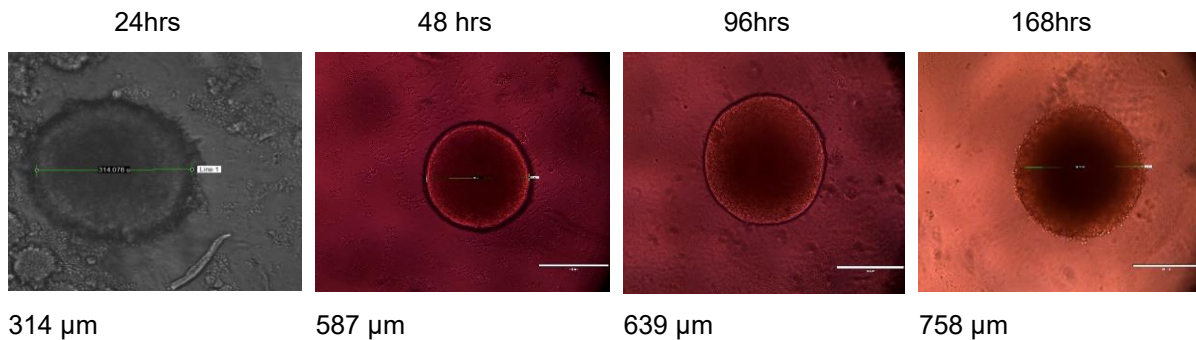
After the optimization process was complete, it was deduced that the optimal seeding density for all cell lines was 1500 cells/well. Fewer cells/well resulted in loose aggregates that took too long to transform into discernible spheroids; while at greater than 1500 cells/well, the spheroids that formed were greater than 1mm after just 24 hrs. It is well documented in the literature that in spheroids with a diameter $\geq 200\text{-}300\ \mu\text{m}$, a hypoxic core begins to form and at $500\ \mu\text{m}$ the spheroid core become necrotic^{22,70}. It was hoped to achieve a seeding density that would produce spheroids of $<500\ \mu\text{m}$ after 24 hrs to allow as many days of experimentation and behavioural observation as possible. However, despite repeated optimization trials this was not achieved nor could it be standardized across all cell lines. After a multitude of seeding densities were trailed for 7 consecutive days, 1500 cells/well was considered to be the most optimal density to form a tightly bound spheroid within 24-48 hrs. Although most spheroids that formed at this density were in the $300\text{--}800\ \mu\text{m}$ range after 24 hrs, a discernible hypoxic core was not seen until day 2-4. Light and EVOS microscopy were used to image the spheroids which only gave a 2D perspective of the structure. As the spheroids grew, a very discernible dark core developed which grew as the spheroid grew in size and time lapsed. This was presumed the hypoxic/necrotic centre and was visually very different to the obviously healthy viable peripheral cells.

Below is a pictorial comparison of the homotypic MCTS formed by all of the cell lines, PDAC and normal, cataloguing how these grew, developed and indeed demised during a 7-day period.

911 cells formed the most compact spheroids that were the most “spheroidal” and regular in shape, formed readily discernible spheroids after 24 hrs and started the smallest after 24 hrs in culture. During the optimization process, in the vast majority of time, 911 cells formed a single spheroid per well (Figure 15, Series A). However, an observation only made with the 911 cell line was at some point during the optimization process they began to form several smaller spheroids per well as shown below in (Figure 15, Series B). It is difficult to deduce which growing conditions favoured the formation of one spheroid over several, however the most likely explanation is again the structural integrity of the crowding agent DMEM/methylcellulose. However, the several smaller spheroids that appeared to behave in the same way as the single large ones; started small after 24 hrs, are overall slower growing compared to the PDAC and developed a hypoxic/necrotic core at the same critical size.

911 MCTS

Series A



Series B

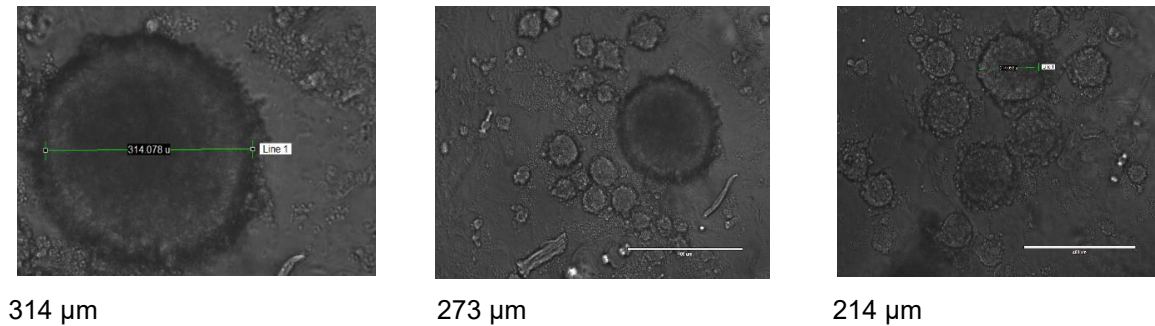


Figure 15 – 911 Homotypic MCTS. Bar represents 1000 μm

Photomicrographs of 911 homotypic MCTS cataloguing their growth kinetic over a 7-day period. 911 MCTS either formed as, for the majority of the time, one spheroid per well (series A) or multiple spheroids per well (series B). It is not known why this change happened but may be due to a change in the crowding agent (DMEM/methylcellulose) or a phenotypic drift of 911 cell line after multiple passages. Series A also demonstrates the formation of the spheroid “capsule” and its demise over the 7-day period as the necrotic core became larger.

All spheroids, derived from normal or cancer cells, formed what appeared to be a peripheral capsule which became less conspicuous and began to disintegrate as the spheroids became larger. This was particularly evident at day 7, when the capsule appeared thinner, had clumps of loose cells forming its edge and disaggregated cells were seen in the well surrounding the periphery of the spheroids. These were true of spheroids generated from all cell lines.

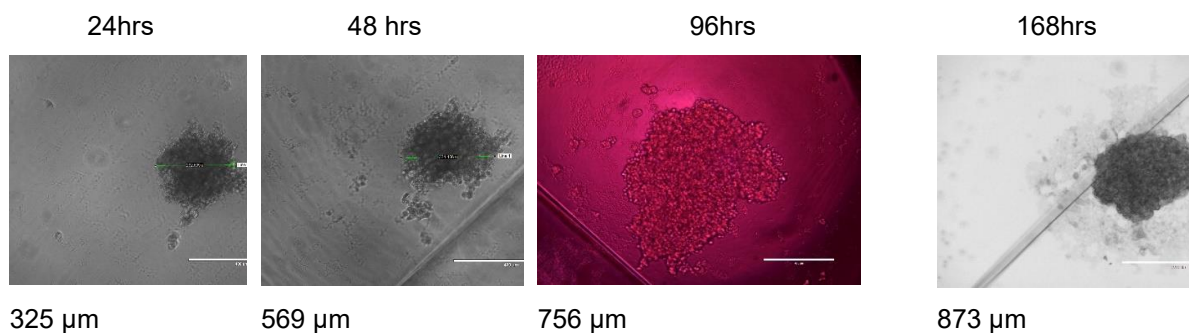
All spheroids became larger in size until day 4, although spheroids derived from normal cell lines were larger still until day 7. The rate of growth between day 4 and day 7 was minimal. PDAC spheroids were all objectively smaller in size by day 7 which coincided with the thinning of the capsule and the observation of disaggregated cells in the well surrounding the periphery of the spheroid.

The PDAC MCTS were much larger after 24 hrs compared to the normal cells. The fastest rate of growth was observed between 24 and 48 hrs (this was true of both cell types) but was greater in the PDAC compared to spheroids from normal cell origin. With the exception of MiaPaCa-2 which is a very rapidly growing cell line that formed significantly larger spheroids after 24 hrs compared to all others, very little growth was observed between day 2 and 4.

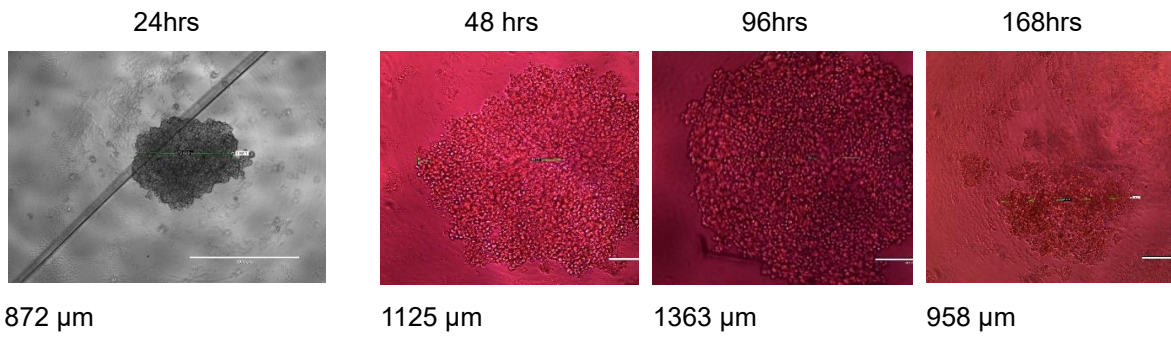
Overall, the PDAC spheroids were morphologically less spheroidal in shape and were much more irregular in appearance compared to normal cell spheroids. This is concordant with the characteristics of cancer cell growth and the irregularity of the size and shape of their cells. Capan-1 formed cohesive spheroids consisting of smaller aggregates with very clear margins. Panc-1 spheroids were larger and with a more irregular outer surface. MiPaCa-2 is a very rapidly growing cell line, that formed very large very irregular sheet like structures within 24 hrs that had less definable outer borders that were very friable and disaggregated on harvesting. It is difficult to ascertain whether the sheet like structures formed by MiPaCa-2 were spheroidal in shape as a 3D perspective could not be captured.

Although hypoxic cores were observed across all spheroids, these were much more conspicuous in spheroids derived from cancer cells and appeared larger with every 24h of growth. This appears to be consistent with the ability of cancer cells to alter their metabolism in severe hypoxic conditions.

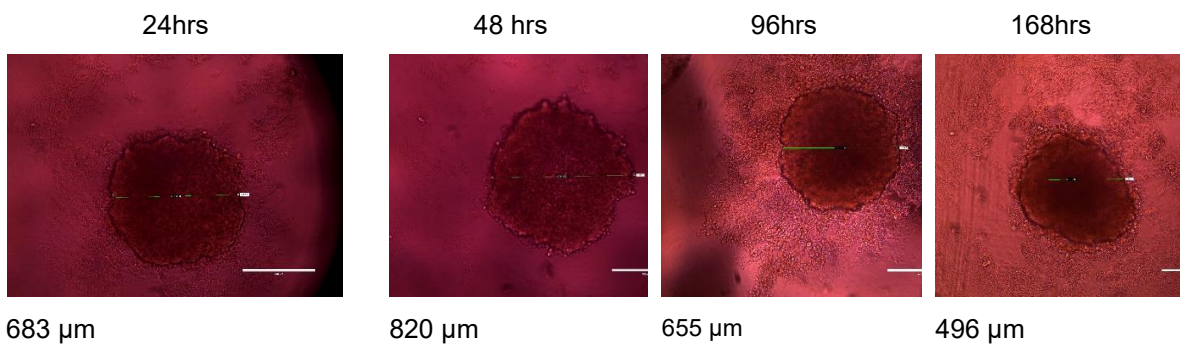
MRC5



Panc-1



Capan-1



MiaPaCa-2

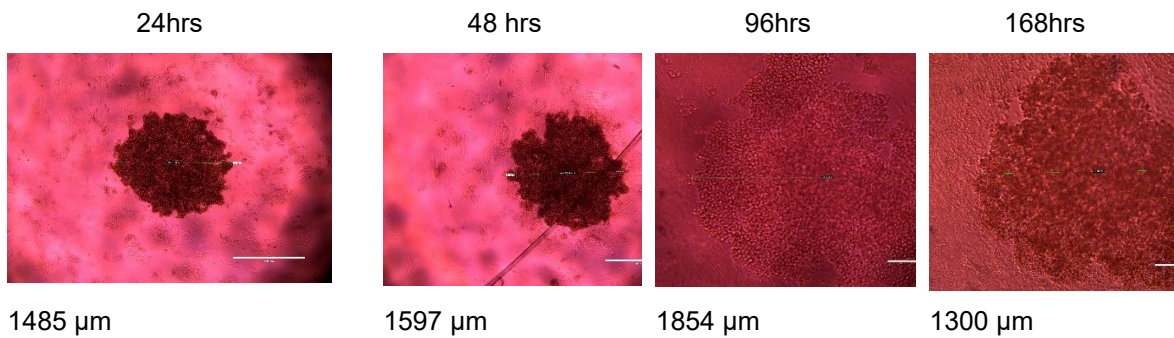


Figure 16 – Homotypic MCTS. Bar represents 1000 μm

7-day catalogue of the growth kinetic of homotypic MCTS of the fibroblast cell line MRC5 and each of the PDAC cell lines demonstrating a growth kinetic that related to the degree of differentiation of the latter. Compact spheroidal spheroids with discernible capsule were formed by the least aggressive most well differentiated Capan-1, tight aggregates by the intermediately differentiated Panc-1 and looser much larger sheet-like aggregates but the most aggressive and most poorly differentiated MiaPaCa-2.

3.2.3. Heterotypic Multicellular Tumour Spheroids

In order to differentiate between normal and cancerous cells in the heterotypic MCTS, cell tracker dyes were used to label the different cell types.

3.2.3.1. Optimizing cell tracker dye labelling in monolayers

It was aimed to use fluorescent cell tracker dyes to label cell types in heterotypic MCTS. Fluorescent cell tracker Orange, Green and Violet (kindly donated by Professor GP Cook, Leeds Institute for Medical Research) were assessed in monolayers of each of the PDAC and normal cell lines to see which dye generated the best signal for each cell line.

The dilutions of the cell tracker dyes for each of the PDAC as well as MRC-5 and DEChTERT were elucidated from monolayer cultures of each cell line that were incubated with dilutions of 1:1000 and 1:2000, the latter suggested by the manufacturer as a starting point. As 911 cells/spheroids were going to be transduced with a replication deficient Ad5F35-EGFP virus, which expresses a green fluorescent protein, they were left unlabelled.

After preliminary experiments were performed and the culture plates reviewed using EVOS microscopy, cell tracker violet imaged poorly with excessive background noise and its use was therefore discontinued after the preliminary stages.

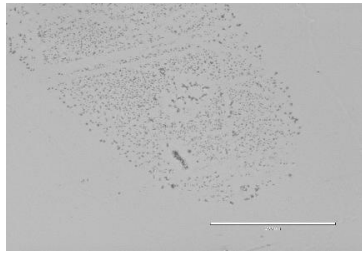
Cell tracker orange and green returned the strongest signals for all cell lines in the monolayers.

Autofluorescence is a characteristic of all tissues. In order to eliminate false positive signal return and to be certain that the signal is specific to the cell progeny that is labelled, unlabelled test sections of paraffin embedded and cut spheroids from each of the homotypic PDAC MCTS were used to assess for i) autofluorescence and ii) to ensure there is no overspill of colour between the green and orange signals. This would therefore allow confident identification of normal and cancer cell populations in the heterotypic MCT spheroids. DAPI (blue), Texas-Red (for orange signal) and GFP (green) filters were used on the EVOS microscope to detect for autofluorescence.

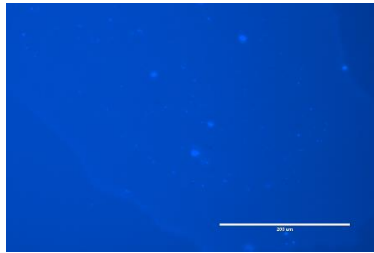
There was strong signal obtained from the DAPI and GFP filters but minimal signal from the Texas-Red filter. This meant that different cell types could be independently labelled as orange or green without there being autofluorescence of green colour from the cells whilst using the Texas-Red filter and vice versa.

The sections below are examples of the Capan-1 and Miapaca-2 test sections:

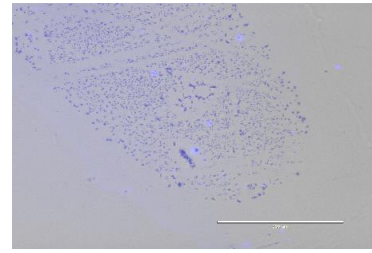
Capan-1



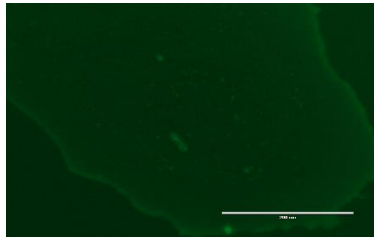
Capan-1 monolayer with transmitted light only



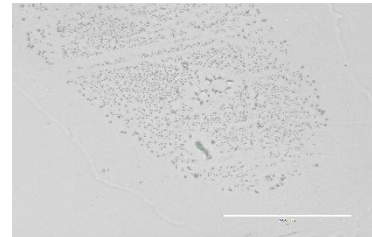
Capan-1 test section with DAPI filter



Overlay of DAPI filter and transmitted light showing blue intracellular autofluorescence



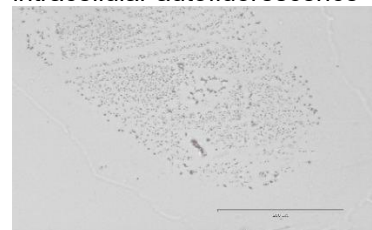
Capan-1 test section with GFP filter



Overlay of GFP filter and transmitted light showing green intracellular autofluorescence



Capan-1 test section with Texas-Red filter

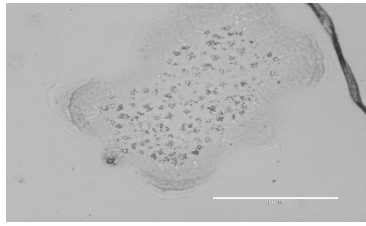


Overlay of Texas-Red filter and transmitted light showing minimal intracellular autofluorescence and no overspill of green autofluorescence

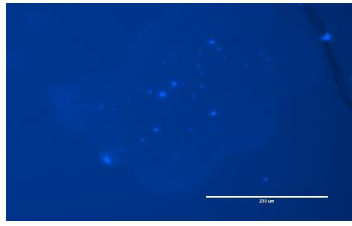
Figure 17 – Capan-1 Test sections for autofluorescence

Representative test sections from Capan-1 to test for innate tissue autofluorescence to ensure true fluorescence is detected from the tracked cells and not false positives from background autofluorescence. Using Texas red filter showed no autofluorescence.

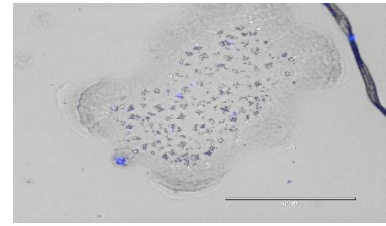
MiaPaCa-2



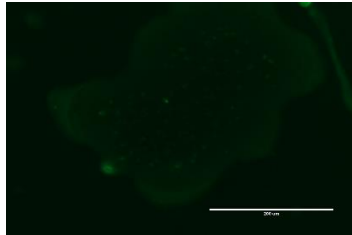
MiaPaCa-2 monolayer with transmitted light only



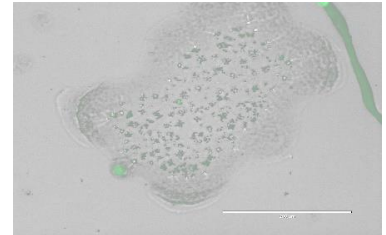
MiaPaCa-2 test section with DAPI filter



Overlay of DAPI filter and transmitted light showing blue intracellular autofluorescence



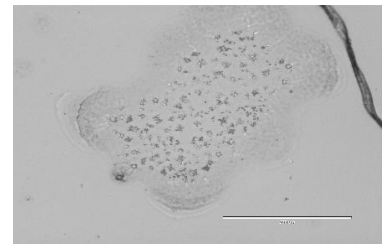
MiaPaCa-2 test section with GFP filter



Overlay of GFP filter and transmitted light showing green intracellular autofluorescence



MiaPaCa-2 test section with Texas-Red filter



Overlay of Texas-Red filter and transmitted light showing no intracellular autofluorescence

Figure 18 – MiaPaCa-2 Test sections for autofluorescence

Representative test sections from MiaPaCa-2 to test for innate tissue autofluorescence to ensure true fluorescence is detected from the tracked cells and not false positives from background autofluorescence. Using Texas red filter showed no autofluorescence.

Both the orange and green cell tracker dyes showed equally strong dye-labelling of cells for all 3 PDAC, however DEChTERT and MRC5 showed stronger cell labelling with cell tracker green. Furthermore, given the limited availability of the cell tracker dyes in our laboratory, the concentration of cell tracker green required for all of the PDAC cell lines were half of that of orange (1:2000 vs 1:1000) and generated an equally strong signal. It was therefore decided that all PDAC would be labelled green and normal cells would be labelled orange in all subsequent experimentations.

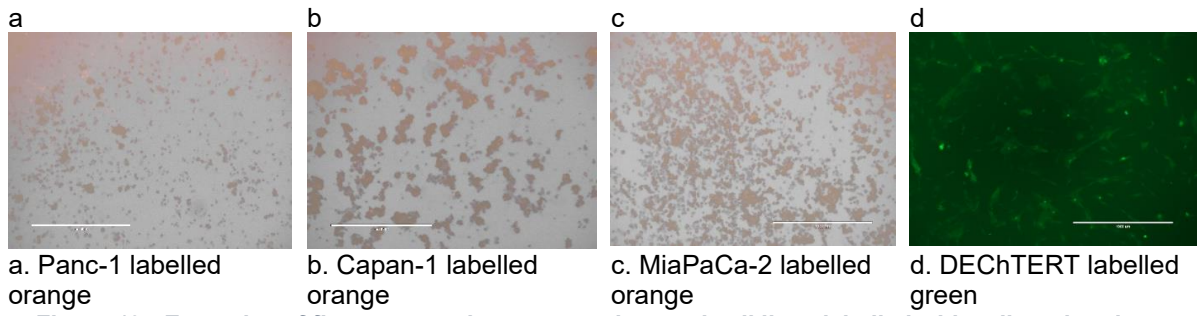


Figure 19 - Examples of fluorescence in cancer and normal cell lines labelled with cell tracker dyes

Stronger labelling was obtained with cell tracker orange in all PDAC lines and increased fluorescence was detected in normal cells using cell tracker green.

3.2.3.2. Heterotypic Multicellular Spheroids

MRC5 and DEChTERT, a fibroblast and epithelial cell lines respectively, were used as representative normal cells in the generation of heterotypic MCTS. Multiple experiments were performed in order to optimize the seeding density of each of the pancreatic cell lines with both MRC5 and DEChTERT with variable success. As the seeding density of the homotypic MCTS was deduced at 1500 cells/well, the heterotypic MCTS were initially set up with a total cell count of 1500 cells/well at a 50:50 ratio of PDAC:Normal cells; 750 of each of the PDAC and 750 of each of DEChTERT or MRC5 in separate 96 well ultra-low adherence cell culture plates.

Despite successfully using MiaPaCa-2 to form homotypic MCTS and transducing these with the adenoviral 5-based vectors, it proved impossible to form heterotypic MCTS containing MiPaCa-2 with either DEChTERT or MRC5 in spite of multiple attempts and optimization processes. MiPaCa-2 was therefore not used to form heterotypic MCTS.

Initially Capan-1 failed to form heterotypic MCTS with either MRC5 or DEChTERT in spite of multiple attempts and optimization processes including alteration of the cell counts. Panc-1 however formed spheroids successfully with MRC5. After optimization processes were performed, the ideal seeding density for these was confirmed at 750/750 of each of Panc-1/MRC5 with a total of 1500cells/well. Panc-1 cells were labelled orange and MRC5 green as per the cell tracker dye assessment in monolayers (see section 3.2.3.1; pg 81). As it was only possible to form heterotypic MCTS with one of the pancreatic cancer cell lines and MRC5, this experiment was used as a proof of concept before trying the PDAC cell lines with DEChTERT.

Although we managed to form multiple homotypic MCTS from a range of different cell line types and established a protocol for this, the process ceased to work and several lengthy optimization processes took place at this point to elucidate the underlying problems (see section 3.2.1; pg 73).

Once the methodology was optimized, we went on to effectively form heterotypic MCTS using Panc-1 and Capan-1 with DEChTERT at a seeding density of 1250cells/well of each of PDAC and 1250 c/w of DEChTERT to a total of 2500c/w for each heterotypic MCTS. In order to speed up the process of heterotypic MCTS formation and given that there were only two cell populations within these, the PDAC cells were labelled green and DEChTERT were left unlabelled. Zeiss inverted microscopy was used to ensure fluorescence. To this end, within the heterotypic MCTS we proved a mixed cellular progeny; some cells showed green fluorescence and others did not. These were then infected with Ad5F35-WT and Ad5F35-

CDC20 with 911 spheroids running in parallel as a positive control and also infected with Ad5F35-WT, Ad5F35-CDC20 and Ad5F35-EGFP (see section 2.3.3; pg 52). The labelled heterotypic MCTS that formed; Panc-1/MRC5, Panc-1/DEChTERT and Panc-1/DEChTERT; were imaged and measured using EVOS microscopy.

The Panc-1/MRC5 were formed as a proof of concept, that spheroids can be formed containing more than one cell type. Indeed, the cell tracker dye labelling clearly demonstrates the presence of two different cell types within the heterotypic MCTS and that the cancer cells far outnumber the normal cells. This is what would be expected within the cancer milieu given their metabolic and mutational selective advantage. Similar to the PDAC MCTS, their shape was far more irregular compared to the homotypic normal cell MCTS, most likely attributable to the uncontrolled growth of cancer cells.

Panc-1/MRC5

24HRS

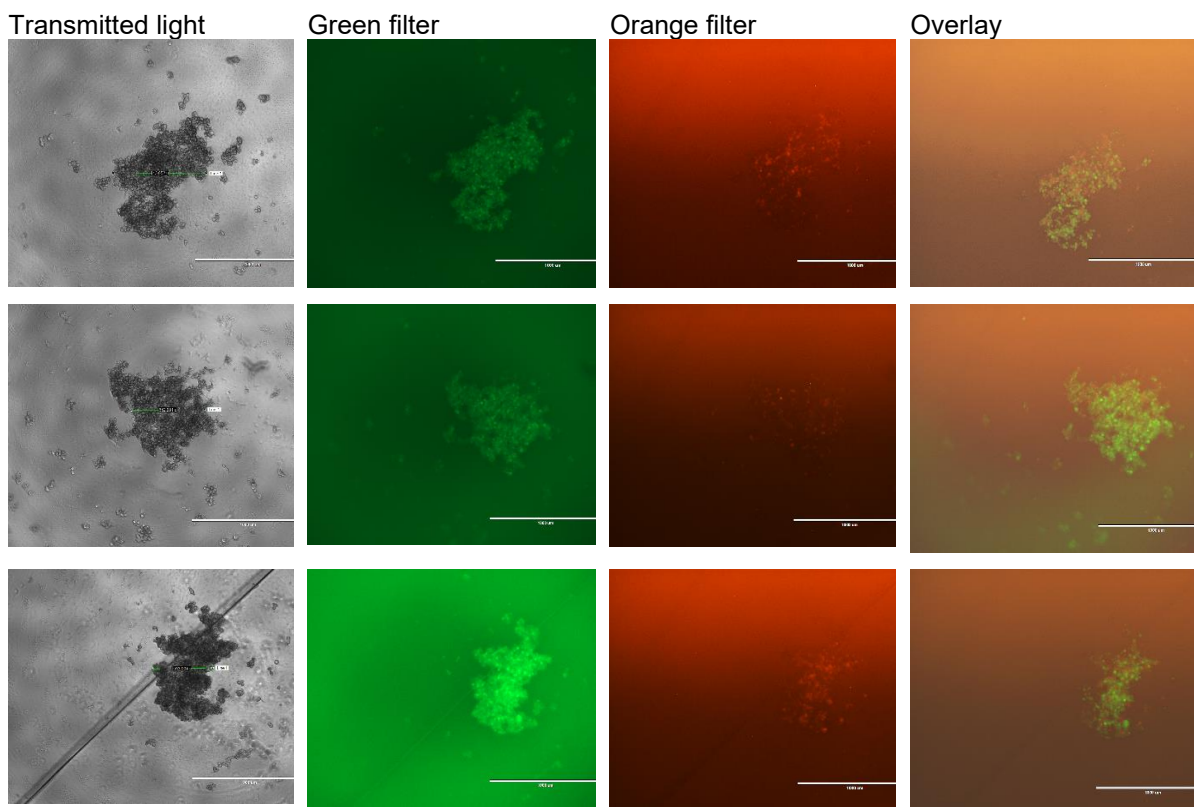


Figure 20 – 3 examples of the heterotypic MCTS formed of Panc-1 and MRC5. Bar represents 1000 μ m

Panc-1 is labelled green and MRC5 labelled orange. The spheroids were imaged after 24 hrs. The images show an existence of both cell progenies within all spheroids. Both the overlaid images on the far right as well as those using just the green and orange filters show that the cancerous cells far outnumber the normal cells. Bars represent 1000 μ m

As with Panc-1/MRC5 heterotypic MCTS, we were again able to form heterotypic MCTS combining one of Panc-1 or Capan-1 with DEChTERT, an epithelial cell line as a representative of normal cells present in PDAC solid tumours. Cancer cell lines were labelled green and normal cells were left unlabelled. All cultures were seeded in triplicate. It is evident in the image gallery below (figures 21 & 22) that with PDAC cell lines after 24 hrs of seeding, some cells were labelled green and some remain unlabelled. The spheroids increased in size during the 4-day period over which they were imaged and, as time progressed, the number of green coloured cancer cells, far outnumbered the normal unlabelled cells as would be expected in cancers. By day 4 almost all of the visualised cells were cancer cells and very few to no normal cells could be seen. This was more conspicuous in the Cap-1/DEChTERT spheroids; although the cells were seeded at the same density and in 50:50 ratio of PDAC:Normal cells as Panc-1/DEChTERT spheroids, were much larger after 24 hrs with greater green labelled cells and far greater cancerous/normal cells by day four. As with the Panc-1/MRC5 and all homotypic MCTS, the greatest rate of growth was seen between 24-48 hrs and the largest number of cancer cells were seen by day 4.

Unlike the pattern of growth seen with the homotypic normal cell MCTS particularly 911, the PDAC containing spheroids, whether heterotypic or homotypic, grew in a much more disorderly fashion with the ultimate spheroid shape being unrepresentative of the spheroid that formed initially after 24hrs, again owing to the growth characteristics of cancer cells.

**Panc-1/DEChTERT
UNINFECTED**

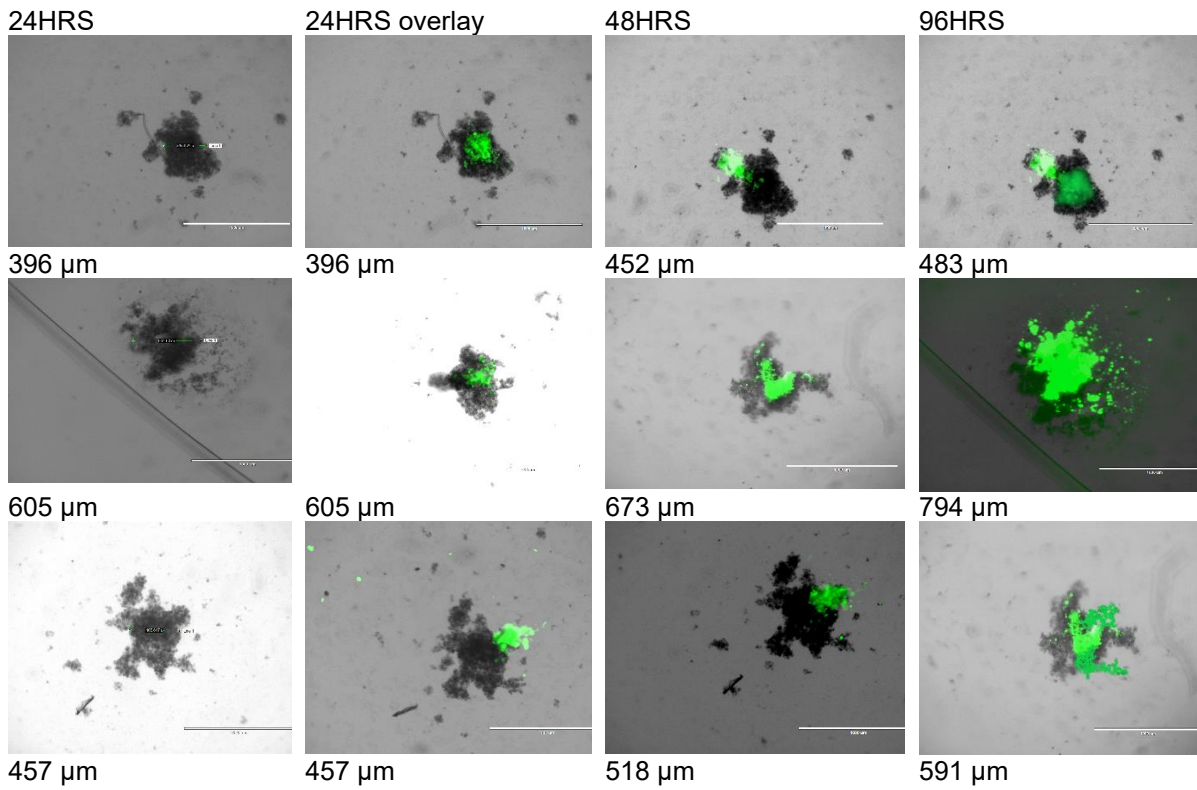


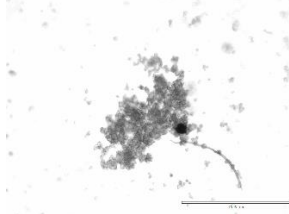
Figure 21 – Uninfected Panc-1/DEChTERT Heterotypic MCTS. Bar represents 1000 μm

Three examples of Panc1-DecHTERT uninfected MCTS imaged over 4 days again with Panc-1 labelled green and DecHTERT left unlabelled.

Capan-1/DEChTERT

UNINFECTED

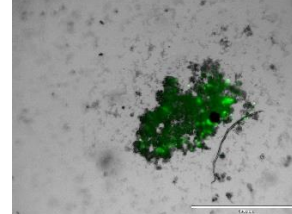
24HRS



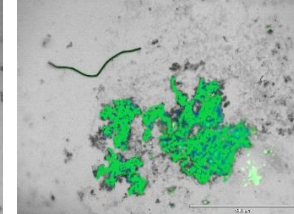
24HRS overlay



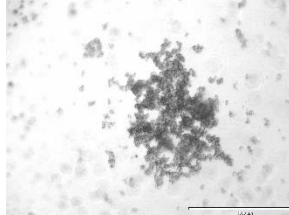
48HRS



96HRS



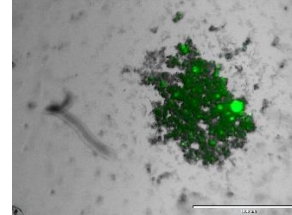
729 μ m



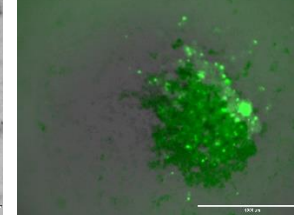
729 μ m



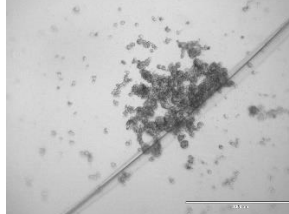
820 μ m



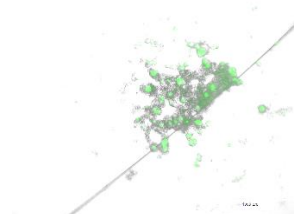
863 μ m



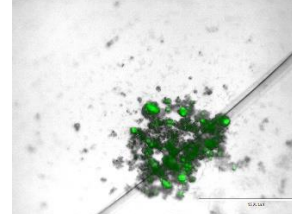
698 μ m



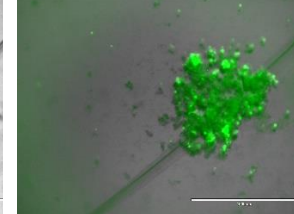
698 μ m



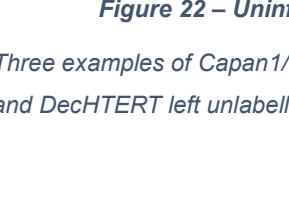
724 μ m



812 μ m



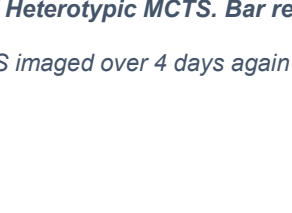
777 μ m



777 μ m



835 μ m



888 μ m



Figure 22 – Uninfected Capan-1/DEChTERT Heterotypic MCTS. Bar represents 1000 μ m

Three examples of Capan1/DecHTERT uninfected MCTS imaged over 4 days again with Capan-1 labelled green and DecHTERT left unlabelled.

3.2.4. Adenoviral Transduction and Infection

Prior to the infection process, viral titres for each of the viruses used were ascertained in 2D monolayers.

3.2.4.1. Ascertaining Viral Titres in 2D Monolayers

Monolayers of each of the cell lines were infected with Ad5F35-EGFP in order to ascertain which concentration of the virus resulted in better uptake and therefore signal for use in the heterotypic MCTS. Ad5F35-EGFP at 100vp/ μ l and 1000 vp/ μ l were used to infect each of the cell lines in duplicates. Duplicates of each of the cell lines were left uninfected and used as negative controls.

Best uptake and signal return were demonstrated using microscopy, light and fluorescent, as well as flow cytometry.

Imaging:

Transmitted light was used to demonstrate cell growth followed by EVOS microscopy to demonstrate the fluorescence of cells after infection. Ad5F35-EGFP at 1000vp/ μ l showed better uptake and hence signal. This was the viral concentration used in all subsequent infection/transduction experiments.

Below are sample images of each of the cell lines in monolayers after infection with Ad5F35-EGFP at the two different concentrations as well as images of the uninfected monolayers demonstrating no fluorescence using EVOS microscopy:

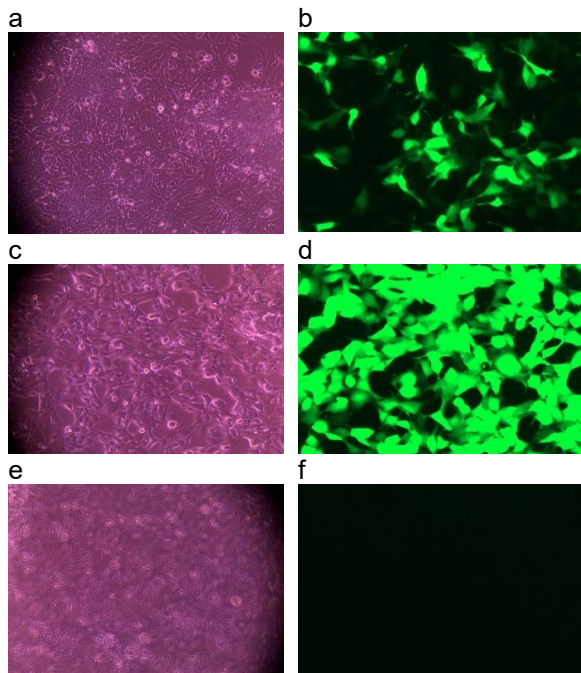
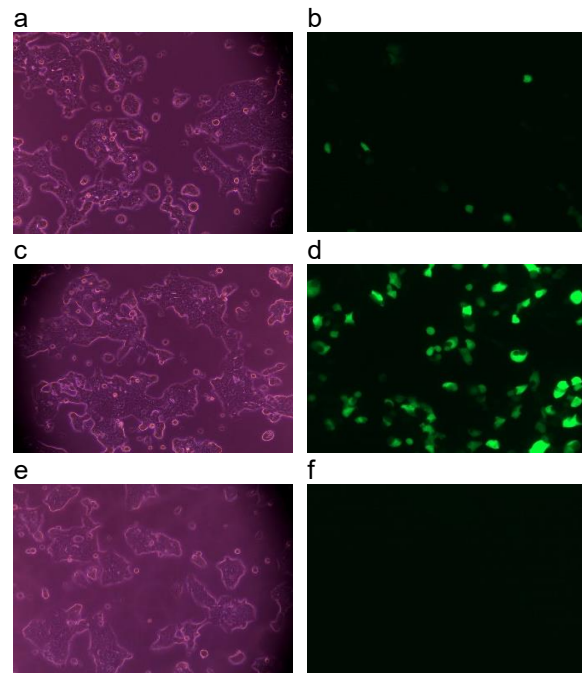
911**Capan-1**

Figure 23 – Cell tracker dye labelling of 911 and Capan-1 monolayers

Images a & b for each of the cells were after infection with Ad5F35-EGFP 100vp/μl; c & d after infection of 1000vp/μl. Images a, c & e are using light microscopy; b, d & f demonstrating fluorescence with EVOS microscopy. The fluorescence imaging clearly demonstrates better uptake and signal return using 1000 vp/μl in all cell lines. Image f shows no fluorescence as these cells were left uninfected as negative controls.

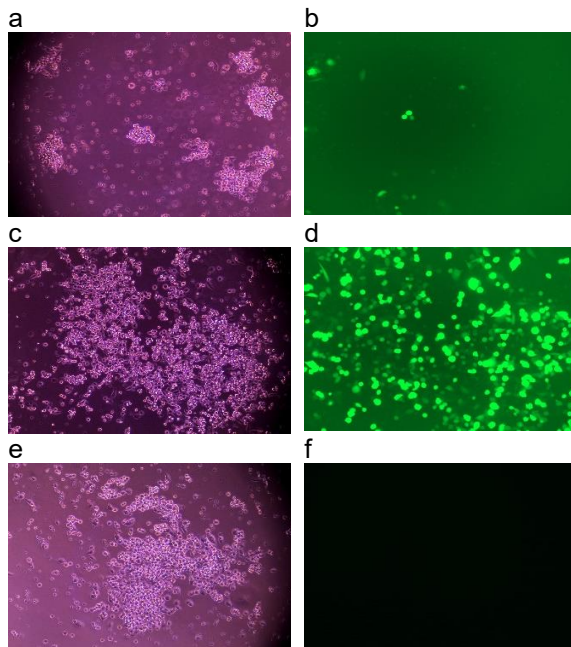
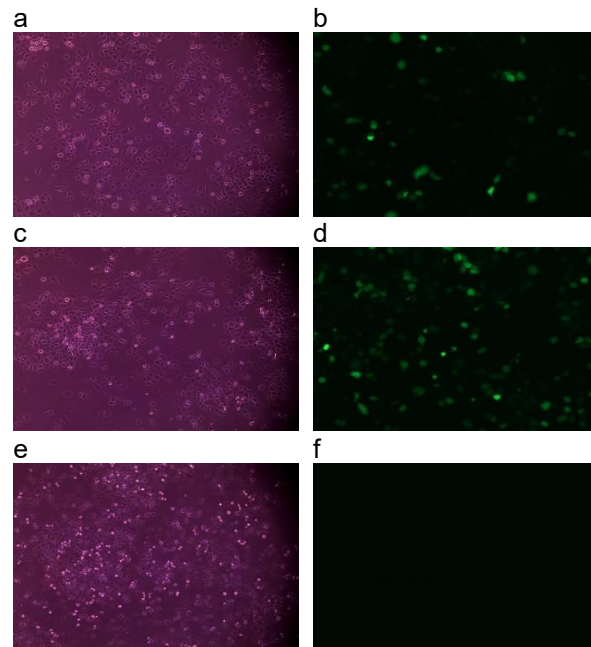
MiaPaCa-2**Panc-1**

Figure 24 – Cell tracker dye labelling of MiaPaCa-2 and Panc-1 monolayers

Images a & b for each of the cells were after infection with Ad5F35-EGFP 100vp/μl; c & d after infection of 1000vp/μl. Images a, c & e are using light microscopy; b, d & f demonstrating fluorescence with EVOS microscopy. The fluorescence imaging clearly demonstrates better uptake and signal return using 1000vp/μl in all cell lines. Image f shows no fluorescence as these cells were left uninfected as negative controls.

3.2.4.2. Flow Cytometry

In order to corroborate the results from the monolayer cell tracker dye experiment, and to objectively measure cellular uptake of the fluorescent dyes in PDAC cells lines, we ran flowcytometric analysis on the supernatants of the monolayers.

One well from each of the monolayer cell lines was left uninfected (in the case of 911) or not incubated with a cell tracker dye in the case of PDAC cell lines as negative controls. 911 monolayers were not incubated with a cell tracker dye but instead incubated and infected with Ad5F35-EGFP as a positive control.

We can see from the above data that all wells used as negative controls show almost 100% green fluorescent negativity. This is with the exception of Capan-1 were 12% of cells were fluorescent green. This may represent an element of autofluorescence.

Similarly, unanimously across all PDAC cell lines there was better uptake with 1000vp/μl vs 100vp/μl: i) Capan-1 41% vs 73%, ii) Panc-1 40% vs 69.5% and iii) MiPaCa-2 6% vs 29%.

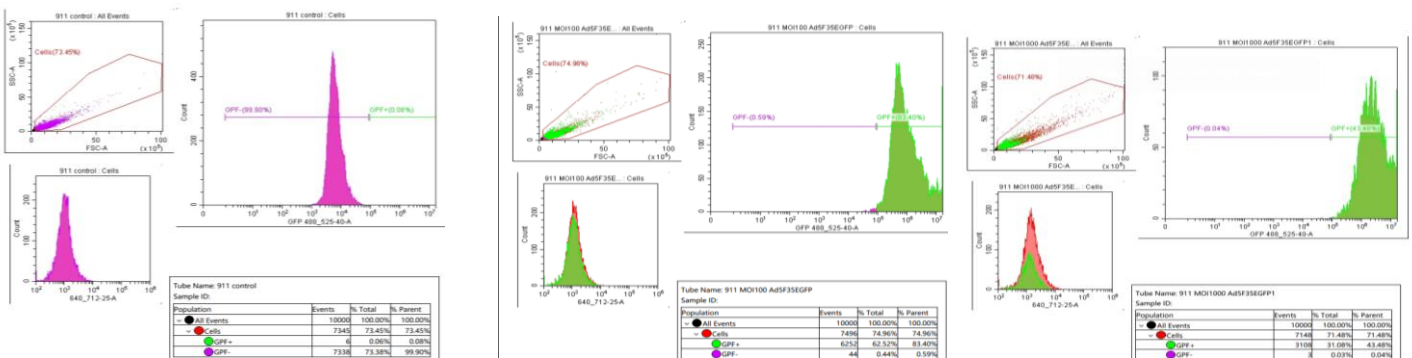
It is difficult to explain why such a low percentage of MiaPaCa-2 cells were positive for green fluorescence despite a high population number and such bright green fluorescence on immunofluorescence microscopy (Figure 25).

Control

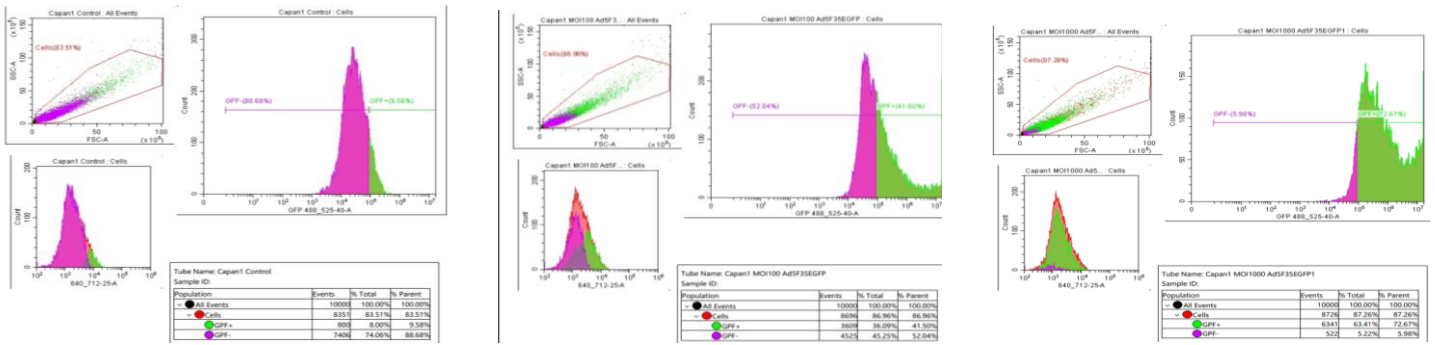
100vp/μl

1000vp/μl

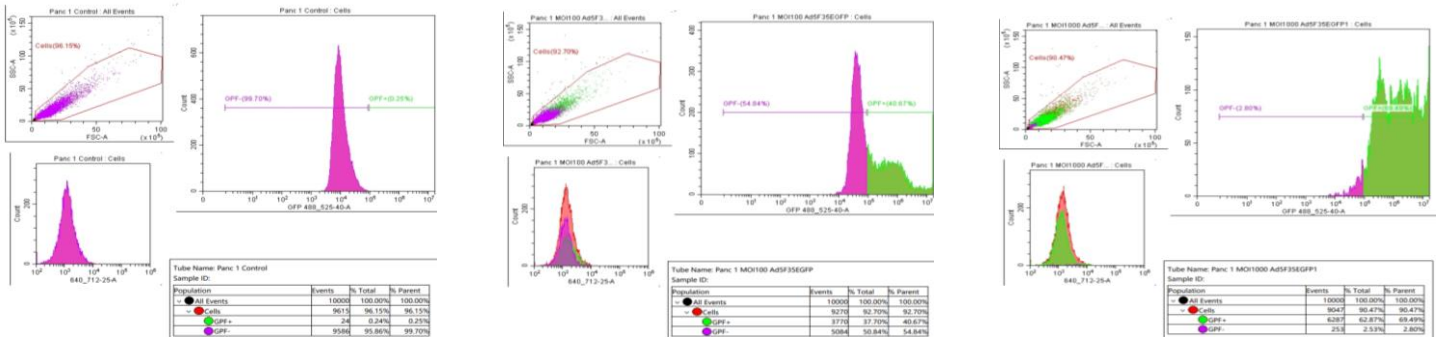
911:



Capan-1:



Panc-1:



MiaPaCa-2:

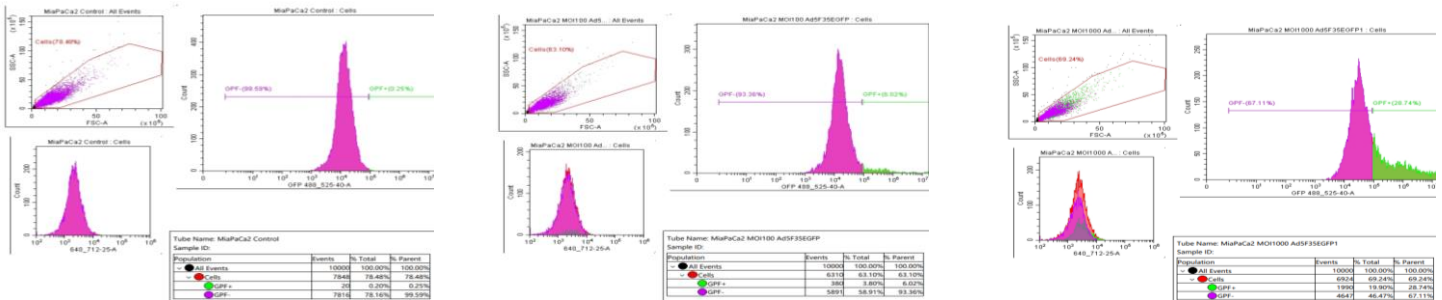


Figure 25 – Flowcytometric analysis of fluorescent tracker dye uptake

The left-hand side column of plots are those from uninfected cells from each of the cell lines, used as negative controls, the middle plots are cells infected at MOI 100 and the right hand side are MOI 1000 of the Ad5F35-EGFP virus. Forward and side scatter gates were applied to identify the cell population of interest. GFP positive and GFP negative gates were set based on the uninfected control sample. The green population on the scatter graph represent GFP positive cells and the pink represent the GFP negative population.

3.2.4.3. Homotypic MCTS Infection

Representative spheroids from each cell line were trypsinised 48 hrs after seeding for cell counting. Two spheroids from each cell line were infected with Ad5F35 (wild type) and two with the recombinant Ad5F35-CDC20. Two 911 spheroids were transduced with Ad5F35-EGFP (replicating in 911 cells, non-replicating in all other cell types) as positive controls and two from each cell line were left uninfected to run in parallel and used as negative controls. Spheroids were imaged and measured using the EVOS microscope at 48, 96 and 168hrs. One of the uninfected spheroids from each cell line was fixed for immunohistochemistry every 48hrs. Panc-1 and MiaPaCa-2 spheroids were too friable at the end of the infection process to pick up and fix for immunohistochemistry.

The 911 homotypic MCTS again here demonstrate that they form the most regular shaped spheroids within the first 24 hrs, with a demonstrable tight capsule. The uninfected spheroids continued to increase in size throughout the 7-day period of observation with the largest growth in size seen between days 2-4. The spheroid capsule remained intact throughout the 7-day period, however appeared to get gradually thinner on days 4-7.

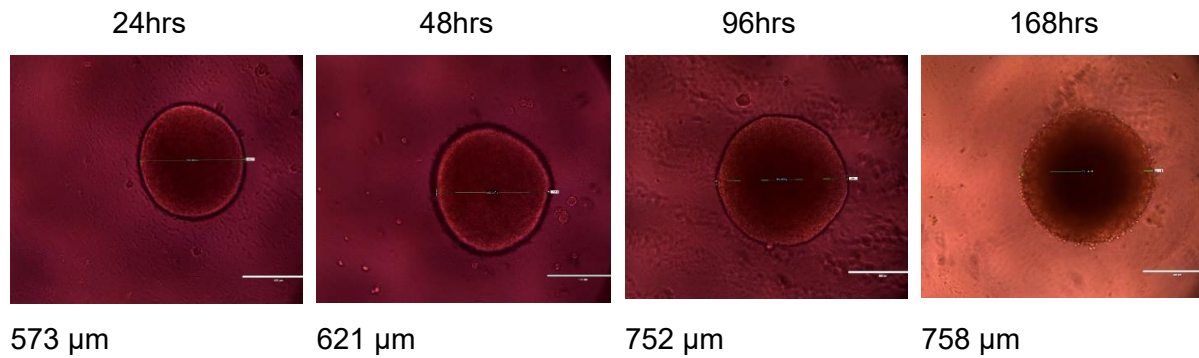
As the spheroids got larger in size a dark, presumably necrotic, core began to appear and this became larger as the spheroids got larger in size. In our experience with the uninfected 911 spheroids, this appeared around 48 hrs when spheroids were around 500 – 600 µm and was very small but became significantly larger as time increased. By day 7, the necrotic core appeared to occupy most of the visible spheroid volume. On day 7, although a very thin capsule is retained, this is much less conspicuous and the periphery of the spheroid appears to slightly disaggregate and clumps of cell appeared. Using a fluorescent microscope however, the uninfected cells did not show any green fluorescence.

Running parallel to the uninfected spheroids, other 911 spheroids were infected 24 hrs after their formation (at 48hrs) with Ad5F35EGFP, a GFP expressing replication defective adenoviral vector, as positive controls. However, the virus can replicate in 911 cells since this cell line contains integrated Ad5 E1A and E1B genes whose products trans-complement the absent E1A and E1B genes in the Ad5F35-EGFP virus. It can be seen from the images above that the virus was able to spread and fully transduce the whole spheroid, which glowed bright green under fluorescence microscopy.

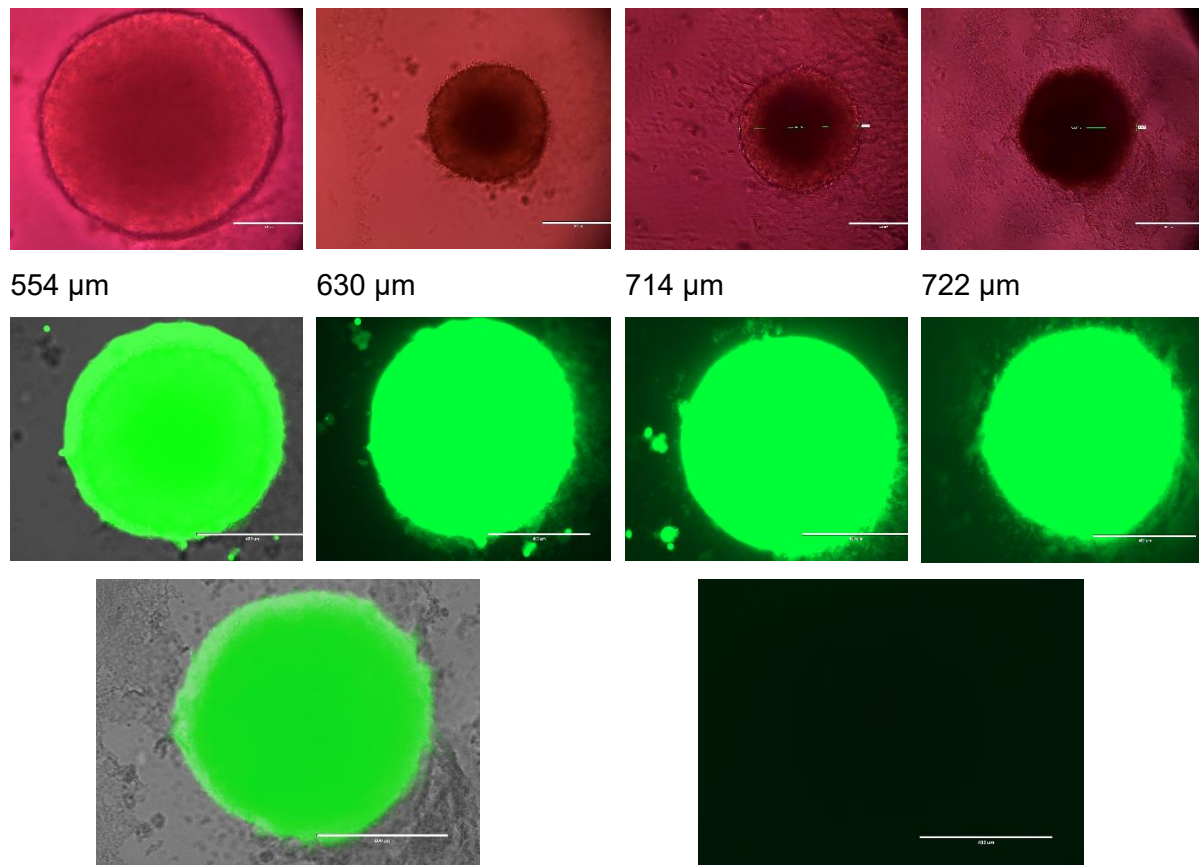
The infected spheroids began to dissociate with the progression of time, similar to their uninfected counterparts, and fluorescent islands of dissociated cells can be seen in the surrounding culture medium as well as a general increasing green glow from the medium.

Towards the end of the week, the crisp green fluorescent capsule of the spheroids appeared hazier when compared to the initial days after formation and infection/transduction.

911; Uninfected



911; Ad5F35-EGFP



168hrs transmitted/inverted microscopy overlay

Uninfected inverted microscopy negative control

Figure 26 – 911 Homotypic MCTS; Uninfected and infected with Ad5F35-EGFP as positive control. Bar represents 1000 μm

911 MCTS infected with Ad5F35-EGFP showing full transduction of the spheroids with the GFP virus proving the ability of the Ad5F35 virus at transducing the spheroids.

The heterotypic MCTS from each of the PDAC were infected with Ad5F35-WT and Ad5F35-CDC20 with spheroids from each left uninfected as negative controls.

All the spheroids were infected 24 hrs after their formation and imaged at 24, 48 and 96 hrs after infection. As seen above (Figure 27, 28 and 29), both viruses blew the spheroids apart within 24 hrs of infection. Although uninfected spheroids from the same cell line began to disaggregate on day 7, this was consistently minimal and from the periphery and all still showed some growth between day 4 and 7.

The uninfected spheroids retained their shape and indeed could be picked up for paraffin embedding for immunohistochemical staining. In contrast with the infected spheroids, there was minimal to no size increase with increasing time, in fact although some spheroids numerically measured larger, this was actually more of a subjective measurement of the disaggregated cell population as no discernible spheroid remained. Most of the infected spheroids at the end of the 7-day period were so friable, they could not be picked up for IHC.

Microscopically this was most conspicuous in MCTS from Capan-1 and Panc-1 with the MiaPca-2 spheroids appearing more intact. However, when harvesting the spheroids for IHC, the MiaPaCa-2 spheroids were equally as friable and disaggregated as spheroids from the other PDAC MCTS.

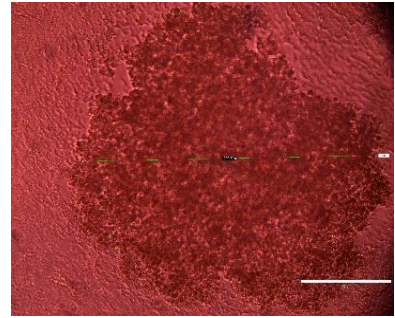
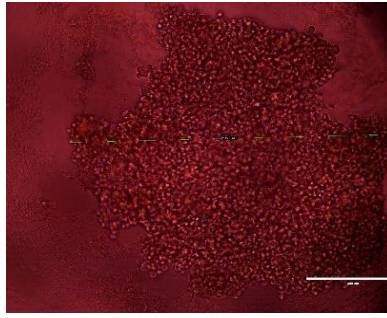
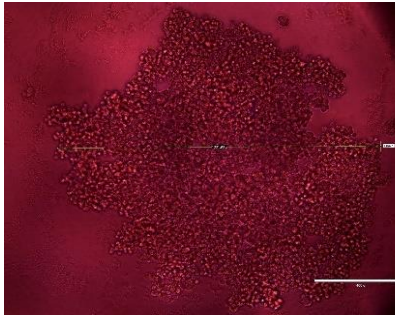
There did not appear to be a difference between the efficacy of Ad5F35-WT and Ad5F35-CDC20 at spheroid disaggregation across all of the cell lines.

Panc-1; Uninfected

24hrs

48hrs

96hrs



1332 μm

1490 μm

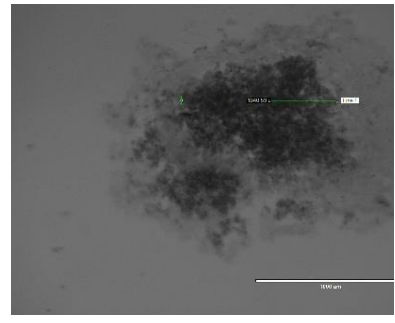
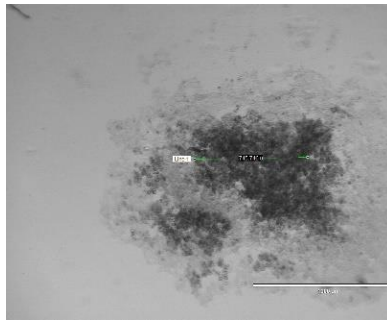
1498 μm

Panc-1; Ad5F35-WT

24hrs

48hrs

96hrs

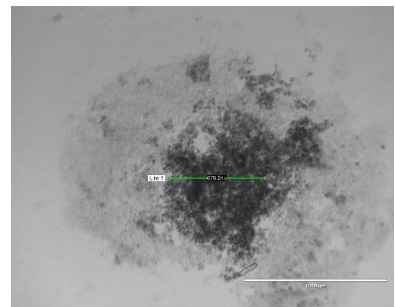
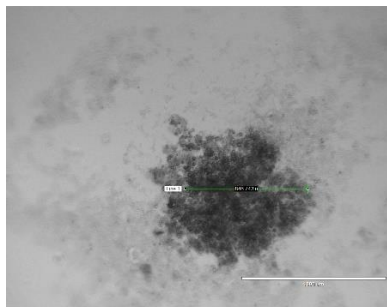
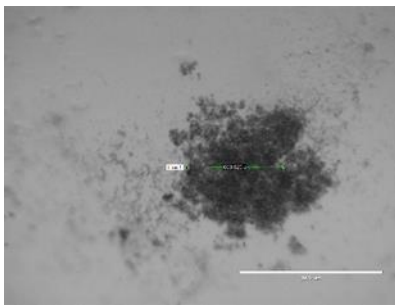


727 μm

746 μm

1041 μm

Panc-1; Ad5F35-CDC20



670 μm

847 μm

678 μm

Figure 27 – Panc-1 Homotypic MCTS Infection. Bar represents 1000 μm

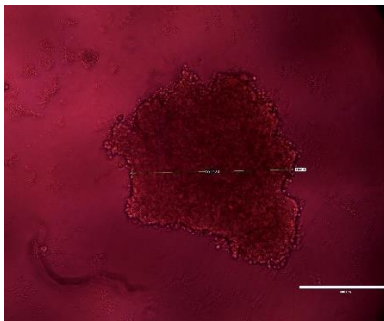
Panc-1 homotypic MCTS. The top series are uninfected spheroids, the middle row infected with Ad5F35-WT parent virus and the bottom infected with the recombinant Ad5F35-CDC20 virus. Each spheroid imaged and measured for 4days. The infected spheroids were blown apart by both viral strains and were objectively different from those left uninfected.

Capan-1; Uninfected

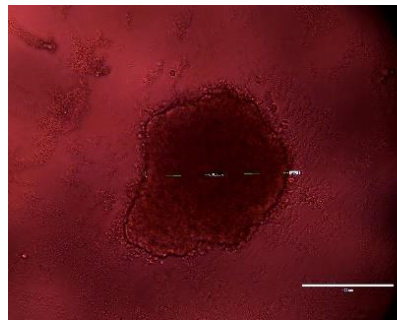
24hrs

48hrs

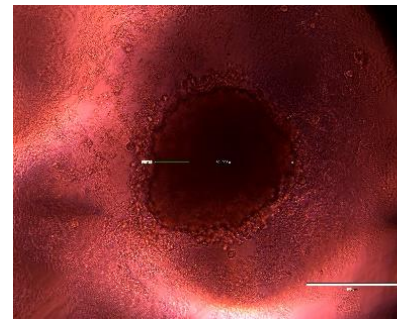
96hrs



699 μm



618 μm



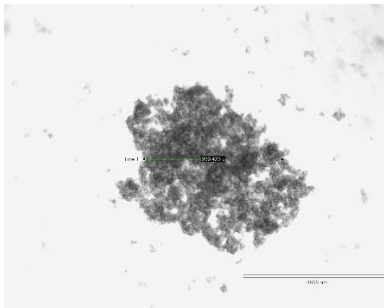
602 μm

Capan-1; Ad5F35-WT

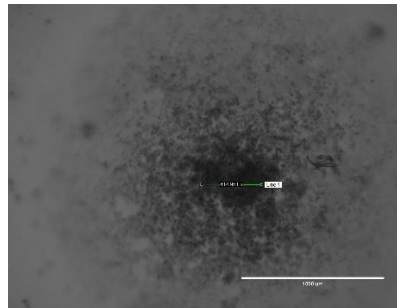
24hrs

48hrs

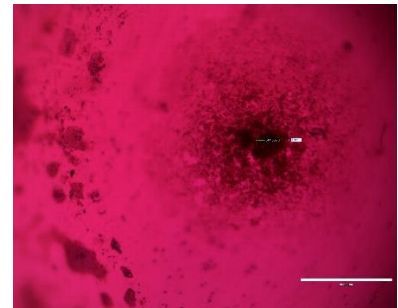
96hrs



939 μm

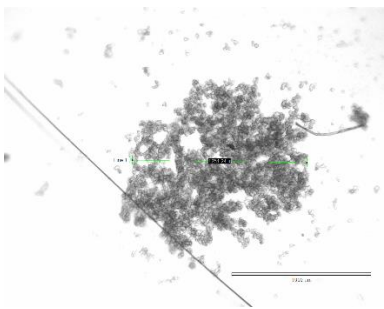


746 μm

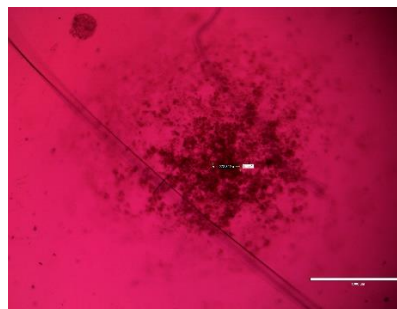


1041 μm

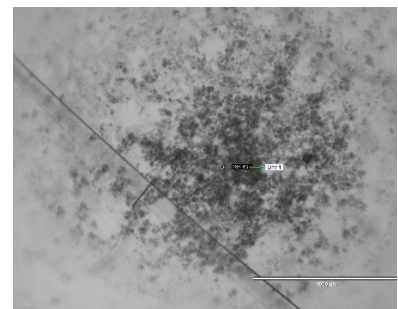
Capan-1; Ad5F35-CDC20



1251 μm



576 μm



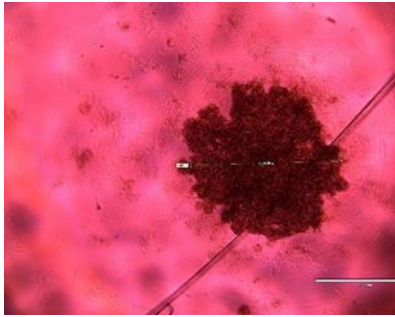
465 μm

Figure 28 – Capan-1 Homotypic MCTS Infection. Bar represents 1000 μm

Capan-1 homotypic MCTS. The top series are uninfected spheroids, the middle row infected with Ad5F35-WT parent virus and the bottom infected with the recombinant Ad5F35-CDC20 virus. Each spheroid imaged and measured for 4days. The infected spheroids were blown apart by both viral strains and were objectively different from those left uninfected.

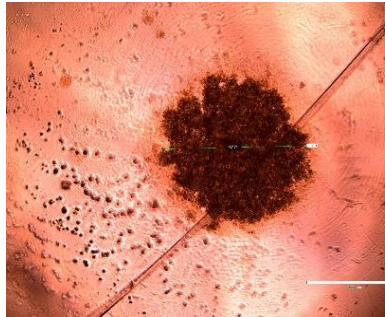
MiaPaCa-2; Uninfected

24hrs



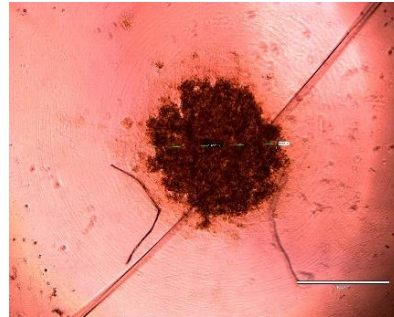
1515 μm

48hrs



1488 μm

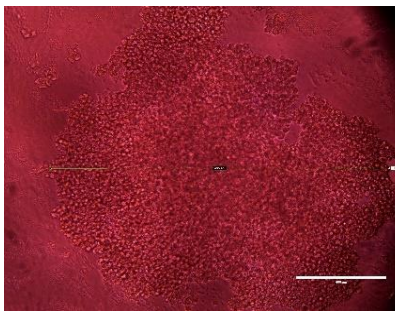
96hrs



1322 μm

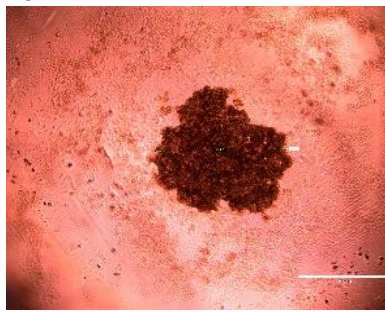
MiaPaCa-2; Ad5F35-WT

24hrs



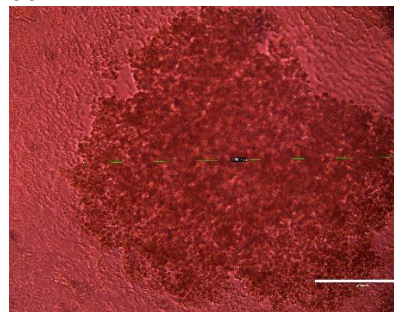
1486 μm

48hrs



1405 μm

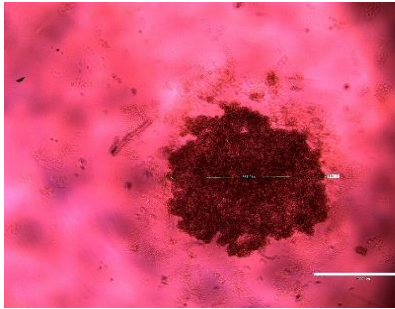
96hrs



1300 μm

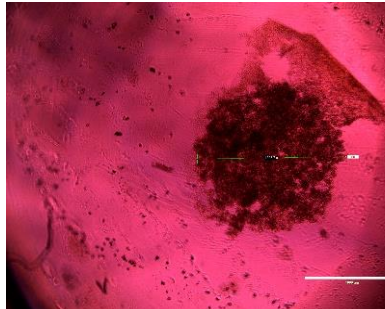
MiaPaCa-2; Ad5F35-CDC20

24hrs



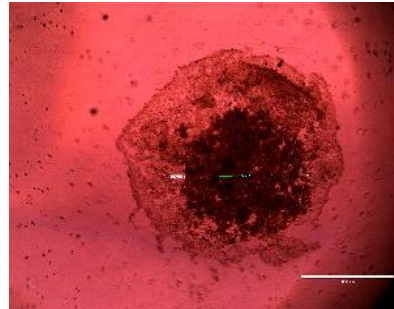
1557 μm

48hrs



1554 μm

96hrs



1325 μm

Figure 29 – MiaPaca-2 Homotypic MCTS Infection. Bar represents 1000 μm

MiaPaCa-2 homotypic MCTS. The top series are uninfected spheroids, the middle row infected with Ad5F35-WT parent virus and the bottom infected with the recombinant Ad5F35-CDC20 virus. Each spheroid imaged and measured for 4days. The infected spheroids were blown apart by both viral strains and were objectively different from those left uninfected.

“Infected Halo”

All infected spheroids appeared to disaggregate in a similar pattern after infection with both the Ad5F35-WT and Ad5F35- CDC20. On day 4 after set up, or 48hrs post infection, all spheroids across all cell lines including 911 appeared to disaggregate from the periphery and the disaggregated cells did not float freely in the surrounding medium but circumferentially surrounded the spheroids. The cells were probably contained by the spheroid capsule giving a “halo” appearance surrounding all infected spheroids as demonstrated below in Figure 30.

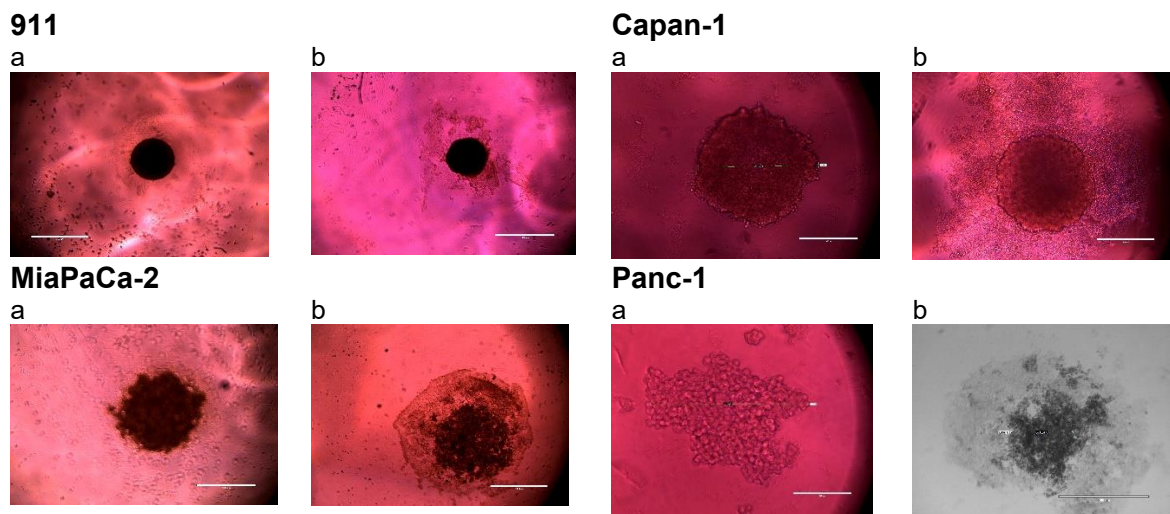


Figure 30 – “Infected Halos”. Bar represents 1000 μm

Example images of the “Infected Halo” surrounding each infected MCTS. Images *a* are infected MCTS and images *b* are infected MCTS.

Z-stack imaging

To get a conceptual 3D image of what was happening within the spheroids with every 24 hrs of growth and post viral infection, Z-stack imaging was attempted in order:

- to look for a hypoxic core and see the size and rate at which it developed
- whether the hypoxic core and its size affected viral transduction/replication
- once spheroids were infected, to see where cell death was initiated, in either the periphery or the core of the spheroids.

Unfortunately, although the spheroids were imaged every 24hrs and Z-stacks produced, the image quality, as we imaged deeper into the spheroid, was too poor to make any sort of assessment. This was true regardless of cell type, infection or lack of, viral vector (whether wild type or CDC20) or day of imaging. When spheroids were imaged with a light/EVOS microscope only 2D images could be taken of a 3D structure. Using the z-stack software,

although imaging went deeper and deeper into a 3D structure, it was impossible to ascertain how much further one set of images were compared to the next, despite the scale being altered. 2D images were produced that were blurred versions of one another and no appreciable differences could be seen between one layer and the next nor any conclusions could be drawn. The only absolute observations made was knowing when we were imaging the top, approximate middle and bottom of the spheroid.

This method of spheroid assessment was not useful and was therefore terminated.

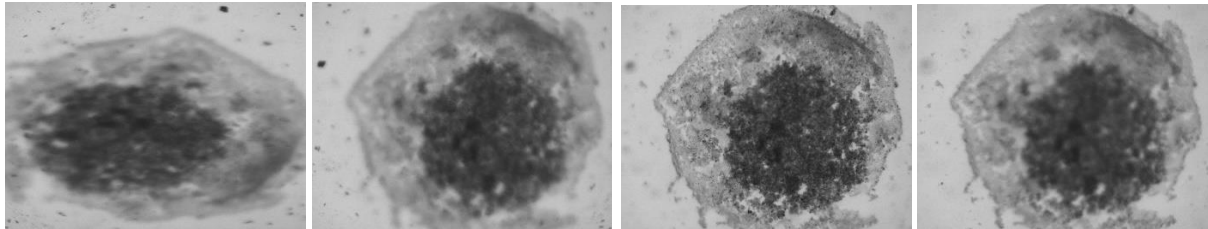


Figure 31 – Example Z-Stack images of MCT at preset sequential depths

Examples of Z-stack imaging performed at preset sequential depths through a spheroid in order to gain a 3D view of the internal structure of the spheroid.

3.2.4.4. Heterotypic MCTS Infection

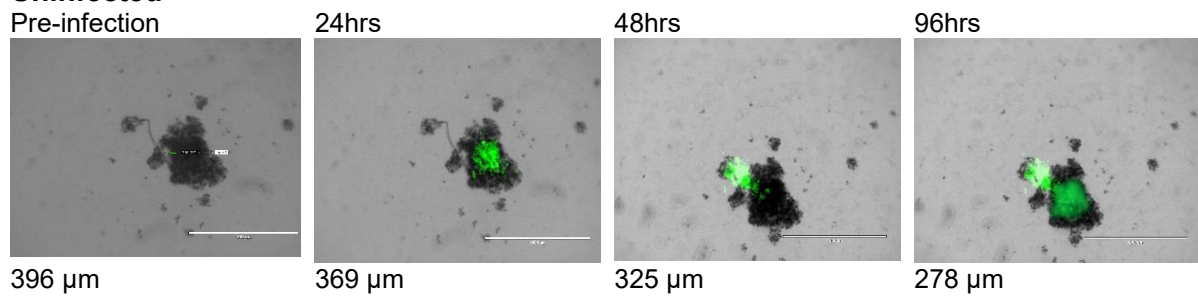
The Panc-1/DEChTERT and Capan-1/DEChTERT heterotypic MCTS that were formed successfully were infected in triplicate with Ad5F35-WT and Ad5F35-CDC20 and three of each were also left uninfected to run in parallel as negative controls. 911 spheroids were generated and infected with Ad5F35-EGFP as positive controls. All spheroids were imaged and measured with EVOS microscopy at 24, 48 and 96 hrs post set up/infection.

The gallery of heterotypic MCTS in Figure 32 - 34 below, demonstrate the presence of two cell types within every spheroid, the PDAC cells labelled green and the rest, normal cells, unlabelled. The uninfected spheroids in every series demonstrate growth in size throughout the observation period and green fluorescent cells that far outnumber the unlabelled normal cells, as would be expected of a tumour environment. The unlabelled spheroids continued to grow in size throughout the observation series retaining their shape without discernible disaggregation. This was opposed to the infected spheroids which again like their homotypic counterparts were blown apart by both viral strains without apparent difference in efficacy between the two. The pattern of disaggregation was again the same as for homotypic MCTS, with peripheral separation and the formation of an infected halo surrounding the spheroids beyond the borders of which no cells were seen in the medium. The cells within this halo appeared primarily green, representing cancer as opposed to normal cells.

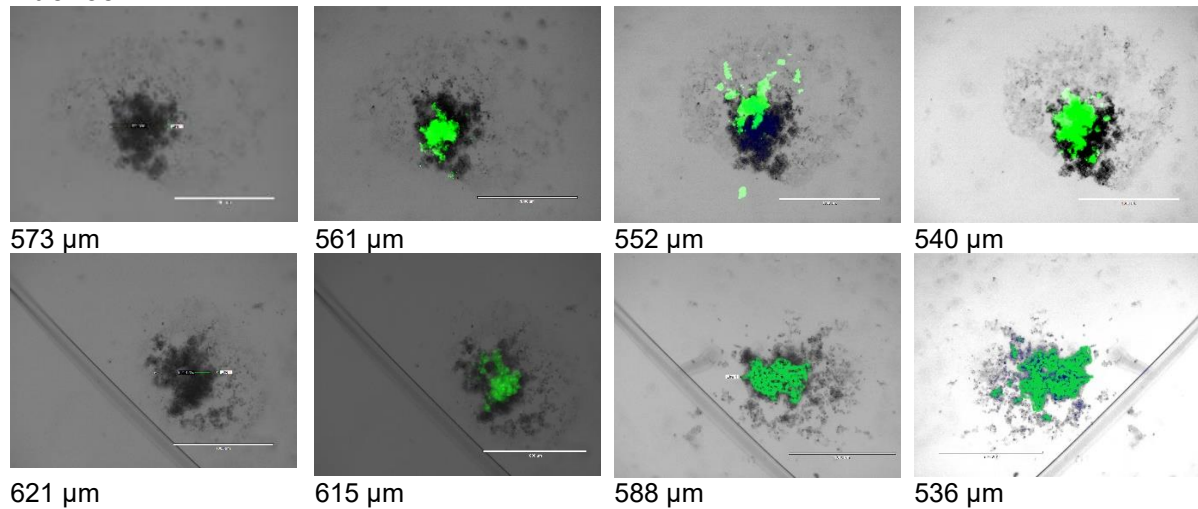
Although the heterotypic MCTS were broken down from apparently the outside in, similar to their homotypic counterparts, larger residual spheroids were present at 7 days compared to the homotypic MCTS and they were also less friable to harvest for IHC. It is presumed, given that green cells were mostly seen in the medium, that it is normal cells which remained and maintained the intact portion of the spheroid (this is difficult to prove however as both cell populations were seen in the residual spheroid and only a 2D view is obtained of them). This would therefore infer that the adenovirus preferentially targeted the tumour as opposed to normal cells.

Imaging

Panc-1/DEChTERT Uninfected



Ad5F35-WT



Ad5F35-CDC20

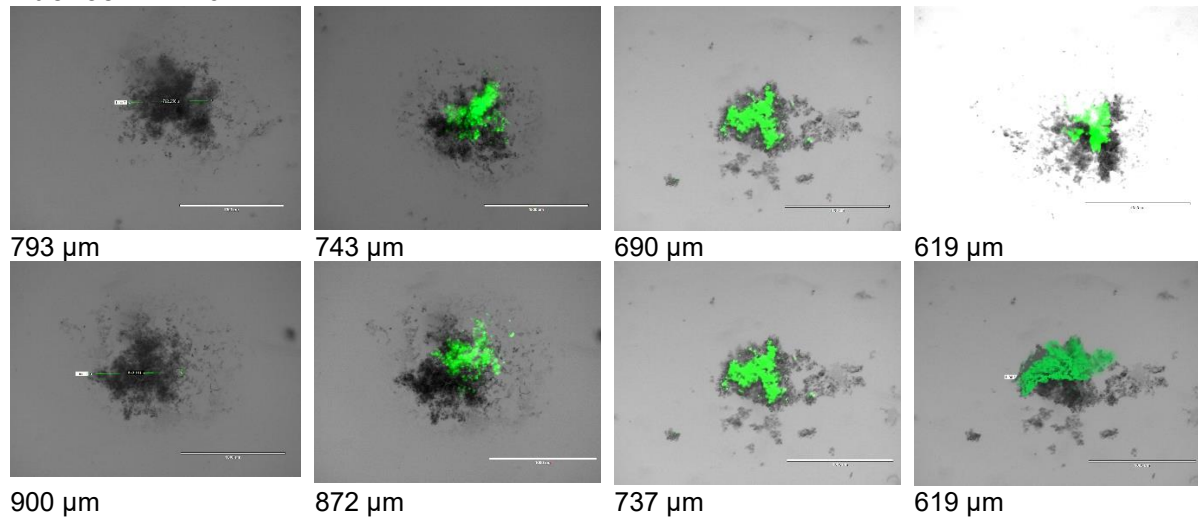


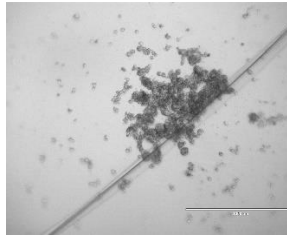
Figure 32 - Panc-1/DEChTERT Heterotypic MCTS infection. Bar represents 1000 μm

Panc-1/DecHTERT heterotypic MCTS. PDAC cells were labelled green and DecHTERT left unlabelled. The top series are uninfected spheroids, the middle row infected with Ad5F35-WT parent virus and the bottom infected with the recombinant Ad5F35-CDC20 virus. Each spheroid imaged and measured for 4days. The infected spheroids were disaggregated by both viral strains and were objectively different from those left uninfected, however this was much less effective compared to the homotypic MCTS.

Capan-1/DEChTERT

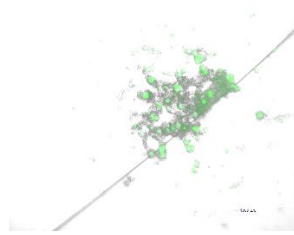
Uninfected

Pre-infection



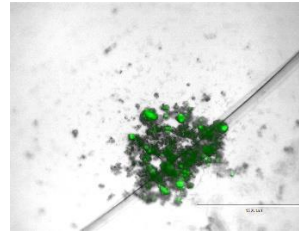
7656 μm

24hrs



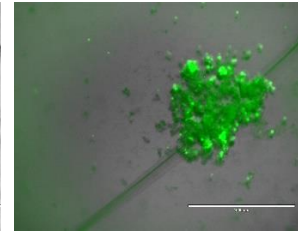
802 μm

48hrs



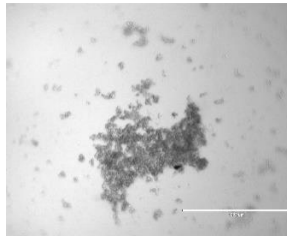
834 μm

96hrs

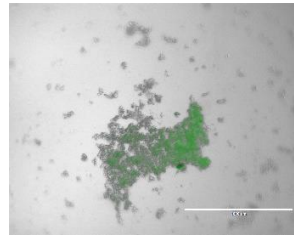


800 μm

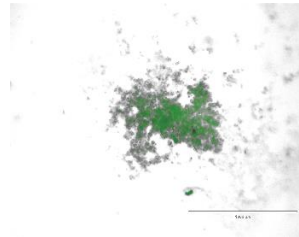
Ad5F35-WT



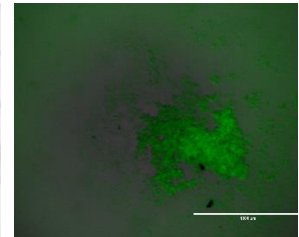
845.435 μm



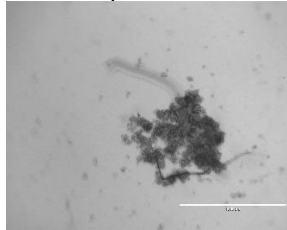
811.876 μm



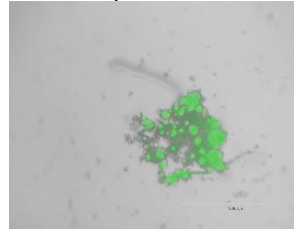
851.083 μm



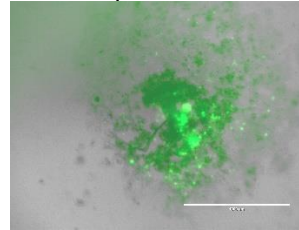
825.679 μm



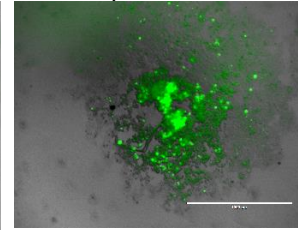
413 μm



360 μm

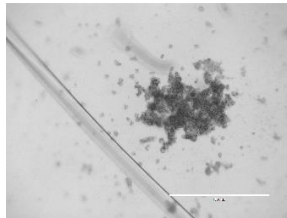


213 μm

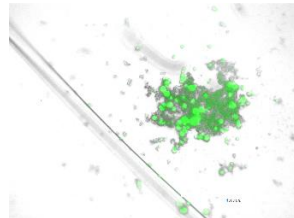


177 μm

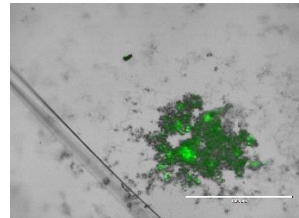
Ad5F35-CDC20



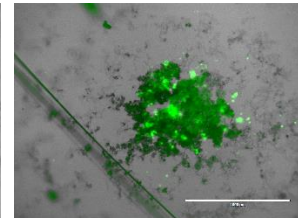
874 μm



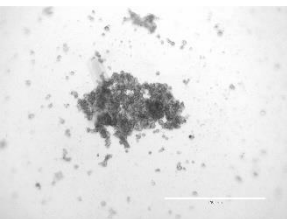
832 μm



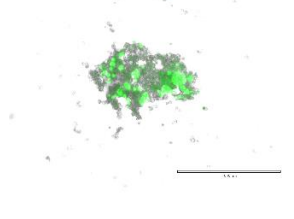
781 μm



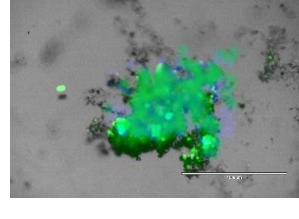
565 μm



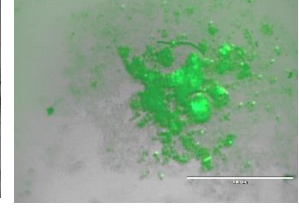
834 μm



790 μm



601 μm



442 μm

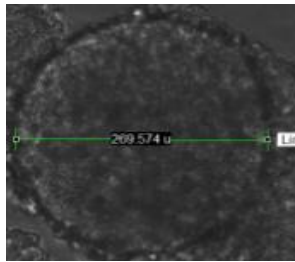
Figure 33 - Capan-1/DEChTERT Heterotypic MCTS infection. Bar represents 1000 μm

Capan-1/DecHTERT heterotypic MCTS. PDAC cells were labelled green and DecHTERT left unlabelled. The top series are uninfected spheroids, the middle row infected with Ad5F35-WT parent virus and the bottom infected with the recombinant Ad5F35-CDC20 virus. Each spheroid imaged and measured for 4 days. The infected spheroids were disaggregated by both viral strains and were objectively different from those left uninfected. However, this was much less effective compared to the homotypic MCTS but greater MCTS oncolysis compared to Panc-1 with both viral strains.

911

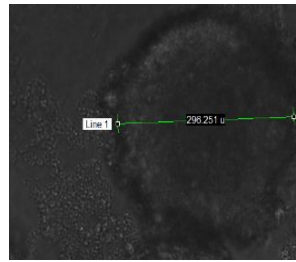
Uninfected

Pre-infection



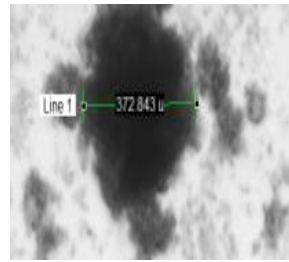
270 μm

24hrs



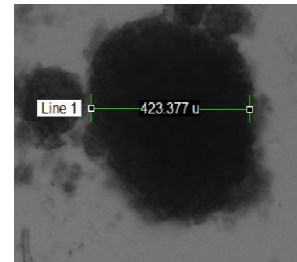
298 μm

48hrs



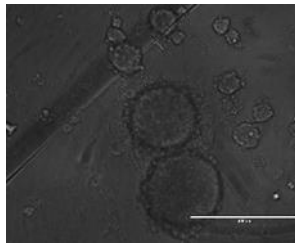
373 μm

96hrs

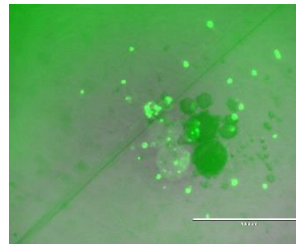


424 μm

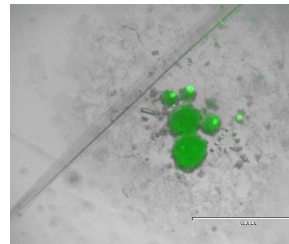
Ad5F35EGFP



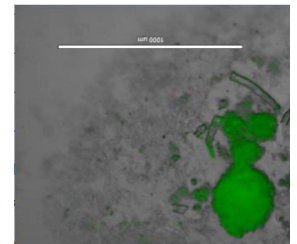
346 μm



388 μm

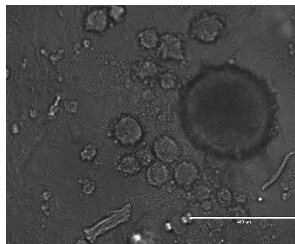


353 μm

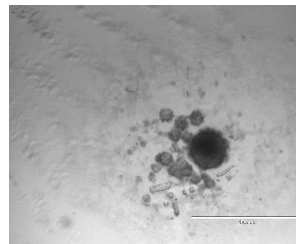


323 μm

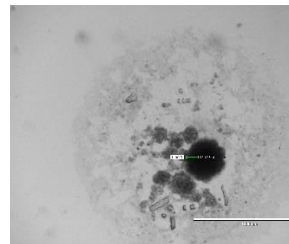
Ad5F35-WT



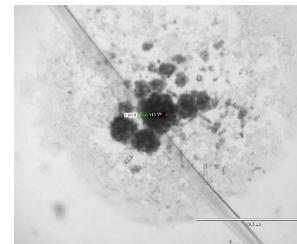
429 μm



390 μm

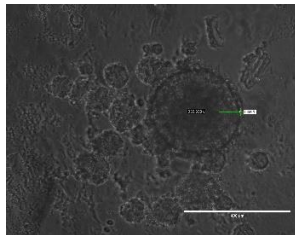


337 μm

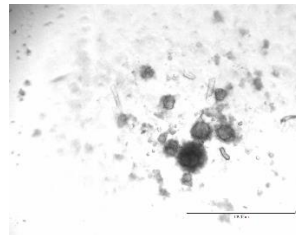


314 μm

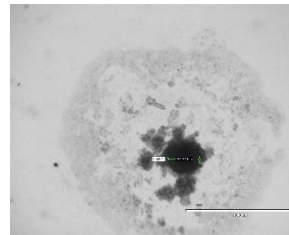
Ad5F35-CDC20



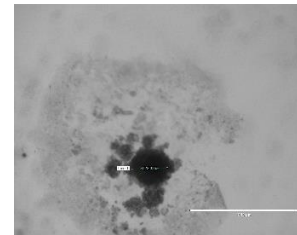
330 μm



311 μm



295 μm



222 μm

Figure 34 – Infected 911 Homotypic MCTS. Bar represents 1000 μm

911 homotypic MCTS. The top series are uninfected spheroids, the second infected with Ad5F35-EGFP, the third row with Ad5F35-WT parent virus and the bottom infected with the recombinant Ad5F35-CDC20 virus. Each spheroid imaged and measured for 4 days.

3.2.4.5. *Flowcytometric Analysis of Viral Selectivity*

We wanted to assess whether there was selective infection of cancer cells over normal cells. To this end, we labelled cancer cells with a green tracker dye and left the epithelial cells unlabelled. We trypsinized the spheroids into single cell and stained these with an anti-hexon antibody stain. We ran flowcytometric analysis to see whether the green fluorescent cells contained more hexon, therefore more viral particles, than normal cells and if so, this would in turn directly mean viral selectivity for cancer cells. Unfortunately, although this laboratory work was performed (Materials and Methods - section 2.3.5), at the time of writing, data files became corrupt and were irretrievable. Time constraints meant that this part of the research could not be repeated.

4. Discussion

4.1. The ex-vivo Tissue Slice Model

The aim of this preliminary part of the project was to optimise the culture system for pancreatic tissue ex-vivo, both normal and cancerous. We also aimed to develop a comprehensive analysis system for the tissue slices covering all aspects of tissue survival including maintenance of morphology and ultrastructure, viability and functionality.

4.1.1. Tissue Morphology

The pancreatic tissue slices were produced using the Leica VT1000s vibrating blade microtome. This allowed the production of uniform sections of fresh pancreatic tissue to use in an organotypic culture system. Although this has been previously done for the culture of various other organs from different species^{57,58,72,74}, it has been notoriously difficult to apply to pancreatic tissue. The limitation with the pancreas is its softness and hence difficulty in handling and cutting, both surgically and ex-vivo. This study has shown that this is possible with the aid of a tissue corer, 3% low melting point agarose and a high frequency and low speed on the microtome. As previously mentioned, resection specimen numbers are low and the amount of tissue available for research is very limited. The size of resection specimens also varied. The combination of low-melting point agarose, tissue corer and the automated tissue slicer allowed i) optimisation of the yield of slices, therefore producing a far larger number of slices from small amounts of tissue compared to when the specimens were manually dissected and ii) production of uniform slices that are comparable in both size and viability.

Other elements were also introduced to the culturing system to determine their effect on the viability and duration of survival of the slices. These variables included i) a shaking platform which keeps the 6-well plates moving constantly at 150 rpms, ii) comparing both coated and uncoated 6-well plates. As the tissue slices produced are relatively heavy, they immediately sunk to the base of the wells, possibly limiting the exposure of the entire surface area to the culture medium. Using uncoated plates, it was hoped that this may minimise the 'sinking' effect and iii) using transwells with either a 0.4µm or 3.0µm micropores as an air-medium interface to prevent the slices from sinking to the base of the well and allow diffusion of the culture medium to the under-surface of the sections whilst allowing adequate oxygenation.

All tissue slices were fixed, embedded and subsequently H&E stained. Although numbers were too low for statistical analysis, morphological examination together with the viability scoring did not reveal an added benefit of using uncoated culture plates, the porous transwells or the shaking platform. Although similar shakers have been used by other groups during ex-vivo culturing of other organs such as breast and liver, its specific benefits have not previously been assessed in human pancreatic tissue^{13,74,75}. Variable revolutions, anywhere between 30 – 150 rpm/minute have been used. Olinga et al⁷⁶ showed that a 6-well shaker incubation system at 60 rpm was beneficial and superior to other agitation methods to improve oxygenation and viability in rat liver slices. In this study, the shaker was set at its lowest setting of 150 rpm, and the overall finding was that this did not offer any additional benefit to the viability of the tissue; on the contrary slices that were shaken seemed to do worse overall, having more grade 0 and I regions than grade II. The higher setting compared to that used by Olinga et al⁷⁶ may be partly responsible for this. However, given that non-shaken slices seemed to survive much better, with a higher proportion of the tissue scored at grade II, the shaker seems unlikely to add any survival benefit even at a lower setting. In contrast to other groups such as van Geer et al¹⁷, we have shown that pancreatic adenocarcinoma explants survived better in our modelling system and retained excellent morphology compared to normal tissue. After 48 hours in culture all tumour tissue without exception had a viability grade II, whereas normal tissue began to show poorer viability and some death. This was not surprising given the biology and heterogeneity of tumour cells, which makes them less vulnerable and better able to adapt and survive in hostile conditions. Not only did the tumour tissues demonstrate better survival, moreover, within 24 hours they began to show signs of hyperplasia, with new tumour cell growth at the periphery of the tissues. This only underlines the aggressive nature of pancreatic adenocarcinoma and its propensity to adapt, survive and grow.

4.1.2. Tissue functionality

The intention of irradiating the pancreatic slices was to define how the level of amylase release from the explants into the culture medium reflected the functionality of the viable tissue. In other words, do healthy pancreatic tissue slices retaining their ultrastructure, morphology, and hence function, release high or low levels of amylase into the surrounding medium? In the clinical context, insult to the pancreatic gland, such as an alcohol binge for example, resulting in acute inflammation causes a reactive serum hyperamylasemia. This is indicative of acute damage or insult. The 'normal' reference range of amylase in human serum used by clinical laboratories cannot be used as a guide in this culture model as in the human body amylase is released from the exocrine pancreas in a very controlled manner secondary to feedback mechanisms. With the pancreatic explants used in this study however, this will not be the case. Much of the release of amylase into the surrounding culture medium is likely to be, at least in the first instance, a result of capillary leakage from the freshly cut surfaces. Furthermore, human serum cannot be compared to conditioned culture medium as they would have differing properties. Additionally, it is not normal to find amylase in human serum, it is only found in the diseased state of the pancreas.

As there was no indication from the literature what concentration of X-irradiation would be required to kill the pancreatic cells, a series of different concentrations were tried. It was hoped that this would generate a trend going in one of two ways, either; 1) an inverse relationship between cell death and amylase activity, i.e., as more cells die, less amylase is released into the surrounding medium, or 2) as more cells die, more amylase is released due to cell lysis.

Unfortunately, irradiating slices from normal pancreas did not answer the question. Looking at the H&E stains of the pancreatic sections, the cells were completely devitalised, yet still intact after the first 10 minutes at maximal irradiation. Despite the peaks and troughs of amylase activity in the surrounding culture medium of the irradiated slices, these could not be directly explained by the tissue morphology. There is a disassociation between morphological appearance and release of amylase by devitalised cells. This does not allow drawing of any conclusions regarding the trend of amylase activity.

The dose of irradiation was evidently too high and a series of lower doses would be required to assess what happens to amylase release with gradual cell loss and hence function. Multiple samples would need testing to produce a general trend.

In conclusion this experiment failed to answer the question of precisely how amylase activity of the normal pancreatic tissue explants behaves over time as the morphology of the slices

deteriorates. In the amylase assay (Section 3.1.2.3) the overall pattern of enzyme activity was a decrease in amylase activity in the supernatants of the normal pancreatic explants over time. It was very high after the first 24 hours of culture, followed by a rapid decline thereafter. This finding was consistent regardless of any variable added to the culturing system. Van Geer et al¹⁷ also demonstrated the same finding in amylase activity, with maximal secretion at day 1 and a decline below detection levels at day 3, also using a colorimetric assay. Although the amylase activity in the medium on day 3 in the experiments performed in this study was very low, they were not below detection levels. As they were able to maintain their slices viable with good morphology for a minimum of 3 days (also assessed using a viability scoring system on H&Es), Van Geer et al¹⁷ interpreted this to mean that the pancreatic slices were not only viable, but they also retained function for at least up to two days. They did not mention however whether their assay was used for normal or cancerous tissue, or both.

Although the results shown here are consistent with those of Van Geer et al¹⁷ both morphologically and on assessment of the amylase activity, their interpretation of the amylase results may not necessarily be true. The irradiation experiment shows that with cellular lysis, amylase is released into the surrounding medium. This could be applied to the peak of activity after 1 day. Because the tissue is sliced, this will cause acinar and ductal leakage and hence release of enzyme into the surrounding culture medium and a 'burst' of amylase release. From that point on, the gradual reduction of amylase activity on the ensuing days could just represent a more controlled release of the enzyme.

Nonetheless, as the results in this study are consistent with those of the Van Geer¹⁷ group and both showed that reduced amylase activity is associated with a poorer morphological grading, it may be assumed that because amylase activity decreases with increased time in culture it may, therefore, also represent poorer tissue function. Nevertheless, as we failed to demonstrate a baseline for the amylase activity of these tissue slices, this remains a poor test for functionality of the normal pancreatic slices.

When the amylase assay was performed on the supernatants of the cancerous sections, the amylase activity was barely above zero. Looking at the H&E sections of the corresponding tissue, they showed 100% cancerous cells with no residual normal pancreatic tissue. This seems to be a very reasonable finding as amylase secretion/release occurs from intact acinar cells and therefore in the absence of these, due to their replacement by tumour cells, no amylase is present. This clearly demonstrates that the amylase assay is not an appropriate test of function of pancreatic cancer tissue slices.

An appropriate test that could be applied to the tissue explants is an ATP assay. This will assess the presence of metabolically active cells and therefore can be applied to either normal or pancreatic tissue.

4.1.3. Tissue viability

TUNEL is an apoptosis assay that detects DNA fragmentation by incorporation of labelled nucleotides onto the free 3' OH ends of DNA fragments using a terminal deoxynucleotidyl transferase enzyme (TdT). The TACS.XL-Blue kit used in this study produced an intense blue stain in cells with DNA fragmentation. This was used with the aim of correlating apoptosis with morphological grading from the H&E stains and functionality from the amylase assay, therefore producing a comprehensive and detailed analysis system for the pancreatic tissue explants.

After optimisation of the assay, the results demonstrated that there was, overall, very low levels of apoptosis in all the pancreatic slices using the TUNEL assay. This was consistent irrespective of whether the tissue was i) in early or late stage of culture, ii) normal or cancerous and iii) variables in culturing conditions (i.e., shaking platform, transwells etc.). DNA fragmentation is a late stage in apoptosis and it could be that apoptotic cells are not being detected with this assay. However, detailed examination of all the H&E sections, whether normal or cancerous tissue, showed that cell death in these pancreatic explants was mainly by necrosis and not apoptosis. There are no other reports in the literature describing mode of death in pancreatic tissue explants.

As there were very few apoptotic bodies on the H&Es and low-level staining using the TUNEL detection kit, this assay was therefore felt an inappropriate method of assessing tissue viability in this culture system and was therefore not applied to further specimens. Although an alternative assay could be used to detect earlier stages of apoptosis, because of the very low level of death through apoptosis detected by H&E, this seemed to be pointless, as well as being very costly and time-consuming. Death detected by necrosis, and indeed apoptosis, is probably best visualised on H&E and quantified using the viability grading system described in this report.

4.2. Multicellular Tumour Spheroids

The aim of the preliminary part of the project was to optimise the culture system for pancreatic tissue *ex-vivo*, both normal and cancerous. We also aimed to develop a comprehensive analysis system for the tissue slices covering all aspects of tissue survival including maintenance of morphology and ultrastructure, viability and functionality.

The *ex-vivo* slice model most closely emulates the *in-vivo* environment, as the work is performed directly on primary human tissue which retains the cellular ultrastructure and human tumour milieu in contrast to simple cell and transgenic mouse models or indeed 2D cellular monolayers. However, because of the aggressive nature of the disease and the late stage of diagnosis in the vast majority of cases, tissue availability was scarce. The limitation in understanding of the biology of pancreatic adenocarcinoma and the failure to find effective therapies is due to these very facts, namely advanced stage at diagnosis, limited resection specimens and hence limited human tissue for research. Therefore, an alternative culture model was required.

In 2D cell cultures, cells are deprived of the cell–cell and cell–extracellular matrix interactions and the level of cellular responsiveness is limited^{77,78}. Moreover, forcing cells to grow on flat surfaces can change their metabolism and function⁷⁹ and it is well documented that the cell culture environment can have an effect on the phenotype of cells and hence affect the cellular response to added substances, e.g., drugs⁸⁰. Therefore, a much better *in-vitro* model is three-dimensional (3D) culture as it more precisely mimics the natural cell microenvironment. As cells grow in 3D, they alter the expression of a number of proteins regulating tissue architecture, matrix interaction and growth factor signalling⁸¹⁻⁸³.

Owing to the fact that many cell lines have the ability to self-assemble, one 3D culture model is the formation of spheroids⁸⁴. Multicellular spheroids are intermediate in complexity between *in-vitro*, 2D monolayers, and *in-vivo* solid tumours in that they facilitate direct cell-cell and cell-extracellular matrix interactions, which may influence metabolism, proliferation and differentiation.

Recently, the three-dimensional (3D) multicellular tumour spheroids model has been gaining increased recognition as an intermediate step between *in-vivo* and *in-vitro* models, thus offering enhanced biological relevance in research fields, such as tumour biology and drug screening^{45,85}.

4.2.1. Homotypic Multicellular Spheroids

Successful formation of spheroids was based on already established protocols by partner laboratories using TC32, a Ewing sarcoma cell line. Although preliminary experiments were successful, the results were certainly not reproducible and therefore it was important for us to establish a protocol that achieved success in our laboratory. This involved breaking down the process of spheroid culture.

All spheroids were cultured in ultra-low adherence round/u-bottomed plates. The well shape forces all the cells to the most dependent point, the base, where they adhere to each other, forming loose or compact spheroids depending on cell type.

The most important step was optimising the seeding of each of the cell lines. We found that the optimal seeding density for the three PDAC cell lines was 1500 cells/well. This allowed for sufficient ECM production^{70,83,86} and the formation of discernible spheroids within the first 24 hrs which continued to grow for a 7-day period. At this density all cell lines formed discernible spheroids within 24 hrs. Across the literature optimal seeding densities varied amongst pancreatic cancer cell lines. This may be related to the method of spheroid formation, of which there are many. Longati et al⁷⁰ used the same methodology of spheroid formation by using the crowding agent methylcellulose, a cellulose-derived inert compound which helps cells to aggregate and form spheroids. Many previous studies^{19,34,70} also tested various starting numbers and found an optimal density of 2500cells/well for a 7-day growth period for all cell lines, including the three used in this study. At this density, the spheroids were maintained below the well documented 500µm diameter at which necrosis starts to develop in the spheroid core⁸⁶. In this study, the optimal density was considerably less. At 1500 cells/well discernible spheroids were formed after 24 hrs and, although their starting size was greater than 500µm for all PDAC, a necrotic core was not apparent until day \geq 4 days and at much greater diameters than described. Indeed, some spheroids did not become centrally necrotic even by day 7 and at diameters of $>1000 \mu\text{m}$ (see figure 16). Although ideally, the aim was to maintain absence of necrosis for the whole 7-day growth period, using fewer cells/well took much longer for the spheroids to form and they still began to disaggregate at the periphery by day 7. Clearly a greater number of cells/well would have initiated necrosis much earlier than at the observed day 4. Many factors could account for the differences in optimal seeding densities and appearance of necrosis, including more/less favourable culture conditions, differences in suppliers and culturing of the cell lines. MCTS formation is linked to various factors, such as cell type, culture technique, medium composition and volume, cell density and mechanical stress. These factors cause variability in MCTS formation, resulting in difficulties in generating reproducible spheroid formation⁸⁷.

The normal cell lines formed the most spheroidal and compact spheroids structures with very definite borders, most notable 911 cells. Similar to Sipos et al⁸⁸, we found that of the PDAC cell lines tested, Capan-1 formed the most compact spheroids in the shortest period of time and Panc-1, which are of more intermediate differentiation, formed looser cell clusters in the first 24 hrs but continued to become gradually more compact and spheroidal-like with time (see figure 16; pg 71). MiaPaCa-2 was the most challenging cell line to culture successfully and, maintain in long-term culture. It also showed a variable growth pattern. All PDAC cell lines formed very large aggregates within the first 24 hrs, some appearing spheroidal and compact but, by day 4, this was not maintained and spheroids began to globally disaggregate (see figure 16; pg 71). Others formed very large cell aggregates that appeared more sheet-like than spheroidal. They continued to grow and, in some cases, outgrew the wells and also disaggregated by day 4. This seems concordant with their documented poorly differentiated phenotype. Although those that were spheroidal demonstrated definite aggregation characteristics, unlike the other PDAC, particularly Capan-1, they had no definable outer border and were very friable on harvesting. Although many other studies recorded similar observations of very aggressive phenotypic behaviour of MiaPaCa-2; i) it had shortest doubling time when grown in monolayers and ii) had friable cell aggregates on harvesting, all studies in the literature documented a total lack of any cell aggregation^{19,70,71,877,88}. In this study, definite cohesive cell aggregation was achieved, however it was more sheet-like and not spheroidal like the other PDAC spheroids. This may be attributable to the inherent differences in cell-to-cell adhesions of different cancer cell lines which result in differences in i) formation and ii) compactness of spheroids⁷. Ivanov et al found that cell lines which formed compact spheroids expressed a high E-cadherin level, those forming tight aggregates showed accelerated expression of N-cadherin, whereas when cells lose the adhesion molecules entirely, they also lose the ability to aggregate into a sphere⁸⁹.

Spheroids that originated from normal cell lines (MRC5, DEChTERT and 911) were approximately 300µm after 24 hrs without an objective necrotic core. As would be expected, the PDAC spheroids were much larger after 24 hrs and their size seemed to correlate to the differentiation characteristics of their cell line. The largest aggregates after 24 hrs were formed by MiaPaCa-2 (\bar{x} = 1450 µm) which is the most poorly differentiated of the three PDAC followed, in descending order, by Panc-1 (\bar{x} = 850µm) which is moderately differentiated then Capan-1 (\bar{x} = 650µm), the most highly differentiated of the three cell lines. Sipos et al characterised pancreatic ductal adenocarcinoma cell lines (which included all three in this study) and part of this was to establish whether there is a relationship between their proliferation rate (measured by the doubling time) in monolayers and their

ultrastructural differentiation. They indeed found the most marked difference in the population doubling rate between the cell lines with the highest degree of differentiation, Capan-1 (longest population doubling rate), and that with the lowest degree of degree differentiation, MiaPaCa-2 (shortest population doubling rate). This seems to be concordant with the cultured spheroids described here, Capan-1 forming the smallest and hence slowest growing spheroids and MiaPaCa-2 forming the largest cell aggregates and hence fastest growing which indeed outgrew the size of the wells on numerous occasions.

Hypoxia is a common feature of solid tumours and develops because of the rapid growth of the tumour that outstrips the oxygen supply. Uncontrolled cell proliferation often exceeds the ability to satisfy the oxygen demand from preexisting blood vessels. This results in the formation of new abnormal vessels to supply the tumour and consequently impaired blood flow⁹⁰. The hypoxic microenvironments within solid tumours are known to contribute to chemoradio-resistance, immune suppression, increased metastasis, and an overall poor prognosis. It has been reported that tumour hypoxia can activate angiogenesis thereby enhancing invasiveness and risk of metastasis, increase tumour survival as well as suppress anti-tumour immunity and hamper the therapeutic response.

As in solid tumours, it has been widely reported by other researchers⁹¹⁻⁹³ that an oxygen gradient is maintained within the spheroid with resultant hypoxia at the spheroid core while cells at the periphery of the spheroid are not affected by oxygen diffusion limitations and therefore experience less to no oxygen deprivation⁹⁴.

Most citations quote critical cut offs, 300 μm for hypoxia and $\geq 500\mu\text{m}$ for central necrosis. This was not the case in this study. The behaviour of normal/control cell spheroids was very different to PDAC spheroids. 911 spheroids developed central necrosis between day 4-7 and an average \bar{x} of 700 μm . MRC5 did not develop central necrosis for the duration of the 7-day growth period, at which point there was evidence of peripheral cellular disaggregation but no necrosis even at diameters approx $\sim 800\mu\text{m}$ (see figure 16; pg 71).

The PDAC spheroids however showed different rates and degrees of development of increasing central necrosis. All three types of PDAC spheroids showed the fastest rates of growth days 2-4 and all began to peripherally disaggregate and lose their capsule by day 7 (see figure 16; pg 17). The most obvious central necrosis was seen in Capan-1 which also formed the most uniform and compact of spheroids with very clear capsules. Panc-1 and MiaPaCa-2 did not appear to have a necrotic core throughout the growth period despite exceeding sizes of $>1\text{mm}$ and in the case of MiPaCa-2 almost reaching 2mm. It is difficult to believe that such large spheroids/aggregates were not stripped of their oxygen and nutrient supply despite having the same culture conditions as their smaller counterparts, Capan-1.

The observation maybe explained by two hypotheses i) cell density and ii) hallmarks of cancer cells. Some of the Panc-1 and particularly MiaPaCa-2 were so large and so cell dense that it was difficult to distinguish individual cells and see if they appeared viable microscopically so a necrotic core simply may not have been detected. MiPaCa-2 is known to be a very poorly differentiated very aggressive cell line and may have just been the most proficient at transforming and demonstrating the hallmarks of cancer cell characteristics: sustaining proliferative signalling, evading growth suppressors, resisting cell death and enabling replicative immortality. Cancer cells respond differently to decreased oxygenation, leading to cell death or cell survival which partially depends on the time of exposure to hypoxia⁹⁵.

Necrosis was assessed by looking for an expanding dark core in the spheroids, the cells of which looked non-viable compared to the periphery. To better assess the precise location of necrosis, visualising evidence of a hypoxic gradient and gaining a three-dimensional view of the whole spheroid structure using Z-stack imaging would be desirable. This technique sequentially images through the spheroid at pre-defined depth intervals. This unfortunately produced very unclear images with no clear view of the cells and it was very difficult to determine exactly where in the spheroid images were derived, except at the very top and the very bottom. It was also aimed to harvest the spheroids for immunohistochemical staining analysis using markers for hypoxia, necrosis and proliferation. Due to limited laboratory time, prolonged preliminary experiments to establish the culture protocol and technical difficulties in harvesting the friable spheroids, immunohistochemical analysis had to be abandoned. Future work needs to establish improved methods for defining hypoxia and necrosis of the spheroids and being able to assess the whole 3D structure. Such methods may include:

- i) assessment of lactate accumulation: cancer cells dramatically consume much more glucose compared to non-transformed cells known as the Warburg effect, when cells make a metabolic switch from oxidative phosphorylation to aerobic glycolysis induced by the lack of oxygen;
- ii) confocal microscopy assessment of spheroids which may reveal an arrangement of cells around a hypoxic core
- iii) continue to develop the methodology in order for this to become a high throughput system and improve spheroid harvesting for immunohistochemical/H&E analysis of hypoxia and necrosis.

4.2.2. Heterotypic Multicellular Tumour Spheroids

The aim of this work was to establish an in-vivo model that most closely recapitulates the in-vitro solid tumour milieu as a replacement for the organotypic tissue slice model and to use these for the assessment of various genetically-modified adenovirus-5 viruses as oncolytic viruses.

Once the protocol for homotypic MCTS generation was established, PDAC were used, combining them with either MRC5 (primary human fibroblast cells) or DEChTERT (pancreatic ductal epithelial cells immortalised by hTERT) as representatives of normal cells to mimic the in-vitro solid tumour environment.

MiaPaCa-2 failed to form MCTS with either cell line, MRC5 or DEChTERT. This is most likely due to its poor aggregational ability as widely reported in the literature and as demonstrated in the homotypic MCTS experiment (see section 3.2.2). This was therefore abandoned as a cell line at this stage.

In the scientific literature, authors have frequently termed cells grown in 3D culture as “multicellular tumour spheroids” or MCTS, despite these being formed of one cell type; most studies have hence based their conclusions, for example on drug responsiveness, oncolytic virus efficacy tumour behaviour etc on these ex-vivo but ‘in-vivo--mimicking’ models. This is however misleading and misrepresentative. Cellular monolayers are also “multicellular” as they contain large cell populations. The idea of developing 3D models such as spheroids is not only to recapitulate the structural and biochemical complexity (presence of multiple cells/multicellular and mimic the physical characteristics such as i) cell-cell and cell-extracellular matrix interactions, ii) hypoxic gradients and iii) developments of ECM components) but also the biological complexity of PDAC. Aside from their physical characteristics and ECM components, solid tumours are heterogenous containing multiple cell types such as non-tumour stromal cells, mesenchymal stem cells, endothelial cells, fibroblasts, connective-tissue cells, and immune cells. All of these cells communicate with one another via specific junctions (tight and gap junction) that maintain and regulate a “perfect” tumour microenvironment. Moreover, it is this heterogeneity and the dynamic interaction between the different cell types that results in tumours acquiring new phenotypes, such as multidrug-resistance, promotion of invasiveness and metastasis. Therefore, we propose that these “multicellular” spheroids should more correctly be labelled as homotypic MCTS as they are formed of a single cell type and hence limiting the reliability and application of the results.

At the time of this research, we found no other studies in the literature that formed heterotypic multicellular PDAC spheroids and hence the formation of heterotypic PDAC MCTS is novel.

Studies on numerous cell lines such as pancreas, breast, HCC, non-small cell lung cancer, colon and renal cancers have shown the importance of the hepatocyte growth factor (HGF) – mesenchymal epithelial transition (MET) signalling pathway in the onset, progression and metastasis of multiple tumours⁹⁶. The HGF-MET signalling pathway is activated in solid tumours from HGF-secreting fibroblasts as a result of the tumour-stroma interactions⁹⁷. HGF-Met signalling pathways are uncontrolled in human cancer with overexpression of HGF. This dysregulation contributes to aspects of tumour progression, such as the disaggregation of neoplastic cells from the tumour mass and colonizing new tissues to form metastases⁹⁶. This peripheral disaggregation was an observation that was particularly prominent in all PDAC containing spheroids when compared to normal cell spheroids towards the end of their observed growth period, as mentioned above.

In order to recapitulate this, we used MRC5, a fibroblast cell type, as it is known to secrete high levels of HGF⁹⁸.

Panc-1 successfully formed MCTS with MRC5. This is clearly demonstrated in figure 20, where the Panc-1 cells are labelled green and MRC5 labelled orange. Although these were not spheroidal in shape, they were cohesive tight aggregates without an obvious capsule. The spheroids formed within 24 hrs with Panc-1 cells far outnumbering the normal cells, as would be anticipated of highly proliferative moderately differentiated cancer cells compared to normal cells and their ability to strip oxygen and nutrients from their environment.

The MRC5 cells have a limited lifespan in culture and the cells in use in the laboratory stopped growing. Although the PDAC cell lines used were at some point derived from either primary pancreatic cancer tissue or metastasis, they have been frozen and cultured in laboratories for unknown periods of time. The cells have undergone numerous passages of culture and almost certainly developed transformations. This makes the cells used less representative of the original human cancers, limiting their representation of the solid tumours. Although spheroids have many advantages as a representative culture platform for preclinical studies, the phenotypic changes occurring in laboratory cultured cells reinforces the need to find more representative models. One such model is organoids. Organoids are derived from patient-derived embryonic stem cells that are expanded and subsequently differentiated through a multistep protocol which eventually achieves the fully differentiated structure that more closely resembles the organ not only in its structure but also in function⁹⁹.

As stem cells are differentiated to achieve this, it avoids the laboratory acquired phenotypic transformations of multiply passaged cell lines.

Therefore, given the difficulties in using MRC5 cells, the research turned to forming heterotypic spheroids with DEChTERT to form MCTS.

Both Capan-1 and Panc-1 successfully formed MCTS with DEChTERT as demonstrated in figure 22. Despite the fact that in homotypic MCTS Capan-1 formed the most cohesive spheroidal and regular shaped spheroids, in combination with DEChTERT they formed loose irregular aggregates (figure 22) in the first 48 hrs. However, these became more cohesive and tightly bound by day 4 when the cellular density had clearly increased, and as anticipated, the green labelled cancer cells far outnumbered the fibroblasts. No peripheral capsule formed in the 4-day growth period. The spheroids did however clearly demonstrate a heterotypic cellular population with green-labelled cancerous cells and unlabelled fibroblasts. Because of the dense cell population and the overlap of green fluorescent labelling it was much more difficult to assess the spheroids for central necrosis.

The spheroids did not dramatically increase in diameter during the 4 days, only by a maximum average $\bar{x} = 150 \mu\text{m}$. They did however become much more cell dense centrally (figure 22) and appeared to be composed of predominantly cancer cells by day 4. Again, this observation was difficult to quantify because of the lack of a three-dimensional view into the body of the spheroid which posed a limitation in making comprehensive observations. If time permitted, confocal microscopy could have been used as a better method of visualising the ultrastructure of spheroids in three-dimension.

On co-culturing Panc-1 with DEChTERT, these formed compact, tightly- bound spheroids within 24 hrs, remained static until day 4 when they showed a growth acceleration, again with a far greater number of cancer cells compared to fibroblasts. The two cell progenies were distributed differently in the two heterotypic MCTS. In Panc-1/DEChTERT, there was a more peripheral distribution of the cancer cells with the fibroblasts remaining more central. Because of the lack of tumour cells centrally, a necrotic core could easily be detected which appeared at an approximate $\bar{x} = 450\mu\text{m}$, in keeping with the widely reported $500 \mu\text{m}$. This arrangement of peripheral tumour cells and central necrotic core reconfirms what many have observed on H&E staining of spheroids and solid tumours where cancer cells are arranged around a necrotic core.

No studies were available at the time of this research that had performed similar co-cultures with fibroblasts and PDAC. However, in a postdated study by Broekgaarden et al⁹⁷, they co-cultured MRC5 with MiaPaCa-2 and ASPC-1, another PDAC cell line. They observed that combining MRC5 with both PDAC cell lines resulted in an initial notable size reduction of the

spheroids for the first 2 days followed by accelerated spheroid growth by day 4 compared to the linear growth pattern of homotypic PDAC MCTS. It is difficult to explain the observation described here and followed later by Broekgaarden et al⁹⁷ in the co-culture of PDAC with fibroblasts and epithelial cells. This may be attributable to the production of downstream signalling pathway products as a result of the interaction of cancer cells with their normal cellular milieu which we attempted to recapitulate in these heterotypic spheroids. PDAC is characterised by a dense fibrous stroma, which varies widely between patients and has been reported to be 40 -80% on histopathology specimens. The fibrotic tissue is not only a major impediment to therapeutic drug penetration into the tumour³⁴, but it also modifies the characteristics of the tumour in complex ways^{100,101}. The desmoplastic reaction is responsible for the generation of these fibrotic lesions and is driven by intricate crosstalk between PDAC tumour cells and cancer-associated fibroblasts (CAFs). Further work is required to understand whether it is the by-products of this cancer cell – fibroblast cross talk that causes the initial pause/regression in spheroid growth followed by a growth acceleration.

4.2.3. Adenoviral Transduction, Infection and Oncolysis

4.2.3.1. Homotypic MCTS Infection

Adenoviruses (Ad) have shown promising results in the therapeutic treatment of cancer. Adenovirus type 5 (Ad5), is a species C virus and is the most extensively utilized type in gene therapy. These viruses can be utilised in cancer therapy in one of two ways, either i) by genetically modifying the virus to render it replication deficient and use it as passive delivery vector or ii) as replication competent oncolytic viruses⁶³.

In this study two strains of the Ad5 were used; Ad5F35 wild type and Ad5F35-CDC20, both replication competent viruses, to transfect spheroids. Ad5F35-CDC20 was made in our laboratory by Magdalena Karwatka as a recombinant virus in which the 200bp promotor fragment of the human CDC20 gene has replaced the endogenous viral E1A promoter. The p53 cellular tumour suppressor gene product binds to represses transcription driven from the 200bp CDC20 promoter. This should permit virus replication specifically in cancer cells that are p53 negative, as it is widely documented at least 75% of PDAC have p53 mutations or deletions¹⁰².

Recombinant oncolytic viruses offer important advantages over traditional methods, one of the most crucial of these is their cancer selectivity. They are designed to be inactive within non-transformed cells but to respond to tumour cell phenotype and achieve cancer selective replication, cell lysis and spread of progeny virus to infect nearby cells⁶³.

Although many wild-type viruses show an intrinsic selectivity for replication within cancer cells⁶²⁻⁶⁴, we wanted to evaluate whether we can achieve a better cancer cell specificity with the recombinant Ad5F35-CDC20. The Ad hexon constitutes the major virus capsid protein and our recombinant Ad5F35-CDC20 has an identical hexon to the wild type Ad5virus. To this end, we labelled cancer cells with a green tracker dye and our aim was to disaggregate the spheroids into single cells and label these with the anti-hexon antibody. We used flowcytometry to evaluate whether the green fluorescent cells contained more hexon, therefore viral particles, which would in turn imply viral selectivity for cancer cells. Unfortunately, although this laboratory work was performed at the time of writing, the data files became corrupt and were irretrievable. Time constraints meant that this part of the research could not be repeated.

Recombinant adenoviruses used as vectors for gene therapy purposes frequently have a deletion in the E1 region of the viral genome (that is often replaced with a therapeutic transgene). The defective gene products are provided in a complementing cell line, thus allowing the defective viruses to be propagated. 911 cells are an immortalised human retinoblast cell line that is an E1-expressing, is highly transfectable and has favourable growth characteristics¹⁰³. This cell line was transduced with an EGFP-expressing non-replicating Ad5F35 virus as a positive control to demonstrate the ability of Adenovirus-5 to transduce spheroids.

It is clear from the immunofluorescence microscopy images that we achieved 100% viral transduction of the 911 spheroids with Ad5F35-EGFP (see figure 26). The first images that were captured of the spheroids were at 24 hrs after infection, however 60 min after incubation these spheroids were viewed using an inverted microscope and within as little as 60min the spheroids were 100% transduced.

The 911 spheroids remained compact for the duration of the 7-day growth period. A similar observation to their uninfected counterparts, is that the spheroids gradually began to peripherally disaggregate and fluorescent clusters of green cells can be seen in the medium surrounding them by day 4 and there was a background green hue to the medium from ≥ 2 .

911 cells are E1a & b gene expressing which complement the E1 defective GFP virus. This allows viral transduction into the spheroids and renders the virus replication competent within the 911 cells only. The spheroids, except for the peripheral disaggregation that is common to all spheroids including those uninfected, remained very much tight, cohesive and spheroidal. This makes it very unlikely that cell lysis, and hence viral replication, occurred. From the imaging it would appear that 100% transduction was achieved (see figure 26) but the virus remained most likely non-replicating which is contrary to what was expected.

Within the homotypic MCTS both the WT and recombinant and Ad5F35 virus blew the spheroids apart by the end of the observation period. After 24 hrs of infection, there appeared to be little effect of either virus on any of the PDAC MCTS except for possibly Panc-1, which showed minimal peripheral disaggregation with a few loose cell clusters in the surrounding medium and a transformation from a tightly bound spheroid to a slightly looser aggregate (see figure 27) By day 4 however all spheroids had largely disintegrated with little residual intact structure. By day 4 the medium was filled with loose cells and there was minimal to no residual spheroidal structure, most dramatically seen in Capan-1 followed by Panc-1 (see figures 27 and 28).

Objectively there was no apparent difference between the WT or recombinant virus's oncolytic efficacy and therefore transduction of both into the PDAC MCTS is assumed equal. The exception is seen with MiaPaCa-2. Very little effect on the spheroids is seen with the WT virus even by the end of the observation period (see figure 28). The recombinant virus however did show some spheroid destruction by day 2 which progressed further by day 4, yet the residual spheroid at the end of the 4-day infection period was the largest of all the PDAC MCTS (see figure 28). This differential oncolysis between the PDAC MCTS may be explained by the known degree of differentiation of each of the PDAC cell lines; Capan-1 most highly differentiated and least aggressive, Panc-1 moderately differentiated and intermediate in aggression and MiPaCa-2 them most poorly differentiated and most aggressive. One would anticipate the most well differentiated tumours to respond best to therapy and the most poorly differentiated to respond the least, which is what we have shown here with these homotypic MCTS.

As mentioned above, the MiaPaCa-2 spheroids only seemed to disaggregate with the recombinant virus. Although all three cell lines are known to have p53 deletions^{9,36,38}, there are several different p53 codon mutations, some more common than others^{39,102}. It may be that the p53 codon mutation in MiaPaCa-2 accounts for its more aggressive phenotype, degree of differentiation and oncolytic virus responsiveness. Further work is required to elucidate whether the specific p53 mutation in each of the PDAC cell lines contribute to their phenotype.

P53 mutations can also occur in either early or late tumorigenesis, depending on the origin of cancer types, and strongly facilitate onset or progression of cancers¹⁰⁴. This too may have a role in the growth kinetic and oncolytic virus responsiveness of the more aggressive PDAC cell lines.

We have have described an 'infected halo' that appears around homotypic MCTS after they have been infected with Ad. 5-base virus. This seemed to only appear in spheroids that weren't completely disaggregated by the virus and had a residual central spheroid at the end of the infection period, i.e., Panc-1 and MiaPaCa-2. Capan-1 was completely blown apart and there was no residual spheroid at the end of the infection period (figure 28). This may be explained by one of two hypotheses or indeed both. Most spheroids developed a peripheral capsule; the halo may simply represent lysed cells contained within a partially intact capsule. The halo also predominately surrounded the more aggressive PDAC which formed larger spheroids and had a residual central spheroid structure at the end of the infection period. This therefore may mean that virus transduction, proliferation and hence cancer cell lysis was restricted to the periphery of the spheroids. Larger spheroids would outstrip their oxygen

and nutrient supply much quicker because of the greater number of cancer cells. They therefore would have a large hypoxic core and a larger residual central spheroid structure at the end of the infection period as transduction efficiency would be reduced. It is well document in the literature that used alone, oncolytic viruses are restricted to the peripheral proliferating zone of spheroids^{36,38,39,102}.

Another element to contemplate when considering efficacy of viral transduction is this phenomenon of the observed spheroid capsule. What is the capsule composed of? A parallel could be drawn with the observed “edge effect” in pancreatic explants, which under light microscopy was seen as an outer circumferential layer of newly grown highly proliferate cells, likely formed here given the maximal exposure to surface nutrients. The spheroid capsule also most likely represents new growth cells with a high turnover, “the proliferative zone”, which is a few cells thick, again positioned on the outer surface of the capsule given its maximal exposure to surface nutrients and akin to the well described “zonation” in spheroids. Do surface exposed cells have preferential growth characteristics purely because of their maximal exposure to nutrients or does this normoxic/hyperoxic positioning stimulate production of surface ligands that aid viral transduction which are not produced in the spheroid core?

The spheroid capsules were most discernible and much more substantial in thickness in i) normal (contrary to the pancreatic explants) and ii) highly differentiated, less aggressive cell lines that responded the most to Ad killing. Are there components of the spheroid capsule that aid viral transduction? Could recombinant viruses be further engineered to include elements that complement the spheroid capsule and enhance viral infection and transduction to a greater extent? Given that the capsule was most conspicuous in normal and less aggressive PDAC cell line spheroids, could increasing the ratio of normal:cancer cells further potentiate oncolysis? Further work on the ultrastructure of the spheroid capsule using, for example confocal microscopy, is required to further understand characteristics of the spheroid capsule.

It is important to remember that several limitations exist to using Ad5 as an oncolytic virus. These include i) high levels of anti-Ad5 neutralizing antibodies in the population, ii) binding of the Ad5-hexon to blood coagulation factor X which leads to liver sequestration and toxicity, and iii) reduced expression of the primary receptor CAR on many tumours. The latter point is frequently overcome (as in this study) by replacement of the Ad5 fibre, the ligand for the CAR receptor, with the Ad35 fibre that interacts with the widely and highly expressed CD46 surface receptor molecule.

Postdating our research in 2021, Varudkar et al¹⁰⁵ used a recombinant oncolytic parainfluenza virus with and without natural killer (NK) cells to see if they mediated the killing of infected and non-infected lung cancer cell spheroids. Varakudar et al¹⁰⁵ showed that combining NK cells with lung cancer spheroids that were infected with a recombinant parainfluenza virus resulted in surface expression of glycoproteins/ligands on infected cells which i) aided viral attachment and ii) mediated entry into target cells. This resulted in significantly increased killing of both the infected outer layers and the uninfected core of 3D lung cancer spheroids.

NK cells are an integral part of the innate immune system and play pivotal roles in clearance of viral infections as well as tumour cells^{106,107}. NK cell adoptive therapy is a promising approach to cancer immunotherapy, since NK cells do not require prior sensitization to antigens to kill transformed cells and they can be highly cytotoxic towards tumour cells¹⁰⁸⁻¹¹⁰. From the observations we have made with oncolytic Ad5 on PDAC MCTS; i) appearance of a spheroid capsule, ii) probable killing of only surface cells on the more aggressive cancer cell lines and iii) remnant intact likely uninfected core; the addition of an immune cell such as NK cells is an exciting area to explore. The presence of a spheroid capsule may mean presence of viral attachment ligands and hence better viral attachment and penetration. Addition of NK cells may result in surface expression of ligands such as glycoproteins, like that seen lung cancer spheroids¹⁰⁵. This could potentiate infection, transduction and killing of those spheroids originating from more aggressive PDAC cell lines that don't possess a spheroid capsule. Having an immune component may also result in the induction of cytokines and increase the susceptibility of cancer cells.

Combining cytotoxic chemotherapies with immunotherapy is certainly an emerging area in the treatment of this lethal disease and is employed in the clinical setting of many cancers including PDAC.

4.2.3.2. Heterotypic MCTS Infection

As PDAC solid tumours have a dense fibrous stroma and it is well documented that's indeed this stroma that at least partially contributes to its resistance to therapy^{18,100,101}, our aim was to co-culture the fibroblast cell line MRC5 with the three PDAC cell lines to make solid tumour representative ex-vivo MCTS. Our objective was to assess their responsiveness to oncolytic viral infection and evaluate whether indeed the presence of fibroblasts makes them more resistant.

At the time of the experimental work, we were the first group to successfully coculture a PDAC cancer cell line and a fibroblast cell line, Panc-1 and MRC5, and form heterotypic

PDAC MCTS (see figure 20). Unfortunately, thereafter, MRC5 ceased to grow in monolayers most likely because of transformations secondary to multiple passages. This line of the work was therefore discontinued. However, given more time it was aimed to make PDAC MCTS with all the PDAC cell lines and infect them with Ad5 as we did with their homotypic counterparts. Furthermore, given the interpatient variability in the density of fibrous content within PDAC, quoted to be 40- 80%^{101,130}, and that the presence of a more dense stroma confers a more aggressive phenotype, our intention was to vary the proportion of fibroblast:cancer cells within the spheroids to assess whether there would be differential response to the oncolytic virus. This is a line of future work.

Another characteristic that renders PDAC so aggressive, is its propensity of early local invasiveness and ability to disseminate to form distant metastasis. Tumour dissemination is based on the so-called epithelial–mesenchymal transition (EMT), a process whereby epithelial cells (known for their apical-basal polarity and attachment characteristics) are transformed into mesenchymal cells possessing high mobility and migration potential¹¹¹. Moreover, EMT has been shown to be a significant contributor to chemoresistance in several cancers including pancreatic cancer¹¹²⁻¹¹⁴. The transition of solid cancer cells from an epithelial to a mesenchymal phenotype increases their migratory and invasive properties, thus promoting metastasis^{112-114,132}.

We therefore went on to evaluate the relationship between PDAC cell lines and an epithelial cell line, DEChTERT, in MCTS. We co-cultured the two to successfully form a second variety of heterotypic PDAC MCTS (see figures 21 and 22) and went on to infect them with Ad.

All PDAC MCTS and 911 MCS, used as a positive control, were infected with Ad5F35-WT and Ad5F35-CDC20. In addition, the 911 cells were again infected with a third virus, Ad5F35-EGFP as a proof of concept – transducibility of the MCTS by Ad5-based virus.

We observed little difference in spheroid destruction between the WT virus and the recombinant virus (see figure 27 and 28) with both Capan-1 and Panc-1/DecHtert MCTS, a finding similar to their homotypic counterparts.

As described earlier, homotypic PDAC MCTS showed little disaggregation in the first 24 hrs but began to disaggregate 24-48hrs which continued to increase until day 4. The viral oncolysis mainly occurred at the periphery with intact residual central spheroids seen with both PDAC MCTS.

In contrast, the degree of spheroid destruction was much less marked in the heterotypic spheroids compared to their homotypic counterparts – fewer disaggregated loose cell clusters in the surrounding medium and larger residual central spheroids. The intact residual

spheroids were observed in both PDAC cell line spheroids, although these were somewhat smaller in the Capan-1/DEChTERT MCTS. Conversely, the homotypic Capan-1 MCTS had minimum/absent central residual central spheroid at the end of the infection period with both viruses.

This would imply that combining PDAC cell lines with epithelial cells in MCTS confers a more resistant phenotype. Like in-vivo solid tumours, the presence of epithelial cells and their interaction with PDAC, may result in a phenotypic transition from epithelial to mesenchymal, i.e., EMT. EMT not only results in invasiveness and cellular migration, but also has a role in the establishment of an immunosuppressive tumour microenvironment^{115,131}. Moreover, the induction of EMT confers therapy resistance in tumour cells that leads to a reduction of proliferation rate and increased expression of both antiapoptotic proteins and transporters belonging to ATP binding cassette that are responsible for drug efflux^{116,133}.

Future work needs to be done to look for molecular markers of EMT in the PDAC cell line/epithelial MCTS. EMT is characterized by a loss of epithelial cell markers, such as cytokeratins and E-cadherin, followed by an upregulation in the expression of mesenchymal cell markers, such as N-cadherin, vimentin, and fibronectin¹¹⁷. Staining for the pattern of change in these proteins would indicate whether there is a shift to a mesenchymal phenotype.

We wanted to assess whether there was selective viral infection of cancer over normal cells. To this end, we labelled cancer cells with a green tracker dye and left the epithelial cells unlabelled. We trypsinized the spheroids into single cells and stained these with an anti-hexon antibody stain. We ran flowcytometric analysis to see whether the green fluorescent cancer cells contained more hexon, therefore viral particles, compared to normal cells and if so, this would in turn directly mean viral selectivity for cancer cells. Unfortunately, although this laboratory work was performed, at the time of writing, data files became corrupt and were irretrievable. Time constraints meant that this part of the research could not be repeated. However, it would be crucial to repeat this work in future as cancer selective oncolytic viruses are essential in the clinical setting. This would allow for i) active cell killing mechanisms which are independent of programmed death mechanisms, therefore should decrease the emergence of acquired drug resistance, ii) amplification of active agent within the tumour thus avoiding unnecessary exposure to normal tissues and maximising therapeutic index, iii) tumour selective expression and secretion of encoded anticancer biologics, providing a new realm of potent and cost-effective-targeted therapeutics and iv) lytic cancer cell death results in a proinflammatory microenvironment and the potential for induction of an anticancer vaccine response⁶³.

There are several studies post-dating our research on non-pancreatic cancer cell lines that have been co-cultured with fibroblasts to form heterotypic MCTS. However, to date there are no studies that have combined any cancer cell line with epithelial cells and therefore we have no point of comparison, whether on PDAC cell lines or other tumour entities. This is a novel area of research that with further exploration will provide invaluable understating of PDAC solid tumour biologics, therapy responsiveness and the emergence of novel therapies.

Conclusion

In summary the ex-vivo culture system for normal and cancerous pancreatic tissue explants has been optimised to generate maximal yield from minimal amounts of tissue from surgical resection specimens. The generated tissue slices were uniform in size and dimensions and hence can be used for comparison of several experimental conditions within a single tumour specimen. It has also been shown that the survival of pancreatic tissue can be maintained for a minimum of three days with excellent morphology and that pancreatic adenocarcinoma explants survive better and, likely longer, compared to normal tissue. It has also been demonstrated that morphological, viability and functionality assays can be applied to the study of organotypic cultures of the pancreas.

We have also, for the first time, produced heterotypic MCTS using pancreatic ductal adenocarcinoma cell lines of varying degrees of differentiation with two different normal cell lines that are normally present in the in-vivo solid tumours, fibroblasts and epithelial cells. We have also shown that the heterotypic MCTS can be infected and transduced by two oncolytic Ad5-based viruses and these show an oncolytic response that is concordant with their grade of differentiation. Furthermore, we have shown that the presence of both epithelial and fibroblast cells has a negative oncolytic effect of Ad5 on spheroid destruction.

PDAC remains a dismal disease with poor prognosis, few therapeutic options and very poor outcome even when diagnosed early. Diagnosis at an advanced stage and low resection numbers results in minimal human tissue available for research purposes as described in this study. This therefore means that any promising therapeutics almost never into clinical research. In spite of the low numbers, we have established and optimised a research platform for the most representative of tumour models, the tissue explants. These slices originate from human normal and cancerous tissue, retain their ultrastructure, cell-cell and cell-matrix interactions. It is this intricate cancer milieu with its rich architecture that hinders drug penetration and efficacy. Now that the ground work for this ex-vivo cancer model has been performed, with collaboration with other centres, this can be expanded for preclinical research to better understand the biologics of PDAC and test the efficacy of therapeutics to produce results of statistical significance. The direct work on human tissue with its preserved TME will also novel therapeutics to enter into clinical research.

Given the limitation in the availability of human tissue, multicellular tumour spheroids are a very attractive laboratory generated 3-dimensional model that recapitulates the tumour microenvironment. We were able to optimise every part of their culture conditions and go on to generate homotypic and heterotypic PDAC MCTS and at the the time of this research, this study was the first of its kind to generate the latter. Furthermore, now that their generation

and culture conditions have been optimised, given the innate heterogeneity of PDAC particularly in the variation of its stromal content, the use of the heterotypic MCTS will be invaluable. Being able to include and modulate the ratio of a variety of non-cancer TME cells:cancer cells will make heterotypic MCTS further representative of solid tumours and serve as an ideal laboratory generated intermediary between tissue slices and solid tumours.

With further laboratory time, MCTS can serve as a high throughput model for the preclinical assessment of much needed new therapeutics, including single agent chemotherapeutics, multiple agent chemotherapeutics as well as other more novel therapies such as immunotherapies, viral vectors and oncolytic viruses, the latter demonstrated here with promising results.

5. Future Work

5.1. *The ex-vivo Tissue Slice Model*

Further work for this part of the project will consist of the following priorities:

- To increase the number of specimens assessed by the methods represented in this report to produce numbers that are statistically significant; collaborations with other centres
- To culture pancreatic tissue slices, both normal and cancerous, for longer and start removing them beyond the 4-day point to see how long they remain viable with good morphology, functionality and ultrastructure
- To replace the amylase assay as a test for functionality with an ATP assay, as this will detect metabolically active cells and will be appropriate for both normal and cancerous tissue
- The long-term goal of this work is to transfect these pancreatic explants with adenoviruses as potentially useful vectors for pancreatic cancer gene therapy or as oncoviruses.
- Adenoviruses are known to cause hepatotoxicity in humans when given via certain routes. The intention is to assess this effect using fresh liver tissue. The first goal will be to optimise the culture conditions for normal liver tissue as has been done for pancreatic tissue
- Human serum Factor X is known to potentiate the delivery of adenovirus to the liver and hence exacerbate its toxic effects. We intend to assess this effect as well as determining whether Factor X can be used to potentiate the delivery of adenovirus to pancreatic tissue.

5.2. Multicellular Tumour Spheroids

Much of the work done in this study remains novel, and an emerging area of cancer research. A considerable amount of the experiments performed were preliminary and proof of concept. However, this has opened up many avenues for further research that is required to explore this evolving platform of organotypic PDAC research, which is desperately needed. The following areas need further exploration:

- Although uniformity was maintained in our methodology by using the same number of cells/well for all cell lines, identical culture methods and conditions, production of uniform sized spheroids whether homo or heterotopic was unreliable. Uniformity and reproducibility are essential for duplicability of results and statistical significance. More time in the laboratory to fine tune the methodology in order to make this model a reliable high-throughput system for evaluation of drugs, oncolytic viruses etc in preclinical trials is essential. There are several methods of generating spheroids including pellet culture, liquid overlay, hanging drop, spinner culture etc. These could be individually trialled with our PDAC cell lines to see which could give the most consistent and reproducible results.
- Increased proficiency of spheroid harvesting in order perform immunohistochemistry on the cut spheroids at different time points in order to i) follow their growth kinetic, ii) observe hypoxic core/differential hypoxia, iii) perform Ki67 staining to see if there is a viable peripheral proliferating zone and iv) H&E staining to look for central hypoxia/necrosis
- Perform lactate accumulation assay on spheroid medium at different time points as a quantifiable method of assessing the metabolic switch from oxidative phosphorylation to aerobic glycolysis as a marker of hypoxia and comparing 3D spheroids with 2D monolayers
- Vary cancer cell:fibroblast ratio to mimic the inter patient variability in stromal density of PDAC solid tumours and its effect on response to oncolysis by Ad5
- Explore the spheroid capsule and its role in viral transduction
- Further engineer recombinant virus to allow for the surface expression of ligands that aid infection and transduction
- Combine oncolytic Ad5 with an immune cell such NK cells to evaluate if this upregulates viral oncolysis in both the infected spheroid periphery and uninfected core such as that observed in lung cancer cell spheroids
- Repeat hexon antibody staining to ensure that Ad5 selectively kills cancer cells

- Further explore the role of epithelial cells in PDAC by testing for biological hallmarks of EMT such as down regulation of cytokeratins and E-cadherin and upregulation of N-cadherin, Vimentin and fibronectin.
- Evaluate the PDAC cell lines for their p53 mutations to see whether this has an effect on differentiation phenotype in order to ultimately produce a recombinant virus that compliments this.
- Compare organoids as an experimental model which better recapitulates the in-vivo solid tumour and avoids transformed laboratory grown cells.

6. References

1. Elghazawy RM, Verbeke CS. Pathology of pancreatic tumours. *Surgery*. 2010;28(5): 189-197.
2. Stanger BZ. About Pancreatic Cancer. Penn Pancreatic Cancer Research Center. 2019.
3. Carpelan-Holmstrom M, Nordling S, Pukkala E. Does anyone survive pancreatic ductal adenocarcinoma? A nationwide study re-evaluating the data of the Finnish Cancer Registry. *Gut* 2005; 54: 385-7
4. Fechner H, Haack A, Wang H, Wang X, Eizema K, Pauschinger M, Schoemaker R, Veghel R, Houtsmuller A, Schultheiss HP, Lamers J, Poller W. Expression of coxsackie adenovirus receptor and alpha-integrin does not correlate with adenovector targeting in vivo indicating anatomical vector barriers. *Gene Ther* 1999; 6: 1520-1535
5. Kitel R., Czarnecka J., Rusin A. Trójwymiarowe hodowle komórek—Zastosowania w badaniach podstawowych i inżynierii tkankowej. *Post Biochem*. 2013; (59):305–314.
6. Sant S., Johnston P.A. The production of 3D tumor spheroids for cancer drug discovery. *Drug Discov. Today Technol*. 2017; (23):27–36. doi: 10.1016/j.ddtec.2017.03.002.
7. Han SJ, Kwon S and Kim k. Challenges of applying multicellular tumor spheroids in preclinical phase. *Cancer Cell International* 21: 152. doi.org/10.1186/s12935-021-01853-8.
8. Gabriel ANA, Jiao Q, Yvette U, Yang X, Al-Ameri SA, Du L, Wang YS, Wang C. Differences between KC and KPC pancreatic ductal adenocarcinoma mice models, in terms of their modeling biology and their clinical relevance. 2020;20 (1):79-88. <https://doi.org/10.1016/j.pan.2019.11.006>.
9. Voutsadakis IA. Mutations of p53 associated with pancreatic cancer and therapeutic implications. *Ann Hepatobiliary Pancreat Surg*. 2021 Aug 31; 25(3): 315–327. doi: 10.14701/ahbps.2021.25.3.315.
10. Reyes G, Villanueva A, Garcia C, Sancho FJ, Piulats J, Lluís F, Capella G. Orthotopic xenografts of human pancreatic carcinomas acquire genetic aberrations during dissemination in nude mice. *Cancer Res*. 1996;56(24):5713-9.
11. Kloppel G, Hruban RH, Longnecker DS, Adler G, Kern SE, Partanen TJ. Ductal adenocarcinoma of the pancreas. In: *Pathology and genetics of tumours of the*

- digestive systems. World Health Organization classification of tumours. Lyon, France: IARC Press, 2000: 221-30
12. Fechner H, Haack A, Wang H, Wang X, Eizema K, Pauschinger M, Schoemaker R, Veghel R, Houtsmuller A, Schultheiss HP, Lamers J, Poller W. Expression of coxsackie adenovirus receptor and alpha-integrin does not correlate with adenovector targeting in vivo indicating anatomical vector barriers. *Gene Ther* 1999; 6: 1520-1535 7.
 13. Van der Kuip H, Murdter TE, Sonnenberg M, McClellan M, Gutzeit S, Gerteis A, Simon W, Fritz P, Aulitzky WE. Short term culture of breast cancer tissues to study the activity of the anticancer drug taxol in an intact tumor environment. *BMC Cancer* 2006; 6:86
 14. Nam S et al. Cellular context-dependent interaction between cancer and stellate cells in hetero-type multicellular spheroids of pancreatic tumor. *Biochemical and Biophysical Research Communications*. 2019; 515(1)183-189.
 15. Gupta P, Pérez-Mancera PA, Kocher H, Nisbet A, Schettino G, Velliou EG. A Novel Scaffold-Based Hybrid Multicellular Model for Pancreatic Ductal Adenocarcinoma—Toward a Better Mimicry of the in vivo Tumor Microenvironment. *Front Bioeng Biotechnol*. 2020; 8: 290. doi: 10.3389/fbioe.2020.00290.
 16. Verbeke CS, Menon KV. Redefining resection margin status in pancreatic cancer. *HPB* 2009; 11: 282-9
 17. Van Geer MA, Kuhlmann KFD, Bakker CT, ten Kate FJW, Oude Elferink RPJ, Bosma PJ. Ex-vivo evaluation of gene therapy vectors in human pancreatic (cancer) tissue slices. *World J Gastroenterol* 2009; 15: 1359-1366
 18. H.Y. Tanaka, M.R. Kano, Stromal barriers to nanomedicine penetration in the pancreatic tumor microenvironment, *Canc. Sci.* 109 (2018) 2085–2092, <https://doi.org/10.1111/cas.13630>.
 19. Zeeberg K, Cardone RA, Greco MR, Saccomano M, Nohr-Nielsen A, Alves F, Pedersen AF, Reshkin SJ. Assessment of different 3D culture systems to study tumor phenotype and chemosensitivity in pancreatic ductal adenocarcinoma. *Int J of Oncology*. 2016;49: 243-252. Doi 10.3892/ijo.2016.3513.
 20. Sajjad H, Imtiaz S, Noor T, Siddiqui YH, Sajjad A, and Zia M. Cancer models in preclinical research: A chronicle review of advancement in effective cancer research. *Animal Model Exp Med*. 2021 Jun; 4(2): 87–103. doi: 10.1002/ame2.12165.
 21. Voskoglou-Nomikos T, Pater JL, Seymour L. Clinical predictive value of the in vitro cell line, human xenograft, and mouse allograft preclinical cancer models. *Clin Cancer Res*. 2003;9(11):4227-4239.

22. Jakeman PG, Hill TE, Tedcastle AB, Fisher YDKD and Seymour L. Improved In Vitro Human Tumour Models for Cancer gene Therapy. *Human Gene Therapy*. 2015; 26:249-256.
23. Shoemaker RH. The NC190 Human tumour cell line anti-cancer drug scree. *Nat Rev Cancer* 1006; 6:813-823.
24. Howes AL, Richardson RD, Finlay D and Vuori K. 3-Dimensional Culture Systems for Anti-Cancer Compound Profiling and High-Throughput Screening Reveal Increases in EGFR Inhibitor-Mediated Cytotoxicity Compared to Monolayer Culture Systems. *PLOS*. 2014;(9):e108282. Doi:10.1372/journal.pone.0108283.
25. Abbott A: Cell culture: biology's new dimension. *Nature* 2003, 424:870-872.
26. Ernst A et al. Genomic and expression profiling of glioblastoma stem cell-like spheroid cultures identifies novel tumour-relevant genes associated with survival. *Clin Cancer Res* 2009, 15:6541-6550.
27. Fernando A, Glaysher S, Conroy M et al. Effect of culture conditions on the chemosensitivity of ovarian cancer cell lines. *Anticancer Drugs*. 2006; 17:913-919.
28. Andreotti PE, Linder D, Hartmann DM et al. TCA-100 tumour chemosensitivity assay: differences in sensitivity in cultured cell lines and clinical studies. *I Biolumin Chemilumin* 1994;9:373-378.
29. Smith J, Stewart BJ, Glaysher S Et al. The effect of pentamidine on melanoma ex vivo. *Anticancer Drugs*. 2010;21:181-185.
30. Stolarek R, Gomez-Manzano C, Jiang H et al. Robust infectivity and replication of Delta-24 adenovirus induce cell death in human medulloblastoma. *Cancer Gene Ther*. 2004;11:713-20.
31. Pol IG, Zhang L, Bridle BW et al. Maraba virus as a potent oncolytic vaccine vector. *Mol Ther* 2014;22:420-429.
32. Zou, W. Regulatory T cells, tumour immunity and immunotherapy. *Nat Rev Immunol* 6: 295-307
33. Mao et al. Crosstalk between cancer-associated fibroblasts and immune cells in the tumor microenvironment: new findings and future perspectives. *Molecular Cancer* volume 20, Article number: 131 (2021). Open access journal.
34. M. Erkan, G. Adler, M. V Apte, M.G. Bachem, M. Buchholz, S. Detlefsen, I. Esposito, H. Friess, T.M. Gress, H.-J. Habisch, R.F. Hwang, R. Jaster, J. Kleeff, G. Klöppel, C. Kordes, C.D. Logsdon, A. Masamune, C.W. Michalski, J. Oh, P.A. Phillips, M. Pinzani, C. Reiser-Erkan, H. Tsukamoto, J. Wilson, StellaTUM: current consensus and discussion on pancreatic stellate cell research, *Gut* 61 (2012) 172–178, <https://doi.org/10.1136/gutjnl-2011-301220>.

35. Jančík S, Drábek J, Radzioch D, and Hajdúch M. Clinical Relevance of KRAS in Human Cancers. *J Biomed Biotechnol.* 2010; 150960. . doi: 10.1155/2010/150960.
36. Ozaki T and Nakagawar A. Role of p53 in Cell Death and Human Cancers. *Cancers (Basel).* 2011; 3(1): 994–1013.
37. Drosten M, Guerra C, and Barbacid M. Genetically Engineered Mouse Models of K-Ras-Driven Lung and Pancreatic Tumours: Validation of Therapeutic Targets. *Cold Spring Harb Perspect Med.* 2018 May; 8(5): a031542. doi: 10.1101/cshperspect.a031542.
38. Hingorani S.R., Wang L., Multani A.S., Combs C., Deramaudt T.B., Hruban R.H., Rustgi A.K., Chang S., Tuveson D.A. Trp53R172H and KrasG12D cooperate to promote chromosomal instability and widely metastatic pancreatic ductal adenocarcinoma in mice. *Cancer Cell.* 2005;7:469–483. doi: 10.1016/j.ccr.2005.04.023.
39. Anderson MD. Mutant KRAS and p53 cooperate to drive pancreatic cancer metastasis. 2021; 4.
40. Herreros-Villanueva M. Mouse models of pancreatic cancer. *World J Gastroenterol.* 2012;18 (12):1286.
41. Qiu W and Su GH. Challenges and advances in mouse modelling for human pancreatic tumorigenesis and metastasis. *Cancer Metastasis Rev.* 2013;32(0). Doi. 10.1007/s10555-012-9408-2.
42. Schuller HM, et al. The cyclooxygenase inhibitor ibuprofen and the FLAP inhibitor MK886 inhibit pancreatic carcinogenesis induced in hamsters by transplacental exposure to ethanol and the tobacco carcinogen NNK. *Journal of Cancer Research and Clinical Oncology.* 2002;128(10):525–532.
43. Al-Wadei HA, Schuller HM. Nicotinic receptor-associated modulation of stimulatory and inhibitory neurotransmitters in NNK-induced adenocarcinoma of the lungs and pancreas. *The Journal of Pathology.* 2009;218(4):437–445.
44. McGuinness EE, Morgan RG, Wormsley KG. Fate of pancreatic nodules induced by raw soya flour in rats. *Gut.* 1987;28(Supp1):207–212.
45. Pampaloni F, Reynaud EG, Stelzer EH. The third dimension bridges the gap between cell culture and live tissue. *Nat Rev Mol Cell Biol.* 2007;8:839–45.
46. Pinto B, henriques AC, Silva P and Boussba H. Three-Dimensional Spheroids as In Vitro Preclinical Models for Cancer Research. 2020; 12(12): 1186. doi: 10.3390/pharmaceutics12121186.
47. Durand RE. Invited review Multicell spheroids as a model for cell kinetic studies. *Cell Proliferation.* 1990 ; 23(3): 141-159. doi.org/10.1111/j.1365-2184.1990.tb01111.x

48. Lamfers MLM and Heminki A. Multicellular tumor spheroids in gene therapy and oncolytic virus therapy. *Curr Opin Mol Ther.* 2004;6(4):403-11.
49. Van Geer MA, Kuhlmann KFD, Bakker CT, ten Kate FJW, Oude Elferink RPJ, Bosma PJ. Ex-vivo evaluation of gene therapy vectors in human pancreatic (cancer) tissue slices. *World J Gastroenterol* 2009; 15: 1359-1366 8.
50. Friedrich J, Ebner R, Kunz-Schughart LA. Experimental anti-tumour therapy in 3-D: Spheroids—old hat or new challenge? *Int J Radiat Biol.* 2007;83(11):849–71.
51. Friederich J, Seidel C, Ebner R et al. Spheroid-based drug screen: considerations and practical approach. *Nat Protoc.* 2009;4:309-324.
52. Muthana M et al. Use of Macrophages to Target Therapeutic Adenovirus to Human prostate Tumours. *Cancer Res.* 2011;71:1805-1815.
53. Grill et al. Oncolytic Virotherapy of Meningiomas in Vitro with replication-competent adenovirus. *Experimental Studies.* 2005; 56 (1):146-154.
54. Grill et al. The Organotypic Multicellular spheroid is a relevant three-dimensional model to study adenovirus replication and penetration in human tumors in vitro. *Molecular Therapy.* 2002; (6): 609-614.
55. Porter RJ, Graeme I. Murray & Mairi H. McLean. Current concepts in tumour-derived organoids. *British Journal of Cancer.* 2020;(123): 1209–1218. Human pancreatic carcinomas acquire genetic aberrations during dissemination in nude mice. *Cancer Res* 1996; 56: 5713-5719.
56. Van der Kuip H, Murdter TE, Sonnenberg M, McClellan M, Gutzeit S, Gerteis A, Simon W, Fritz P, Aulitzky WE. Short term culture of breast cancer tissues to study the activity of the anticancer drug taxol in an intact tumor environment. *BMC Cancer* 2006; 6:86 6.
57. WA, Buskens CJ, Wesseling JG, Offerhaus GJ, Bergman JJ, Tytgat GN, van Lanschot JJ, Bosman PJ. Gene therapy for oesophageal carcinoma: the use of an explant model to test adenoviral vectors ex vivo. *Cancer Gene Ther* 2004; 11: 289-296
58. Kirby TO, Rivera A, Rein D, Wang M, Ulasov I, Breienbach M, Kataram M, Contreras JL, Krumdieck C, Yamamoto M, Rots MG, Haisma HJ, Alvarez RD, Mahasreshti PJ, Curiel DT. A novel ex vivo model system for evaluation of conditionally replicative adenoviruses therapeutic efficacy and toxicity. *Clin Cancer Res* 2004; 10: 8697-8703
59. Jones S and 35 authors. Signalling pathways in human pancreatic cancers revealed by global genomic analyses. *Science* 2008; 321: 1801-1806
60. Hall KH, Blair Zajdel ME, Blair GE (2010). Unity and diversity in the human adenoviruses: exploiting alternative entry pathways for gene therapy. *Biochem J* 2010;

61. Al-Wadei HA, Al-Wadei MH, Schuller HM. Prevention of pancreatic cancer by the beta-blocker propranolol. *Anti-Cancer Drugs*. 2009;20(6):477–482.
62. Shalhout SZ, Miller DM, Emerick KS & Kaufman HL. Therapy with oncolytic viruses: progress and challenges. *Nature Reviews Clinical Oncology*. 2023(20): 160–177.
63. Seymour LW and Fisher KD. Oncolytic viruses: finally delivering. *British Journal of Cancer*. 2016; 114: 357-361. Doi: 10.1038/bjc.2015.481.
64. Mizuguchi H, Hayakawa T. Targeted adenovirus vectors. *Hum Gene Ther* 2004; 15: 1034-1044 .
65. Garnett CT, Erdman D, Xu W and Gooding LR. Prevalence and Quantitation of Species C Adenovirus DNA in Human Mucosal Lymphocytes. *Journal of Virology*. 2002; 76(21). doi.org/10.1128/jvi.76.21.10608-10616.2002.
66. Peter M and Kühnel F. Oncolytic Adenovirus in Cancer Immunotherapy. *Cancers (Basel)*. 2020; 12(11): 3354. doi: 10.3390/cancers12113354.
67. Parkin DM et al. Global cancer statistics, 2002. *C A Cancer J Clin* 2005; 55: 74–108.
68. Mantwill K et al. Concepts in Oncolytic Adenovirus Therapy. *Int J Mol Sci*. 2021;22(19): 10522. doi: 10.3390/ijms221910522.
69. Wang et al. The function of the HGF/c-Met Axis in Hepatocellular Carcinoma. *Sec. Signalling*. 2020 (8):1-15. Doi:10.3389/fcekk.2020.00055.
70. Longati et al. 3D pancreatic carcinoma spheroids induce a matrix-rich, chemoresistant phenotype offering a better model for drug testing. *BMC Cancer*. 2013; (13):95: 1-20. Doi:10.1186/1471-2407-13-95.
71. Vinci M, Gowan S, Boxall F, Patterson L, Zimmermann M, William C, et al. Advances in establishment and analysis of three-dimensional tumor spheroid-based functional assays for target validation and drug evaluation. *BMC Biol*. 2012;10(1):29.
72. De Kanter R, Monshouwer M, Meijer DK, Groothuis GM. Precision-cut organ slices as a tool to study toxicity and metabolism of xenobiotics with special reference to non- hepatic tissues. *Curr Drug Metab* 2002; 3: 39-59.
73. Rots MG, Elferink MG, Gommans WM, Oosterhuis D, Schalk JA, Curiel DT, Olinga P, Haisma HJ, Groothuis GM. An ex vivo human model system to evaluate specificity of replicating and non-replicating gene therapy agents. *J Gene Med* 2006; 8: 35-41
74. Stoff-Khalili MA, Stoff A, Rivera AA, Banerjee NS, Everts M, Young S, Siegal GP, Richter DF, Wang M, Dall P, Mathis JM, Zhu ZB, Curiel DT. Preclinical evaluation of transcriptional targeting strategies for carcinoma of the breast in a tissue slice model system. *Breast Canc Res* 2005; 7: R1141-R1152.
75. Stoff-Khalili MA, Stoff A, Rivera AA, Mathis JM , Everts M, Wang M, Kawakami Y, Waehler R, Mathews QL, Yamamoto M, Rocconi RP, Siegal GP, Richter DF, Dall P,

- Zhu ZB, Curiel DT. Gene transfer to carcinoma of the breast with fiber-modified adenoviral vectors in a tissue slice model system. *Canc Bio & Ther* 4; 11: 1203-1210.
76. Olinga P, Groen K, Holf IH, De Kanter R, Koster HJ, Leeman WR, Rutten AA, Van Twillert K, Groothuis GM. Comparison of five incubation systems for rat liver slices using functional and viability parameters. *J Pharmacol Toxicol Methods* 1997; 38: 59-69
77. Do Amaral J.B., Rezende-Teixeira P., Freitas V.M., Machado-Santelli G.M. MCF-7 cells as a three-dimensional model for the study of human breast cancer. *Tissue Eng. Part C Methods*. 2011;17:1097–1107. doi: 10.1089/ten.tec.2011.0260.
78. Lee J., Lilly G.D., Doty R.C., Podsiadlo P., Kotov N.A. In vitro toxicity testing of nanoparticles in 3D cell culture. *Small*. 2009;5:1213–1221. doi: 10.1002/smll.200801788.
79. Andersen T., Auk-Emblem P., Dornish M. 3D cell culture in alginate hydrogels. *Microarrays*. 2015;4:133–161. doi: 10.3390/microarrays4020133.
80. Goodman T.T., Ng C.P., Pun S.H. 3-D tissue culture systems for the evaluation and optimization of nanoparticle-based drug carriers. *Bioconjug. Chem*. 2008;19:1951–1959. doi: 10.1021/bc800233a.
81. Hebner C, Weaver VM and Debnath J. Modelling morphogenesis and oncogenesis in three-dimensional breast epithelial cultures. *Annu Rev Pathol*. 2008; 3: 313-339.
82. Yamada KM, Cukierman E. Modelling morphogenesis and cancer in 3D. *Cell*. 2007; 130:601-610.
83. Edmondson R, Broglie JJ, Adcock AF, Yang L. Three-dimensional cell culture systems and their application in drug discovery and cell-based biosensors. *Assay Drug Dev Technol*. 2014; 12:207-218.
84. Kamila Białkowska,1,2,* Piotr Komorowski,2,3 Maria Bryszewska,1 and Katarzyna Miłowska1 Spheroids as a Type of Three-Dimensional Cell Cultures—Examples of Methods of Preparation and the Most Important Application.
85. Maddaly R, Paramesh V, Kaviya SR, Anuradha E, Paul Solomon FD. 3D cell culture systems: advantages and applications. *J Cell Physiol*. 2015;230:16–26.
86. Kunz-Schughart LA, Freyer JP, Hofstaedter F, Ebner R. The use of 3-D cultures for high-throughput screening: the multicellular spheroid model. *J Biomol Screen*. 2004 Jun;9(4):273-85. doi: 10.1177/1087057104265040.
87. Cheng G, Tse J, Jain RK, Lance L, Munn LL. Micro-environmental mechanical stress controls tumour spheroid size and morphology by suppressing proliferation and inducing apoptosis in cancer cells. *PLoS ONE*. 2009;4(2):e4632.
88. Sipos B, Moser S, Kalthoff H, Turuk V, Luhr M and Kloppel G. A comprehensive characterisation of pancreatic ductal adenocarcinoma cell lines: towards the

- establishment of an in vitro research platform. *Virchows Arch.* 2003;(442): 444-452. Doi 10.1007/s00428-003-0784-4.
89. Ivanov D and Grabowska A. Spheroid arrays for high-throughput single-cell analysis of spatial patterns and biomarker expression in 3D. *Scientific Report.* 2017; (7):41160.
90. Nejad E et al. The role of hypoxia in the tumour microenvironment and development of cancer stem cell: a novel approach to developing treatment. *Cancer Cell Int.* 2021; 21:62-88. Doi:10.1186/s12935-020-01719-5.
91. Walenta S, Doetsch J, Mueller-Klieser W, Kunz-Schughart LA. Metabolic imaging in multicellular spheroids of oncogene-transfected fibroblasts. *J Histochem CytoChem.* 2000;48(4):509-522. doi: 10.1177/002215540004800409.
92. Groebe, K., and Mueller-Klieser, W. (1991). Distributions of oxygen, nutrient, and metabolic waste concentrations in multicellular spheroids and their dependence on spheroid parameters. *Eur. Biophys. J.* 19, 169–181. doi: 10.1007/BF00196343
93. Barisam, M., Saidi, M. S., Kashaninejad, N., and Nguyen, N. T. (2018). Prediction of necrotic core and hypoxic zone of multicellular spheroids in a microreactor with a U-shaped barrier. *Micromachines* 9, 1–19. doi: 10.3390/mi9030094.
94. Schmitz C, Potekhina E, Irianto T, Belousov VV. Hypoxia onset in mesenchymal stem cell spheroids: Monitoring with hypoxia reporter cells. *Front Bioeng Biotechnol.* 2021; 9:1-11. Doi:103389/fbioe2021.6f1837.
95. Muz B, de la Puente P, Azab F, and Azab AA. The role of hypoxia in cancer progression, angiogenesis, metastasis, and resistance to therapy. *Hypoxia (Auckl).* 2015; 3: 83–92.
96. Wang Y, Thorne S, Hannock J, Francis J, Au T, Reid T, Iemoine N, Kirn D, Hallden G. A novel assay to assess primary human cancer infectability by replication-selective oncolytic adenoviruses. *Clin Cancer Res* 2005; 11: 351-360.
97. Broekgaarden M et al. Cabozantinib Inhibits Photodynamic Therapy Induced Auto- and Paracrine MET Signalling in Heterotypic Pancreatic Microtumors. *Cancers.* 2020; 1-17.
98. Matsunaga, T.; Gohda, E.; Takebe, T.; Wu, Y.L.; Iwao, M.; Kataoka, H.; Yamamoto, I. Expression of Hepatocyte Growth Factor Is Up-Regulated through Activation of a cAMP-Mediated Pathway. *Exp. Cell Res.* 1994, 210, 326–335, doi:10.1006/excr.1994.1045.
99. Gunti S, Hoke T.K. A, Vu P. K, London NR Jr. Organoid and Spheroid Tumor Models: Techniques and Applications. 2021; 13(4): 874. DOI:10.3390/CANCERS13040874.
100. C.J. Tape, S. Ling, M. Dimitriadi, K.M. McMahon, J.D. Worboys, H.S. Leong, I.C. Norrie, C.J. Miller, G. Poulgiannis, D.A. Lauffenburger, C. Jørgensen, *Oncogenic*

- KRAS regulates tumor cell signaling via stromal reciprocation, *Cell* 165 (2016) 910–920, <https://doi.org/10.1016/j.cell.2016.03.029>.
101. D. Thomas, P. Radhakrishnan, Tumor-stromal crosstalk in pancreatic cancer and tissue fibrosis, *Mol. Canc.* 18 (2019) 14, <https://doi.org/10.1186/s12943-018-0927-5>.
 102. Brody JR, Costantino CL, Potoczek M, Cozzitorto J, McCue P, Yeo CJ, Hruban RH and Witkiewicz AK: Adenosquamous carcinoma of the pancreas harbors KRAS2, DPC4 and TP53 molecular alterations similar to pancreatic ductal adenocarcinoma. *Mod Pathol.* 22:651–659. 2009.
 103. Fallaux F et al. Characterization of 911: A New Helper Cell Line for the Titration and Propagation of Early Region 1-Deleted Adenoviral Vectors. 2008. doi.org/10.1089/hum.1996.7.2-215.
 104. Zhu G, Pan C, Bei X, Li B, Liang C, Xu Y and Fu X. Mutant p53 in Cancer progression and targeted Therapies. *Sec. Molecular and Cellular Oncology.* 2020; 10. [Doi.org.10.3389/fonc.2020.595187](https://doi.org/10.3389/fonc.2020.595187).
 105. Varudkar N, Oyer JL, Copik A, and Parks GD. Oncolytic parainfluenza virus combines with NK cells to mediate killing of infected and non-infected lung cancer cells within 3D spheroids: role of type I and type III interferon signalling. *J Immunother Cancer.* 2021; 9(6): e002373. doi: 10.1136/jitc-2021-002373.
 106. Colonna M, Jonjic S, Watzl C. Natural killer cells: fighting viruses and much more. *Nat Immunol* 2011;12:107–10. [10.1038/ni0211-107](https://doi.org/10.1038/ni0211-107).
 107. Marotel M, Hasim MS, Hagerman A, et al.. The two-faces of NK cells in oncolytic virotherapy. *Cytokine Growth Factor Rev* 2020;56:59–68. [10.1016/j.cytogfr.2020.06.005](https://doi.org/10.1016/j.cytogfr.2020.06.005)
 108. Halama N, Braun M, Kahlert C, et al. Natural killer cells are scarce in colorectal carcinoma tissue despite high levels of chemokines and cytokines. *Clin Cancer Res* 2011;17:678–89. [10.1158/1078-0432.CCR-10-2173](https://doi.org/10.1158/1078-0432.CCR-10-2173)
 109. Melero I, Rouzaut A, Motz GT, et al.. T-Cell and NK-cell infiltration into solid tumors: a key limiting factor for efficacious cancer immunotherapy. *Cancer Discov* 2014;4:522–6. [10.1158/2159-8290.CD-13-0985](https://doi.org/10.1158/2159-8290.CD-13-0985)
 110. Shifrin N, Raulet DH, Ardolino M. Nk cell self tolerance, responsiveness and missing self-recognition. *Semin Immunol* 2014;26:138–44. [10.1016/j.smim.2014.02.007](https://doi.org/10.1016/j.smim.2014.02.007)
 111. V. Gaponova, S. Rodin, A. A. Mazina, and P. V. Volchkov. Epithelial–Mesenchymal Transition: Role in Cancer Progression and the Perspectives of Antitumor Treatment. *Acta Naturae.* 2020; 12(3): 4–23. doi: 10.32607/actanaturae.11010.
 112. Lee T.K., Poon R.T.P., Yuen A.P., Ling M.T., Kwok W.K., Wang X.H. Twist overexpression correlates with hepatocellular carcinoma metastasis through

- induction of epithelial-mesenchymal transition. *Clinical Cancer Research*. 2006;12(18):5369–5376. doi: 10.1158/1078-0432.ccr-05-2722.
113. Hugo H., Ackland M.L., Blick T., Lawrence M.G., Clements J.A., Williams E.D. Epithelial-mesenchymal and mesenchymal-epithelial transitions in carcinoma progression. *Journal of Cellular Physiology*. 2007;213(2):374–383. doi: 10.1002/jcp.21223.
114. Wang X, Zhong L and Zhao Y. Oncolytic adenovirus: A tool for reversing the tumor microenvironment and promoting cancer treatment (Review). *Oncology Reports*. 2021; 45(4). doi.org/10.3892/or.2021.8000.
115. Kudo-Saito C., Shirako H., Takeuchi T., Kawakami Y. Cancer metastasis is accelerated through immunosuppression during Snail-induced EMT of cancer cells. *Cancer Cell*. 2009;15(3):195–206. doi: 10.1016/j.ccr.2009.01.023.
116. Shibue T., Weinberg R.A. EMT, CSCs, and drug resistance: the mechanistic link and clinical implications. *Nature Reviews Clinical Oncology*. 2017;14(10):611–629. doi: 10.1038/nrclinonc.2017.44.
117. Sethi S et al. Molecular Markers of Epithelial-to-Mesenchymal Transition Are Associated with Tumor Aggressiveness in Breast Carcinoma. *Transl Oncol*. 2011; 4(4): 222–226. doi: 10.1593/tlo.10244.
118. Centeno E.G.Z., Cimarosti H., Bithell A. 2D versus 3D human induced pluripotent stem cell-derived cultures for neurodegenerative disease modeling. *Mol. Neurodegener*. 2018;13:27. doi: 10.1186/s13024-018-0258-4.
119. Baghban et al. Tumour microenvironment complexity and therapeutic implications at a glance. *Cell Communication and Signalling*. 2020; 59(18), :1-19. Doi:10.1186/s12964-020-0530-4.
120. Bullard BL, Corder BN, and Weaver EA. Species D Adenoviruses as Oncolytic Viral Vectors. *Viruses*. 2020; 12(12): 1399. doi: 10.3390/v12121399.
121. Kang S, Gao X, Zhang L, et al.. The advances and challenges of NK cell-based cancer immunotherapy. *Curr Oncol* 2021;28:26:1077–93. 10.3390/curroncol28020105
122. Mazzoleni G, Di Lorenzo D, Steimberg N: Modelling tissues in 3D: the next future of pharmaco-toxicology and food research? *Genes Nutr* 2009, 4:13-22.
123. Ghosh S, Spagnoli GC, Martin I, Ploegert S, Demougin P, Heberer M, Reschner A: Three-dimensional culture of melanoma cells profoundly affects gene expression profile: a high density oligonucleotide array study. *J Cell Physiol* 2005, 204:522-531.
124. De Witt Hamer PC, Van Tilborg AA, Eijk PP, Sminia P, Troost D, Van Noorden CJ, Ylstra B, Leenstra S: The genomic profile of human malignant glioblastoma is altered

- early in primary cell culture and preserved in spheroids. *Oncogene* 2008, 27:2091-2096.
125. Sivaraman A, Leach JK, Townsend S, Iida T, Hogan BJ, Stolz DB, Fry R, Samson LD, Tannenbaum SR, Griffith LG: A microscale in vitro physiological model of the liver: predictive screens for drug metabolism and enzyme induction. *Curr Drug Metab* 2005, 6:569-591.
126. Cree IA, Glaysher S, Harvey AL. Efficacy of anti-cancer agents in cell lines versus human primary tumour tissue. *Curr Opin Pharmacol* 2010;10:375-379.
127. Longnecker DS. Hormones and pancreatic cancer. *International Journal of Pancreatology*. 1991;9:81–86.
128. Lhoste EF, Longnecker DS. Effect of bombesin and caerulein on early stages of carcinogenesis induced by azaserine in the rat pancreas. *Cancer Research*. 1987;47(12):3273–3277.
129. Valentich MA, et al. Effect of the co-administration of phenobarbital, quercetin and mancozeb on nitrosomethylurea induced pancreatic tumors in rats. *Food and Chemical Toxicology*. 2006;44(12):2101–2105.
130. Ouyang N, et al. Nitric oxide-donating aspirin prevents pancreatic cancer in a hamster tumor model. *Cancer Research*. 2006;66(8):4503–4511.
131. Kuroiwa Y, et al. Protective effects of benzyl isothiocyanate and sulforaphane but not resveratrol against initiation of pancreatic carcinogenesis in hamsters. *Cancer Letters*. 2006;241(2):275–280.
132. Heukamp I, et al. Effects of the antioxidative vitamins A, C and E on liver metastasis and intrametastatic lipid peroxidation in BOP-induced pancreatic cancer in Syrian hamsters. *Pancreatology*. 2005;5(4–5):403–409.
133. Strouch MJ, et al. A high omega-3 fatty acid diet mitigates murine pancreatic precancer development. *Journal of Surgical Research*. 2011;165(1):75–81.

7. Appendices

7.1. Appendix 2 Manufacturer's Amylase standard curve

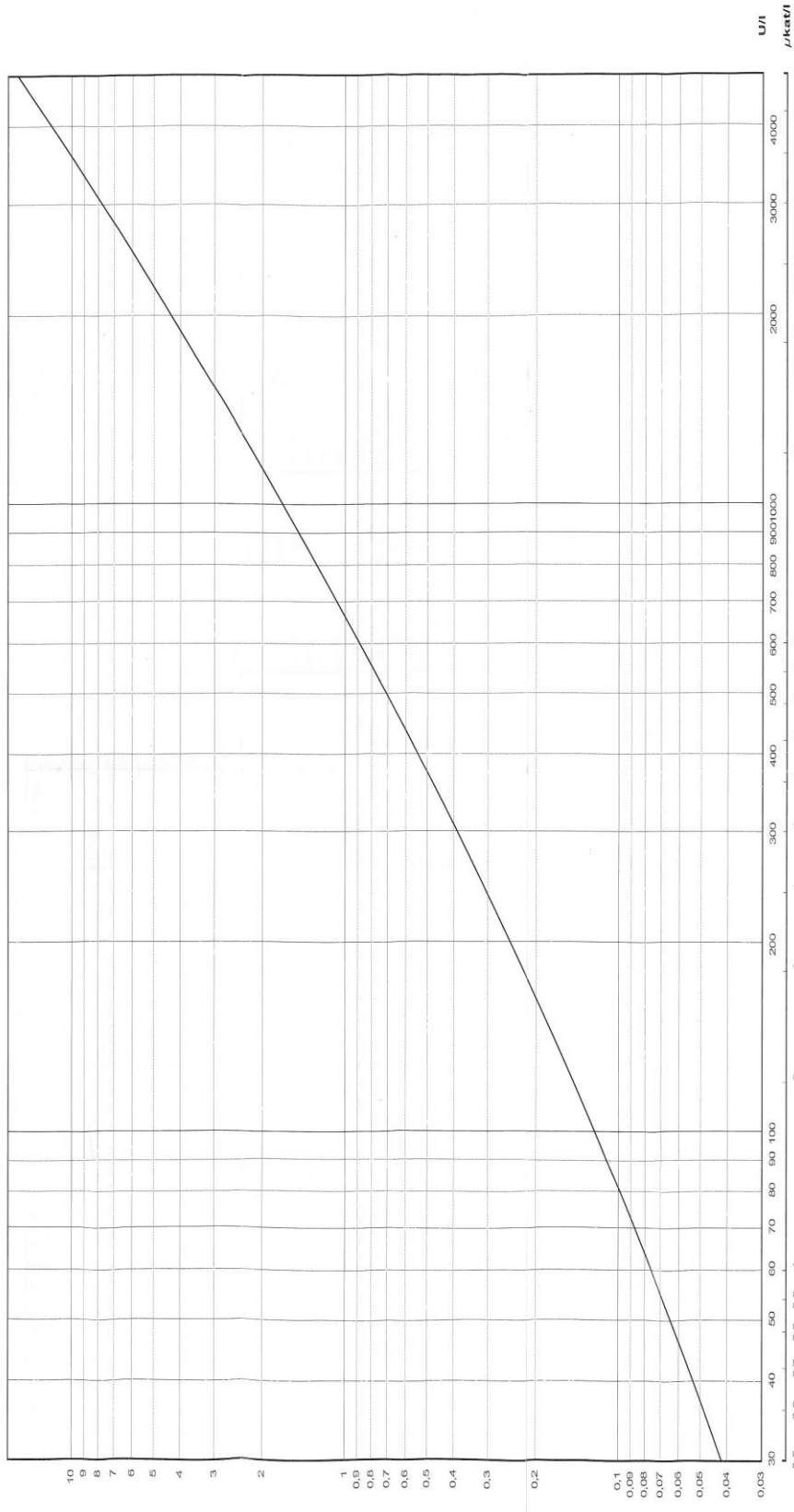
Phadebase® Amylase Test table, activity expressed in $\mu\text{mol/s} \cdot \text{s}^{-1}$
Batch no.: 9M15001

OD 620nm	$\mu\text{mol/s} \cdot \text{s}^{-1}$	$\mu\text{mol/s} \cdot \text{s}^{-1}$	OD 620nm	$\mu\text{mol/s} \cdot \text{s}^{-1}$								
0.040	0.47	0.200	2.71	0.360	0.540	0.860	9.78	1.900	18.2	5.000	37.0	
0.045	0.55	0.205	2.78	0.365	0.550	0.870	9.87	1.950	18.6	5.200	38.0	
0.050	0.62	0.210	2.84	0.370	0.560	0.880	9.97	2.000	18.9	5.400	39.0	
0.055	0.70	0.215	2.91	0.375	0.570	0.890	10.06	2.100	19.7	5.600	40.0	
0.060	0.77	0.220	2.97	0.380	0.580	0.900	10.15	2.200	20.4	5.800	41.0	
0.065	0.84	0.225	3.03	0.385	0.590	0.910	10.24	2.300	21.1	6.000	42.0	
0.070	0.92	0.230	3.01	0.390	0.600	0.920	10.33	2.400	21.7	6.200	43.0	
0.075	0.99	0.235	3.16	0.395	0.610	0.930	10.42	2.500	22.4	6.400	43.9	
0.080	1.06	0.240	3.22	0.400	0.620	0.940	10.51	2.600	23.1	6.600	44.9	
0.085	1.14	0.245	3.29	0.405	0.630	0.950	10.60	2.700	23.7	6.800	45.8	
0.090	1.21	0.250	3.35	0.410	0.640	0.960	10.69	2.800	24.3	7.000	46.7	
0.095	1.28	0.255	3.41	0.415	0.650	0.970	10.78	2.900	25.0	7.200	47.6	
0.100	1.35	0.260	3.47	0.420	0.660	0.980	10.87	3.000	25.6	7.400	48.5	
0.105	1.42	0.265	3.55	0.425	0.670	0.990	10.96	3.100	26.2	7.600	49.4	
0.110	1.49	0.270	3.60	0.430	0.680	1.000	11.05	3.200	26.8	7.800	50.3	
0.115	1.57	0.275	3.66	0.435	0.690	1.050	11.49	3.300	27.5	8.000	51.2	
0.120	1.64	0.280	3.72	0.440	0.700	1.100	11.92	3.400	28.1	8.200	52.1	
0.125	1.71	0.285	3.78	0.445	0.710	1.150	12.35	3.500	28.7	8.400	52.9	
0.130	1.77	0.290	3.84	0.450	0.720	1.200	12.77	3.600	29.2	8.600	53.8	
0.135	1.84	0.295	3.90	0.455	0.730	1.250	13.19	3.700	29.8	8.800	54.6	
0.140	1.91	0.300	3.96	0.460	0.740	1.300	13.60	3.800	30.4	9.000	55.4	
0.145	1.98	0.305	4.02	0.465	0.750	1.350	14.01	3.900	31.0	9.200	56.3	
0.150	2.05	0.310	4.08	0.470	0.760	1.400	14.41	4.000	31.5	9.400	57.1	
0.155	2.12	0.315	4.14	0.475	0.770	1.450	14.81	4.100	32.1	9.600	57.9	
0.160	2.18	0.320	4.20	0.480	0.780	1.500	15.21	4.200	32.7	9.800	58.7	
0.165	2.25	0.325	4.26	0.485	0.790	1.550	15.61	4.300	33.2	10.000	59.5	
0.170	2.32	0.330	4.32	0.490	0.800	1.600	16.01	4.400	33.8			
0.175	2.39	0.335	4.37	0.495	0.810	1.650	16.37	4.500	34.3			
0.180	2.45	0.340	4.43	0.500	0.820	1.700	16.74	4.600	34.8			
0.185	2.52	0.345	4.49	0.510	0.830	1.750	17.12	4.700	35.4			
0.190	2.58	0.350	4.55	0.520	0.840	1.800	17.49	4.800	35.9			
0.195	2.65	0.355	4.61	0.530	0.850	1.850	17.86	4.900	36.4			

Phadebase® Amylase Test table, activity expressed in U/L
Batch no.: 9M15001

OD 620nm	U/L	U/L	OD 620nm	U/L	U/L	OD 620nm	U/L	U/L	OD 620nm	U/L	U/L
0.040	28	0.200	163	0.360	280	0.540	398	0.860	587	1.900	1094
0.045	35	0.205	167	0.365	285	0.550	405	0.870	592	1.950	1115
0.050	37	0.210	171	0.370	287	0.560	411	0.880	598	2.000	1137
0.055	42	0.215	174	0.375	290	0.570	417	0.890	604	2.100	1179
0.060	46	0.220	178	0.380	294	0.580	425	0.900	609	2.200	1221
0.065	51	0.225	182	0.385	297	0.590	430	0.910	614	2.300	1265
0.070	55	0.230	186	0.390	301	0.600	442	0.920	620	2.400	1305
0.075	59	0.235	190	0.395	304	0.610	448	0.930	625	2.500	1344
0.080	64	0.240	193	0.400	307	0.620	454	0.940	631	2.600	1385
0.085	68	0.245	197	0.405	311	0.630	460	0.950	636	2.700	1422
0.090	73	0.250	201	0.410	314	0.640	466	0.960	642	2.800	1461
0.095	77	0.255	205	0.415	317	0.650	472	0.970	647	2.900	1499
0.100	81	0.260	208	0.420	321	0.660	478	0.980	652	3.000	1537
0.105	85	0.265	212	0.425	324	0.670	484	0.990	658	3.100	1574
0.110	90	0.270	216	0.430	327	0.680	488	1.000	663	3.200	1611
0.115	94	0.275	219	0.435	331	0.690	496	1.050	689	3.300	1647
0.120	98	0.280	223	0.440	334	0.700	501	1.100	715	3.400	1685
0.125	102	0.285	227	0.445	337	0.710	507	1.150	741	3.500	1719
0.130	107	0.290	230	0.450	341	0.720	513	1.200	766	3.600	1754
0.135	111	0.295	234	0.455	344	0.730	519	1.250	792	3.700	1789
0.140	115	0.300	238	0.460	347	0.740	525	1.300	816	3.800	1824
0.145	119	0.305	241	0.465	350	0.750	530	1.350	841	3.900	1858
0.150	123	0.310	245	0.470	354	0.760	536	1.400	865	4.000	1892
0.155	127	0.315	248	0.475	357	0.770	542	1.450	889	4.100	1926
0.160	131	0.320	252	0.480	360	0.780	548	1.500	912	4.200	1959
0.165	135	0.325	255	0.485	363	0.790	553	1.550	936	4.300	1993
0.170	139	0.330	259	0.490	367	0.800	559	1.600	960	4.400	2025
0.175	143	0.335	263	0.495	370	0.810	565	1.650	982	4.500	2058
0.180	147	0.340	266	0.500	373	0.820	570	1.700	1005	4.600	2090
0.185	151	0.345	270	0.510	379	0.830	576	1.750	1027	4.700	2122
0.190	155	0.350	273	0.520	386	0.840	581	1.800	1050	4.800	2154
0.195	159	0.355	276	0.530	392	0.850	587	1.850	1072	4.900	2186

Absorbance 620 nm



Standard Curve
 The standard curve was prepared using human α -amylases. From this curve, the activity of α -amylase in U/l can be determined for fluids assayed with Phadebas Amylase Test.
 Activity = $A - 0.0351$
 $\times 75.2465$
 = U/l
 U/l = 0.0167 μ kat/l

Standard Curve
 Die Standardkurve wurde unter Verwendung von Human α -Amylase herangezogen. Durch diese Kurve kann die α -Amylase-Aktivität in U/l in Flüssigkeiten bestimmt werden.
 Aktivität = $A - 0,0351$
 $\times 75,2465$
 = U/l
 U/l = 0,0167 μ kat/l

Curve etalon
 Cette courbe a été préparée en utilisant α -amylases humaine. A partir de cette courbe, l'activité de α -amylase en U/l peut être déterminée en U/l dans les échantillons de fluides avec Phadebas Amylase Test.
 L'activité amylase supérieure à l'intervalle 0,5-80 μ kat/l
 Actuelle = $A - 0,0351$
 $\times 75,2465$
 Pour exprimer en U/l, multiplier par 60.
 U/l = 0.0167 μ kat/l

Curva estándar
 Esta curva estándar se ha elaborado utilizando α -amilasas humanas. A partir de esta curva, la actividad de α -amilasa en U/l puede ser determinada en U/l para fluidos ensayados con el test Phadebas Amylase.
 La actividad de amilasa para el intervalo comprendido entre 0,5 y 80 μ kat/l
 Actividad = $A - 0,0351$
 $\times 75,2465$
 Para expresarla en U/l es necesario multiplicar 60.
 U/l = 0.0167 μ kat/l

Phadebas®
Amylase Test
 Standard Curve
 Standardkurve
 Courbe étalon
 Curva estándar
 Batch No 9946001
 © Magle AIE 2008
 www.phadebas.com

magle
 LIFE SCIENCES

7.2. Appendix 3 Ethical approval letter



National Research Ethics Service

Leeds (East) Research Ethics Committee

Room 5.2, Clinical Sciences Building
St James's University Hospital
Beckett Street
Leeds
LS9 7TF

Tel: 0113 2065652
Fax: 0113 2066772

17 June 2009

Prof Alan Melcher
Professor of Clinical Oncology and Biotherapy
Leeds Institute of Molecular Medicine
St James's University Hospital
Beckett Street
Leeds
LS9 7TF

Dear Prof Melcher

Study title: Preclinical Assessment of Anti-cancer Cellular Vaccines
REC reference: 06/Q1206/106
Amendment number: 5
Amendment date: 11 June 2009

The above amendment was reviewed at the meeting of the Sub-Committee held on 16 June 2009.

Ethical opinion

The members of the Committee taking part in the review gave a favourable ethical opinion of the amendment on the basis described in the notice of amendment form and supporting documentation subject to the following conditions:

The first point on the consent form should be corrected to read, 'I have read the information sheet (version 3.0 dated 03 June 2009) for the above study'.

Approved documents

The documents reviewed and approved at the meeting were:

Document	Version	Date
Participant Information Sheet	3	03 June 2009
Participant Information Sheet: Tracked Changes	3	03 June 2009
Participant Consent Form	3	03 June 2009
Participant Consent Form: Tracked Changes	3	03 June 2009
Protocol: Tracked Change	3	03 June 2009
Protocol	3	03 June 2009
Notice of Substantial Amendment (non-CTIMPs)		11 June 2009
Covering Letter		11 June 2009

This Research Ethics Committee is an advisory committee to Yorkshire and The Humber Strategic Health Authority
The National Research Ethics Service (NRES) represents the NRES Directorate within
the National Patient Safety Agency and Research Ethics Committees in England

Membership of the Committee

The members of the Committee who took part in the review are listed on the attached sheet.

R&D approval

All investigators and research collaborators in the NHS should notify the R&D office for the relevant NHS care organisation of this amendment and check whether it affects R&D approval of the research.

Statement of compliance

The Committee is constituted in accordance with the Governance Arrangements for Research Ethics Committees (July 2001) and complies fully with the Standard Operating Procedures for Research Ethics Committees in the UK.

06/Q1206/106:	Please quote this number on all correspondence
----------------------	---

Yours sincerely



Miss Amy Beckitt
Committee Assistant Co-ordinator
E-mail: Amy.Beckitt@leedsth.nhs.uk

Enclosures: List of names and professions of members who took part in the review

Copy to: Dr Derek Norfolk, University of Leeds
R&D office for Leeds Teaching Hospitals NHS Trust

This Research Ethics Committee is an advisory committee to Yorkshire and The Humber Strategic Health Authority
The National Research Ethics Service (NRES) represents the NRES Directorate within the National Patient Safety Agency and Research Ethics Committees in England.

Leeds (East) Research Ethics Committee

Attendance at Sub-Committee of the REC meeting on 16 June 2009

<i>Name</i>	<i>Profession</i>	<i>Capacity</i>
Ms Caroline Bedford	Pharmacist	Expert
Dr Carol E Chu	Vice Chair: Consultant Clinical Geneticist	Expert

This Research Ethics Committee is an advisory committee to Yorkshire and The Humber Strategic Health Authority
*The National Research Ethics Service (NRES) represents the NRES Directorate within
the National Patient Safety Agency and Research Ethics Committees in England.*

7.3. *Appendix 1 Consent form*

7.4. Publications

Elghazawy RM, Fox N, Orchard-Webb D, Speirs V, Smith AM, Lodge JPA, Verbeke CS and Blair GE. The Journal of Pathology. 228;(1). Abstract

09.30-09.45

[O41]

An Ex-Vivo Model of Human Pancreatic Cancer

© RM Elghazawy¹; N Fox²; D Orchard-Webb²; V Speirs³; AM Smith¹; JPA Lodge¹; CS Verbeke⁴; GE Blair²

¹Dept of HPB & Transplant Surgery, St James's University Hospital, Leeds, United Kingdom; ²Faculty of Biological Sciences, University of Leeds, Leeds, United Kingdom; ³Leeds Institute of Molecular Medicine, Leeds, United Kingdom; ⁴Division of Pathology, Department of Laboratory Medicine, Karolinska Institute, Stockholm, Sweden

Pancreatic cancer is a major leading cause of cancer death in the Western world, with approximately 40,000 deaths per year occurring in Europe and around 26,000 in the USA. The incidence of pancreatic adenocarcinoma has been steadily increasing over the past 20 years and is now the fourth most common cause of cancer deaths. Fatality is due to a lack of effective screening strategies, inconspicuous early symptoms and poor response to existing therapies leading to a median survival of around one year. New forms of treatment for this disease are therefore urgently needed. A critical requirement for pre-clinical studies is a suitable model system in which to analyse the effects of therapeutic agents. Most in-vitro models fail to reflect the complex tissue architecture of an individual tumour. In this study human pancreatic tissue samples, both malignant and normal, were obtained from surgical specimens and processed to precision-cut 250µm x 0.5cm slices. Various elements were introduced to the modelling system (e.g. minimising the time from surgical resection to culture; coated vs uncoated culture plates; using low melting point agarose) in order to maximise the yield from minimal amounts of tissue and optimise the culture conditions. Pancreatic normal and cancer tissue slices could then be cultured for up to four days whilst maintaining good to excellent morphology. A comprehensive analysis of tissue morphology, function and viability established that histopathological examination together with a morphological grading was shown to be the best approach for the assessment of the preservation of structural integrity. It was found that cellular death in such cultured slices occurs by necrosis rather than apoptosis. This organotypic culture model presents a representative and reproducible system of the in-vivo situation that will allow the prediction of the clinical efficacy of novel therapies such as gene therapy.

36

Visit our website: www.pathsoc.org | Summer Meeting (202nd) 3 – 5 July 2012 | Scientific Programme

